DEVELOPMENT AND PATTERN ANALYSIS OF SUPERHYDROPHOBIC NANOCOMPOSITE COATING

by Amrita Hooda

DEVELOPMENT AND PATTERN ANALYSIS OF
SUPERHYDROPHOBIC NANOCOMPOSITE COATING

A thesis submitted to the
University of Petroleum and Energy Studies

For the Award of
Doctor of Philosophy
in
Electronics & Communication Engineering

BY
Amrita Hooda

October 2019

SUPERVISOR (s)

Dr. Rajeev Kumar Gupta
Dr. Adesh Kumar

UPES
UNIVERSITY WITH A PURPOSE

Department of Electrical & Electronics Engineering
School of Engineering
University of Petroleum & Energy Studies
Dehradun - 248007: Uttarakhand

DEVELOPMENT AND PATTERN ANALYSIS OF SUPERHYDROPHOBIC NANOCOMPOSITE COATING

A thesis submitted to the
University of Petroleum and Energy Studies

For the Award of
Doctor of Philosophy
in
Electronics & Communication Engineering
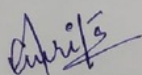
BY
Amrita Hooda

October 2019

SUPERVISOR (s)

Dr. Rajeev Kumar Gupta
Dr. Adesh Kumar

UPES
UNIVERSITY WITH A PURPOSE

Department of Electrical & Electronics Engineering
School of Engineering
University of Petroleum & Energy Studies
Dehradun - 248007: Uttarakhand

i

October, 2019

DECLARATION

I declare that the thesis entitled "**DEVELOPMENT AND PATTERN ANALYSIS OF SUPERHYDROPHOBIC NANOCOMPOSITE COATING**" has been prepared by me under the guidance of Dr. Rajeev Kumar Gupta, Associate Professor of Physics and Dr. Adesh Kumar, Assistant Professor of Electrical & Electronics Engineering, University of Petroleum & Energy Studies. No part of this thesis has formed the basis for the award of any degree or fellowship previously.
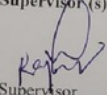
Amrita Hooda

Department of Electrical & Electronics Engineering,

School of Engineering,

University of Petroleum and Energy Studies,

Bidholi, via Prem Nagar, Dehradun-248007, Uttarakhand, India.

Date: 31, October 2019

ii

CERTIFICATE

I certify that Amrita Hooda has prepared her thesis entitled "**DEVELOPMENT AND PATTERN ANALYSIS OF SUPERHYDROPHOBIC NANOCOMPOSITE COATING**", for the award of PhD degree of the University of Petroleum & Energy Studies, under my guidance. She has carried out the work at the Department of Electrical & Electronics Engineering, University of Petroleum & Energy Studies.

Internal Supervisor (s)

Research Supervisor

Dr. Rajeev Kumar Gupta

Research Co-supervisor

Dr. Adesh Kumar

School of Engineering,
University of Petroleum and Energy Studies,
Bidholi, via Prem Nagar, Dehradun-248007, Uttarakhand, India.
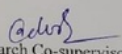
Date: 31, October 2019

iii

This dissertation is dedicated to my parents,

Shri DharamVeer Hooda and Smt. Rajbala Hooda,

my husband Dr. Manjeet Singh Goyat and

my beloved children Aliena and Rudraksh.

ACKNOWLEDGEMENTS

Dated: **AMRITA HOODA**

ABSTRACT

Over the past few years, water-repelling coatings, especially superhydrophobic coatings, have gathered remarkable attention of researchers and industrialists due to their exclusive self-cleaning, anti-reflection, anti-adhesion, anti-icing, etc. properties. The idea of superhydrophobicity emerges out from the lotus plant leaves. The lotus leaves have micro-, nano hierarchical surface roughness which leads the rolling of water droplet during rain and behaves like a self-cleaning surface. The mimicking of such surface provides the artificial superhydrophobic coatings that have contact angle more than 150° and SA less than 10°. Two important parameters need to address to prepare a superhydrophobic coating: (1) low surface energy of the coating and (b) nano-level roughness of the coating. The surface energy of the coating can be reduced using low surface energy materials (Fluoro containing silane groups) deposition on the surface and the nano-level roughness can be induced by introducing nanoparticles in the coating material. The development of transparent superhydrophobic surfaces is quite challenging and very useful of various energy applications such as anti-dust and anti-icing for photovoltaic cells, etc. The surface roughness and transparency of the coatings are competitive properties. If the surface roughness increases transparency decreases due to scattering of light and vice-versa.

This work is focused on the development of transparent superhydrophobic coatings via sol-gel method. ZnO and SiO_2 nanoparticles were functionalized and embedded into polystyrene polymer to develop the coatings. The roughness of the coatings was optimized with respect to the concentration of the nanoparticles, functionalizing agents and process parameters. The ZnO nanoparticles were dual-functionalized using TMCS and MPMS functionalizing agents and uniformly dispersed in PS to achieve the surface roughness of ~ 28 nm with a maximum contact angle of 152° and SA of 3°. The transparency close to the transmittance of bare glass has been obtained for the PS/ZnO based superhydrophobic coatings. However, TOS-

functionalized SiO_2 nanoparticles were embedded in PS to prepare transparent SHC using a simple sol-gel technique. The dip/pull speed and dipping time were optimized to control the superhydrophobicity and the transparency of the developed coating. The maximum roughness of 65.39 ± 6.7 nm with unique morphology was obtained, which was found responsible for the high contact angle of $162 \pm 2°$ and SA of $3 \pm 1°$. High average transmittance of $91.8 \pm 0.5\%$ which was close to the average transmittance of bare glass ($92.6 \pm 0.2\%$) achieved for the superhydrophobic coating.

FESEM images were processed, segmented and applied under wavelet processing. The machine learning approach based on K-means clustering estimated the roughness of superhydrophobic coatings using FESEM images. The MATLAB was used for the FESEM image segmentation, wavelet processing, analysis and score prediction. The performance of the roughness estimation using FESEM images was found good as the tool predicted the score 91.70 % against roughness parameter.

The sol-gel method assisted with spin coating and dip/pulling route has a great potential to prepare transparent superhydrophobic coatings for the self-cleaning application of the cover glass of commercial solar panels. Additionally, digital image processing can assist in a great manner to understand the important features of superhydrophobic coatings. MATLAB is a powerful tool to apply the K-means clustering on SEM or AFM images to determine the various parameters of the superhydrophobic surfaces more precisely and quite helpful for understanding the basic mechanisms of the superhydrophobicity.

Table of Contents

List of Figures

xiii

xiv

xv

List of Tables

List of Symbols

θ_A	Advancing angle
θ	Angle
θ_e	Contact angle
$^{\circ}$	Degree
ρ	Density
$\emptyset_A$	Fraction term
β	FWHM
θ_R	Receding angle
r_f	Roughness factor
P_S	Spreading power
γ_{LV}	Surface tension (liquid-vapour)
γ_{SL}	Surface tension (solid-liquid)
γ_{SV}	Surface tension (solid-vapour)
θ_D	Tilting or slipping or sliding angle
λ	Wavelength of radiation
θ_W^*	Wenzel's contact angle
c_i	Set points
cm^{-1}	Centimetre inverse
g	Acceleration due to gravity
h	Hour
k	No. of groups or no. of clusters
mm	Millimeter
n	Arbitrary number
nm	Nanometer
s	Second
D	Particle size
K	A constant

L	Length
N	Vector points
Jm^{-2}	Joule per meter square
Nm^{-1}	Newton per meter
R_{avg}	Average roughness
X_i	Data points

List of Abbreviations

2 D	2 Dimensional
3 D	3 Dimensional
AFM	Atomic force microscope
APS	Approximate particle size
CA	Contact angle
C-H	Carbon-hydrogen
CH_2	Methylene
CO_2	Carbon dioxide
CVD	Chemical vapour deposition
DA	Discriminant Analysis
Deg.	Degree
DSA	Drop shape analyzer
DWT	Discrete wavelet transform
FESEM	Field emission scanning electron microscope
FTIR	Fourier Transform Infra-red
FWHM	Full width at half maximum
g	Gram
GLM	Generalized Linear Model
GPR	Gaussian process regression
HAAR	Square-shaped function
Hkl or hkil	Crystallographic planes
ITO	Indium tin oxide
MATLAB	Matrix laboratory
Min	Minutes
MPMS	3-Mercaptopropyltrimethoxy silane
Mw	Molecular weight
Nano-ZS	Nano-zeta sizer
NB	Naive Bayes

PDMS	Polydimethylsiloxane
pH	Potential of Hydrogen
PS	Polystyrene
Rad.	Radian
R_{rms}	Root mean square roughness
SA	Sliding angle
SEM	Scanning electron microscope
SHC	Superhydrophobic coating
SHS	Superhydrophobic surface
Si-O	Silicon monoxide
SiO_2	Silica or silicon dioxide
Si-OH	Silicon-hydroxyl
Si-O-Si	Silicon-oxygen-silicon
SVM	Support vector machine
SVM	Support Vector Machines
SVR	Support vector regression
TEOS	Triethoxyoctylsilane
THF	Tetrahydrofuran
TiO_2	Titania or Titanium dioxide
TMCS	Chlorotrimethylsilane
$TOS-SiO_2$	Triethoxyoctylsilane modified nano-silica
UV	Ultra-violet
UV/VIS	Ultraviolet/visible
wt%	Weight percentage
XRD	X-ray diffraction
ZnO	Zinc oxide
Zn-OH	Zinc oxide-hydroxyl

CHAPTER 1. INTRODUCTION

1.1. STATEMENT OF THE PROBLEM

Superhydrophobic surfaces (SHSs) showed a great potential of 'dust-phobicity' and low dust adhesion due to their self-cleaning characteristics. The development of super-hydrophobic surfaces for preventing dust accumulation is an active area of investigation [1], [2]. Water droplets can easily slide on such surfaces, owing to low contact angle (CA) hysteresis. Two main parameters desired to design an SHS: (1) low surface energy and (2) micro- and nano-hierarchical roughness of the solid substrate. The dust accumulation problem on solid surfaces can be easily dealt by reducing its surface energy and generating micro-, nano-level roughness which significantly reduces the adhesion between the solid surface and water droplets and also favours the adhesion between water droplets and dust particles useful for self-cleaning of the surface. Nano-structures are an attractive option for creating nano-scale roughness on the solid surfaces by depositing their layer on the surfaces because nanomaterials generally have at least one dimension in the range of 1-100 nm [3]. The nano-size of nanostructures makes them exhibit unique physical and chemical properties especially due to their high specific surface area to volume ratio [3]–[5]. The surface energy of the solid surfaces can be reduced by attaching low surface energy materials on the surface that can be done in two ways either attaching low surface energy materials directly on the surface in form of the coating of that material or attaching low surface energy materials on the surface of the nanostructures and then depositing the layer of those nanomaterials on the solid surfaces. The latter case is quite useful for developing SHSs because it consists both the low surface energy and nano-level roughness on the solid surface [6].

1.2. BACKGROUND

This is a well-known concept that the rough surfaces exhibit better hydrophobicity compared to flat surfaces [7], [8]. According to Wenzel' theory [8], better hydrophobicity of a rough surface is owing to less contact area between the water droplet and a solid surface. Cassie and Baxter [9] suggest that low CA hysteresis and high CA on a porous surface is owing to air trapping in the pores of the structure which in turn is responsible for diminishing the contact between water droplets and the solid surface. Further, the trapped air also reduces the bonding between subsequent layers of deposited dust and thereby prevents the dust deposition more efficiently. Additionally, superhydrophobic coatings (SHCs) exhibit anti-dust and anti-ice deposition potential [10], [11]. Polymer-based coatings modified with low surface energy materials like tetrafluoroethylene and organopolysiloxane demonstrated a significant reduction in dust deposition. So, these can be considered as the potential candidates for self-cleaning coatings. A durable and eco-friendly SHC can be used as the potential coating to sustain the efficiency of a solar panel by inhibiting the dust deposition. Optical transparency is a must for solar panel which increases the transmission of solar radiation and thereby increasing the efficiency. SHCs usually have high surface roughness that results in significant light scattering which hampers the efficiency of solar panels. Transparency and superhydrophobicity are contradictory properties so an accurate roughness control is imperative to fabricate transparent SHCs.

1.3. MOTIVATION/NEED FOR THE RESEARCH

Plenty of reports available on developing SHCs to reduce the dust deposition on solid surfaces for application in the field of wind power, aviation, building construction and heat-exchanger. But reports of its application in energy conversion devices are limited.

Wang et al [12] developed robust SHCs with excellent transparency using a facile solidification-prompted phase-separation route. The transparency and superhydrophobicity of the hybrid nanoporous coating based on

Polydimethylsiloxane (PDMS) were obtained by optimizing the roughness of the coating which was controlled by varying the PDMS viscosity. The developed coatings exhibited high transparency (an average transmittance > 85% for the visible light radiations) and superhydrophobicity (CA ~ 155°, and SA < 1°). Furthermore, the SHC revealed worthy mechanical durability and thermal stability that makes it worthy for real-life applications.

Zhao et al [13] demonstrated the fabrication of highly transparent SHC via a facile casting method. Polycarbonate in solution form was casted on a micro-level roughness possessing solid substrate. Additionally, the SHC demonstrated heat-resistance and revealed the stability up to 390 °C. Such transparent and SHCs are highly desired for advanced technology and in electronics industries.

Cao et al [14] demonstrated the fabrication of nanoparticle-reinforced polymer nanocomposites. The polymer nanocomposites exhibited the anti-icing property due to their superhydrophobic character. It was demonstrated that the superhydrophobic polymer nanocomposite coatings avert ice-deposition in presence of supercooled water at laboratory scale and in ordinary surroundings outside the laboratory.

Similarly, Bahadur et al [15] and Jung et al. [16], [17] demonstrated the mechanisms of SHCs responsible for anti-icing property considering various parameters such as heterogeneous ice nucleation, heat transfer and water-droplet impact dynamics.

In another study, Mishchenko et al [18] focused on the study on droplet-impact dynamics onto micro- and nano-level roughness possessing surfaces. The nucleation classical theory was clubbed with wetting-dynamics and heat transfer theory to fabricate anti-dust coatings by considering the contributing factors such as water droplet deposition, pinning and retraction. Some researchers reported non-transparent SHCs with a very high CA.

Satyaprasad et.al [19] demonstrated a unique strategy to prepare the SHS on stainless steel analogous to nano-structured Teflon coating via plasma arc

method. The synthesized coating exhibit 80–200 nm nanostructural features with very high water CA ~ 165°.

In another study, Mahendra et. al [20] obtained superhydrophobic methyl-trimethoxysilane based silica coating by utilizing polymethylmethacrylate through simple dip-coating method instead of using silylating reagents. The synthesized SHC exhibit water CA about 171°.

However, Yu et al. [21] developed superhydrophobic nano ZnO consisting of self-cleaning coatings onto Indium tin oxide (ITO) coated glass substrate by growing polystyrene spheres supported ZnO nanoarrays. The developed coating revealed CA ~ 152°.

For solar panel application, Perkas et al. [22] developed a highly hydrophobic film of GaAs material consisting of ZnO nanostructures via ultrasound aided technique. The developed coating presented the CA more than 141° to get-rid off dew-deposition on the solar panel.

However, Jiang et al. [23] described a simplistic approach to synthesize micro-nano feature consisting of Co_3O_4 coatings with outstanding superhydrophobicity and anti-icing character. The synthesized coatings exhibited maximum CA > 169° with SA < 3°.

Dudem et al. [24] described the fabrication of SHCs based on nano titania via a combination of self-assembly and photosensitive sol-gel approach. The maximum water CA of more than 162° was achieved. Additionally, the superhydrophobic character of the coating could be transformed into the superhydrophilic by exposing the coating to ultraviolet radiation.

1.4. OBJECTIVES
- To prepare the nanoparticle filled polymer-based transparent SHCs
- To characterize the developed transparent SHCs
- To analyze the surface pattern of developed coatings using image processing and machine learning tools

4

1.5. SCHEME OF THE CHAPTERS

The chapter-wise summary of the thesis is given below:

Chapter 1 introduces the statement of the problem, background information, motivation/ need for the research objectives and scheme of chapters for the development of nanoparticles filled polymer-based transparent SHCs.

Chapter 2 presents a comprehensive literature review on the fundamentals of superhydrophobicity concept, theoretical wetting models required to understand the wetting theory of surfaces, most commonly used preparation techniques for the development of transparent SHCs and challenges in fabrication of transparent SHSs based on polymer nanocomposites including a glimpse of potential applications of SHCs.

Chapter 3 portrays the detailed methodology of synthesis of nanoparticles and preparation of nanoparticles embedded polymer-based transparent SHCs. It also consists of detailed information about the materials used for the development of the coatings. This chapter describes the characterization techniques including XRD, FESEM, FTIR, Zeta Sizer, AFM, Drop Shape Analyzer, UV/VIS spectrometer used to obtain the data form transparent SHCs. It also presents the pattern analysis approach using K-means clustering to obtain the roughness data from the FESEM images of the developed coatings.

Chapter 4 describes the synthesis of nano-textured polystyrene/ZnO coatings with excellent transparency and superhydrophobicity. It explains how the transparent superhydrophobic polystyrene/ZnO nanocoating, possessing an average roughness of 28 nm and high CA more than 150º has been synthesized through a modified facile sol-gel route. It explains how to control hierarchical roughness of the coating using dual functionalization of ZnO nanoparticles. The effect of experimental parameters on transparency and superhydrophobicity of developed coatings was examined to obtain optimum conditions.

Chapter 5: describes a facile approach to develop modified nano-silica embedded polystyrene-based transparent SHC. It describes how the triethoxyoctylsilane modified nano-silica embedded polystyrene-based transparent SHC has been

synthesized on a glass substrate via a facile sol-gel method. It describes the optimization of dip-pulling process to synthesize the coating. It explains the role of unique morphology of the coating to obtain the static water CA more than 162° with a SA of 3° including the high average transmittance of 91.8%, which is close to close to the average transmittance of the bare glass.

Chapter 6: describes the pattern analysis and machine learning approach. It also illustrates the detailed approach for the pattern analysis data collection based on the roughness of the FESEM images. It portrays the results and discussions on Pattern Analysis and Machine Learning.

Chapter 7: describes the conclusions and future scope of transparent SHCs and their pattern analysis using machine learning approach.

Chapter 8: comprises the references.

CHAPTER 2. LITERATURE SURVEY

2.1. RUDIMENTS OF SUPERHYDROPHOBICITY

2.1.1. SURFACE TENSION

Superhydrophobicity is based on surface tension and surface free energy. Surface tension is related to the surface of a liquid. The lower number of liquid molecules lies at the surface compared to the molecules in the bulk. The variation in the number of molecules at the surface and in the bulk is responsible for the generation of surface tension (γ_{LV}) in the liquid. The surface tension is a force that stems from the attractive forces among the neighbouring molecules of a liquid within the surface layer so that the liquid layer can act as an elastic sheet. The surface tension aids the small insects to float on the surface of water. Conventionally, surface tension is force/unit length (Nm^{-1}) or energy/unit area (Jm^{-2}) [25]. A small drop of any liquid can change its shape in order to reduce its surface free energy in form of a sphere because spherical shape of a liquid drop attributed to the minimum surface free energy, the most stable state of a liquid drop. However, comparatively larger water drops are non-spherical in nature; the gravitational force distorted the shape of water drops especially when the water drops encounter any solid surface. For small sizes of liquid drops, the surface tension dominates whereas, for large sizes, the gravitational force dominates. The surface tension depends on the length (L) whereas the gravity depends on the mass of the liquid drop, in other words, it is a function of cube of the length and the density of the drop (ρ). The gravity to surface tension ratio for a liquid drop is equal to $\rho gL^3/\gamma_{LV}L \sim L^2$ (where g is acc. due to gravity). This ratio indicates that when the length of the liquid drop is large; its shape will be distorted due to the dominance of gravitational force over surface tension, whereas when the length of the drop is small, its shape will be spherical due to the dominance of surface tension over the gravity.

If the surface tension and gravitational forces are plotted against each other for the size of water droplets (Fig. 2.1), then both the plots will intersect at 2.73 mm that is known as the capillary length of the water droplet. The droplets smaller than 2.73 mm will exhibit spherical shape due to the dominance of surface tension while the drops equal and larger than 2.73 mm will exhibit non-spherical shape because of the dominance of the gravitational force. The dominance transition of gravitational force to surface tension can be easily understood by gently dropping a paper clip in water (Fig. 2.1). A heavy and large paper clip when putting into water that breaks the elastic water surface layer easily and sinks, however a lightweight small paper clip floats on the water surface due to elastic layer of water produced by the surface tension. Many tiny insects exist in nature those have the ability to play with the surface tension of a liquid and can easily float and sink in water, for example, water spider (Argyroneta Aquatica) [26], [27].
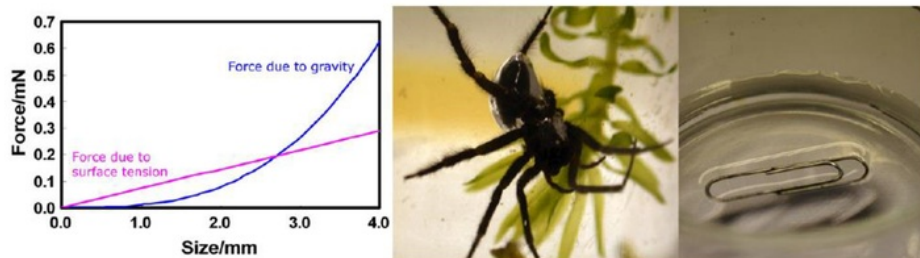
Fig. 2.1 Gravitational force v/s surface tension for the water droplets, a water spider floating on the water film and a paper clip floating on the water [26], [27].

2.1.2. SURFACE FREE ENERGY

Surface free energy is one of the essential parameters of a surface or interface. Generally, in substance chemical bonds occur among the molecules. A particular amount of energy is required to break such bonds in the substance. The molecules, which do not involve in chemical bonding because of their exposure especially at the outer sides of the surface, exhibit high potential energy compared to the molecules that are involved in chemical bonding inside the bulk of the substance. The exposed molecules at the sides of the surface with higher energy are responsible for generation of surface free energy. In other words, the additional

8

energy of such molecules is known as the surface free energy. Such surface/ interface free energy is usually represented by energy/ unit area (Jm^{-2}) [28]. Thermodynamically, all the terms such as surface free energy, surface tension force, surface energy density, surface tension are different [29], [30]. In the study of SHSs especially at thermodynamic equilibrium i.e., at constant temperature and pressure, all such terms become almost equal [31]. In an ideal situation, when adsorption is almost negligible (or zero) at the interfaces then the surface tension can be considered same as the surface free energy. Usually, the dry surface has lesser surface energy compared to the wet surface. Due to the low surface energy of an SHS, a water drop on such surface become spherical in order to reduce its energy so that the preferred liquid-air interface is obtained. Additionally, the roughness of a surface can alter the surface energy by reducing it. Thus, a water drop exhibits a higher CA on a rough surface (low surface energy) and lower CA on a smooth surface (high surface energy) [32].

2.1.3. INTERACTIONS WITH SURFACES

Interfacial tension is the expansion of work (a form of energy) to enhance the interface size between two neighbouring phases that do not blend entirely with each other. In other words, the interfacial tension belongs to the liquid-solid and liquid-liquid phases. However, the liquid-gas interface is attributed to the surface tension (γ_{LV}) and the solid-gas interface corresponds to the surface free energy. The γ_{LV} is related with the liquid-vapour interface. Another two interfaces such as solid-vapour and solid-liquid turn out to be appropriate when a water drop lies on a solid substrate and found responsible for interfacial tensions (γ_{SV}), (γ_{SL}) respectively. The combined effect of all three interfacial tensions γ_{SL}, γ_{LV} and γ_{SV} decides whether a water drop on a solid substrate will turn out into a film or that will persist as a spherical drop. On a plane (or even) and dry surface interaction-energy/ unit area is indicated by γ_{SV}, however if the surface is coated with thin layer of water then two interfaces will come into picture with a joint interaction energy/

9

unit area in form of $\gamma_{SL} + \gamma_{SV}$ and overall surface energy will be lowered and the modified condition will be given by equation (1) [33], [34].

$$P_S = \gamma_{SL} + \gamma_{LV} - \gamma_{SV} > 0 \qquad (2.1)$$

where P_S is spreading power. For an uneven rough surface, the water drops will convert into non-spherical shapes to reduce their surface free energy by changing the comparative areas of all three interfaces and keeping volume constant [35]. The size of water drop will decide that up to what extent gravitational force is a manipulating parameter. Generally, a small water drop on a smooth surface will try to remain in form of a spherical shape, while comparatively a larger water drop will try to flatten on the surface due to the gravitational force.

Once the water drop does not flatten on a surface and rests on the surface in a semi-wetting form, then an equilibrium CA (θ_e) forms at the edges of the water drop. The θ_e is a tangent angle at the liquid-vapour interface involving three phases such as solid-liquid, liquid-vapour, and solid-vapour as shown in Fig. 2.2. The equilibrium CA generally does not dependent on the size of the liquid droplet and can be easily defined using Young's equation [25],

$$\cos \theta_e = \frac{\gamma_{SV} - \gamma_{SL}}{\gamma_{LV}} \qquad (2.2)$$
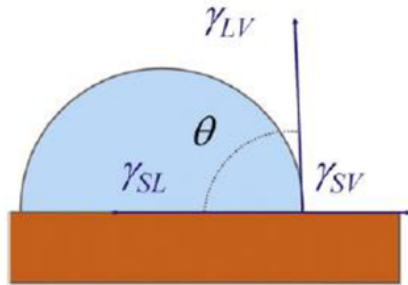
Fig. 2.2 Schematic diagram of the formation of an equilibrium CA (θ_e) at the edges of a water drop on a solid surface involving three phases such as solid-liquid, liquid-vapour, and solid-vapour.

2.1.4. HYDROPHILICITY, HYDROPHOBICITY AND SUPER-HYDROPHOBICITY

When liquid drops fall on a solid surface and turn up immediately into a flat liquid film on the surface and exhibit the spreading power, S = 0 (Equation 2.1). The threshold for such surface corresponds to equilibrium CA, θ_e= 0° (Equation 2.2). Such surface is known as an ideal hydrophilic surface. However, when a liquid drops fall on a solid surface and remain in the form of a spherical liquid droplet without converting into a flat liquid film on the surface, which is energetically uncomplimentary condition for a liquid drop having any contact with the solid surface leading to θ_e= 180°. Such surface is known as an ideal hydrophobic surface. The Young's equation is quite useful to identify whether the surface is hydrophilic or hydrophobic. If γ_{SV} is less than γ_{SL} then the liquid droplet CA will reduce to < 90° so that the surface can be designated as hydrophilic in nature. While if γ_{SV} is greater than γ_{SL}, then the liquid droplet CA will increase to > 90° so that the surface can be designated as hydrophobic in nature [36].

When If γ_{SV} is equal to γ_{SL} then the liquid droplet CA becomes 90°, which is considered as a boundary between a hydrophilic and hydrophobic surface. Generally, it is assumed by the scientific community that if the CA is lying between 150° to 180° then that surface is superhydrophobic in nature. There is a great possibility to convert a hydrophobic surface to the superhydrophobic one by developing a unique type of topography. The topography of a solid surface can be altered by introducing a typical type of roughness on it by various means that will be discussed in detail in the following sections [37]. The increase in CA can be obtained up to 180° under certain circumstances by increasing the surface roughness which is beyond the surface chemistry of the surface alone. The CA can be reduced to 0° which is not possible if we consider the surface chemistry alone of the surface.

2.1.5. THEORETICAL WETTING MODELS

Three theoretical models are well-known to understand the wetting properties of a solid surface. The first and most basic theoretical wetting model is suggested by Young's equation.

2.1.5.1. Young's wetting model

This model is based on certain assumptions such as a steady liquid droplet, a perfect inelastic, uniform, smooth and passive surface. There is a contact line between the liquid droplet and solid substrate consisting of all three phases such as solid-liquid, liquid-vapour, and solid-vapour as shown in Fig. 2.2. The droplet touches the rigid substrate at an angle θ. All the three interfaces draw a contact line in order to reduce the surface area in each case, harmonizing the surface tension of the droplet motion in order to produce a mathematical relation which corresponds to Young's equation (Young's wetting model) as depicted in Equation 2.2. However, Young's publication [38] does not reveal clearly such type of equation. The Young's model explicitly establishes the relation between CA and the interfacial energies. Though practically, the surfaces are not uniform and characteristics of such surfaces usually based on the various parameters during the preparation of a surface and Young's model is based on ideal surfaces so this model is not accurate enough to describe the wetting behaviour of practical surfaces. Then another model comes into the picture named as Wenzel's wetting model.

2.1.5.2. Wenzel's wetting model

Wenzel's wetting model is much better than Young's model because this model establishes relation among the CA, surface energies and the surface roughness [39], [40]. The additional parameter surface roughness is one of the important parameters to study the wetting behaviour of a surface having uniform roughness. Wenzel's equation is:

$$r_f(\gamma_{SV} - \gamma_{SL}) = \gamma_{LV} \cos \theta_W^*$$ (2.3)

where θ_W^* is Wenzel's CA that determines the CA affected by the roughness of the surfaces. r_f is attributed to the "roughness factor". The improved Wenzel's equation is:

$$\cos \theta_W^* = r_f \cos \theta \qquad\qquad (2.4)$$

The Wenzel's model is based on the assumption of a uniform wetting system that allows the piercing of water droplets into the grooves of the rough surface. The CAs can show random values for a surface if one considers its bulk surface or the surface at molecular/atomic dimensions. Practically, it is quite possible to classify smooth and rough surfaces. According to Wenzel's model, a hydrophilic surface can be converted to more hydrophilic one by increasing the roughness of a hydrophilic surface. However, the hydrophobicity of a hydrophobic surface can be significantly improved by increasing the roughness of that surface [46]. Generally, the wetting states can be classified into three categories: (i) stable homogeneous wetting state, (ii) stable heterogeneous wetting state, and (iii) the metastable state (a state between homogeneous and heterogeneous state). The Wenzel's wetting model is valid only for a homogeneous state, while some additional wetting models are required to understand the wetting behaviour of other two types of states.

2.1.5.3. Cassie–Baxter's wetting model

Cassie–Baxter's wetting model is applicable to the heterogeneous wetting state. The schematic diagrams of rough surfaces are illustrated in Fig. 2.3. This infers that for a homogeneous wetting state, the droplet touches the surface of a solid substrate and pierces into the trenches due to the lumps on the surface (Fig. 2.3a) and Wenzel's theoretical model is applicable. However, for a heterogeneous state, the droplet touches only the top of the lumps of the solid surface and traps air below into the trenches (Fig. 2.3b) and Cassie–Baxter's theoretical wetting model is applicable.
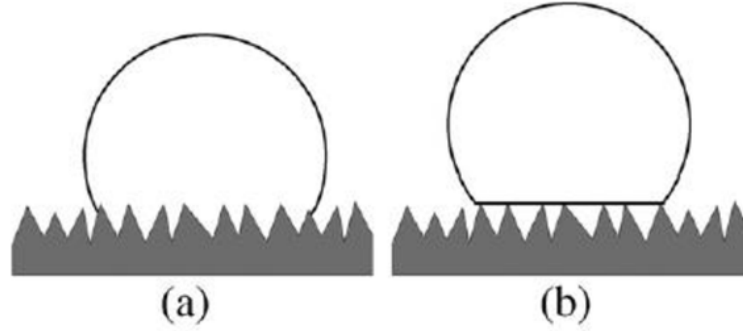
Fig. 2.3 (a) Homogeneous and (b) heterogeneous wetting states. In a homogeneous wetting state, the droplet touches the surface of a solid substrate and pierces into the trenches due to the lumps on the surface whereas, in a heterogeneous wetting state, the droplet touches only the top of the lumps of the solid surface and traps air below into the trenches [41].

When a liquid drop touches only the top of the lumps of a solid surface instead of the complete surface consisting trenches (heterogeneous surface) then a fraction term $(\emptyset_A)$ [38] can be defined as the ratio of the whole area of a solid-liquid interface and the entire area of liquid-air and solid-liquid interfaces considering total area equivalent to unity for an uneven surface. The presence of air between solid and liquid phase can result the maximum CA such as 180°. Such CA can be defined by an equation given below [38]:

$$\cos \theta^* = -1 + \emptyset_A(\cos \theta + 1) = \emptyset_A . \cos \theta + \emptyset_A - 1 \qquad (2.5)$$

If one considers the ratio of the real drenched area and the expected drenched area, then a revised Cassie–Baxter's equation is obtained [42] as mentioned below:

$$\cos \theta^* = r_f . \emptyset_A . \cos \theta + \emptyset_A - 1 \qquad (2.6)$$

where, r_f is the roughness ratio of the fraction. When $\emptyset_A = 1$ and $r_f = r$ then the transition of Cassie–Baxter's equation into Wenzel's equation happens. The equation 2.6 suggests that a multilayered roughness is more appropriate for a hierarchical surface that is morphologically similar to the natural SHSs [43]. This

14

confers that both the roughness and morphology of a surface are possibly responsible for controlling the wetting properties of a solid surface.

Thus, all the theoretical wetting models are correct up to a certain extent but not appropriate for exclusively reciting the wetting behaviour of solid surfaces. To have thorough knowledge about the wetting of solid surfaces further investigation is required.

2.1.6. CONTACT ANGLE HYSTERESIS

To define an SHS, the accurate measurement of both the static CA and CA hysteresis is required. A steady SHS must exhibit highest possible immobile CA with smallest possible CA hysteresis, otherwise the attained wetting state can transfer to another state. The procedure espoused for the measurement of CA also responsible for different values of CA [44]. Some most commonly used methods for the CA measurement are Laplace-Young fitting, circle fitting, ellipse fitting and tangent fitting etc (Fig. 2.4). Thus, to compare the CA and to realize the actual wetting scenario of a surface, the CA measurement method must be clearly stated.
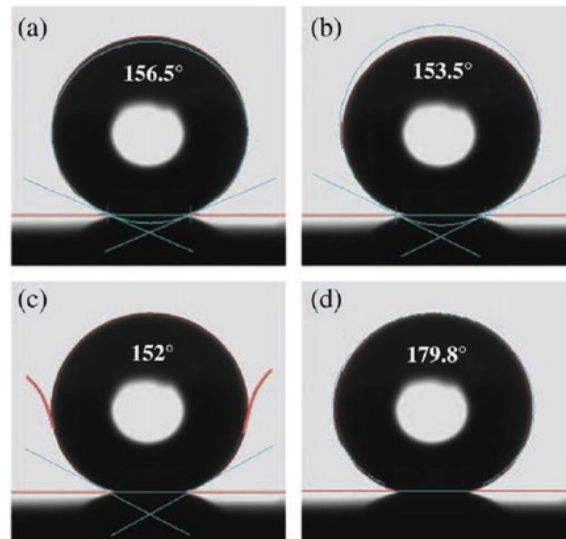
Fig. 2.4 Different CAs measured by different fitting approaches for the same waterdrop such as (a) ellipse (b), circle (c), tangent and (d) Laplace−Young fitting [44].

15

Generally, the CA hysteresis is described by two means. Firstly, the water droplet will move toward the lower side and regress toward the upper side (Fig. 2.5), if the solid surface is inclined at an angle θ_D known as the tilting or slipping or SA [45]. For rolling off a water drop, the solid surface should be inclined at some angle known as the tilting angle. In such a situation, the water droplet wets the solid surface towards the advancement of the droplet and de-wets the surface at the regressing side. Therefore, θ_A is defined as the advancing angle and θ_R is defined as the receding angle. Both the advancing and receding CAs remain unchanged throughout the sliding of liquid droplet until the no variation in surrounding conditions.
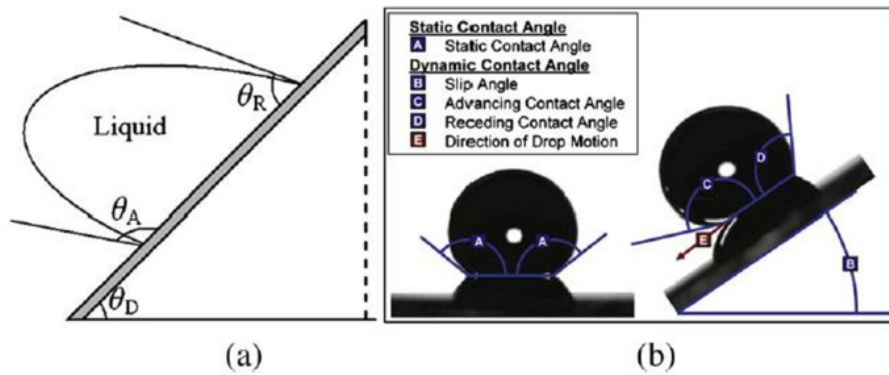
Fig. 2.5 (a) A schematic illustration of uniform sliding of a liquid drop at a declination angle of θ_D with an advancing angle of θ_A and a receding angle of θ_R. (b) The graphic representation of static and dynamic CAs [45].

Secondly, if water from the droplet lying on a solid substrate is sucked slowly via a syringe then the volume of water drop and its contact will reduce without affecting its contact area on the substrate until it starts to regress (Fig. 2.6). Correspondingly, if the water is added slowly to the liquid droplet via a syringe then the volume of water drop and its contact will increase without affecting its contact area on the substrate until it starts to advance (Fig. 2.6). Therefore, when the liquid drop

16

advances, the CA is known as the advancing angle (θ_A) and when liquid droplet regresses, the CA is known as the receding angle (θ_R).
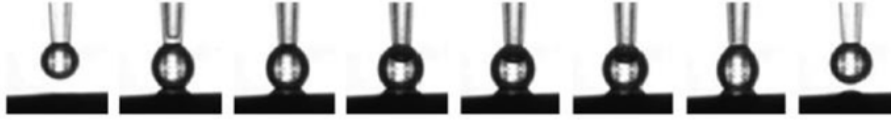
Fig. 2.6 The optical images of the growth and shrinkage of a liquid drop on a solid substrate [46].

Therefore, the difference between θ_A and θ_R angles are defined as the CA hysteresis [46]. According to some reports, the CA hysteresis lies within 5° [47] that hardly affect the superhydrophobic properties of a solid substrate. But, but in some cases the CA hysteresis is quite high such as 40° [48], that can significantly alter the superhydrophobic properties of a solid substrate. Thus, it can be inferred that both the immobile CA and CA hysteresis are equally important to describe the wetting behaviour of a solid substrate.

2.2. CONSTRAINTS OF SUPERHYDROPHOBIC SURFACES

Over the past few decades, many researchers have been describing the astounding water repellent nature of SHSs as well as materials. However, at present, there are many concerns need to address to develop commercial products based on the SHCs or SHS [49]. The major concerns are described below:

1. **Expensive superhydrophobic materials:** The starting materials required for the synthesis of SHCs and surfaces are quite expensive. The process obligatory for the growth of micro as well as nanostructural features on a surface to convert it superhydrophobic are expensive. For instance, in early times, photolithography process and the process employed to produce superhydrophobic micro and nanostructure surfaces were very costly [50]. Eventually, the overall amount and

17

performance can be excessively high, if we combine the fact that photolithography process produces small chip dies at nanoscale for covering significant area.

2. **Nano feature durability:** For achieving an exceptional SHC, high water CA mandatory. Therefore, it is necessary to have a low energy surface based on the water-repelling chemistry consisting durable micron as well as nano-sized topographical features. Usually, it is little tricky to achieve all these difficult experimental parameters simultaneously. For example at nano-scale, some polymers consisting nano-textural feature behave like 'wet noodles'. Such polymer strings i.e. 'wet noodles' entangled down with ease and therefore stop behaving like an SHS [51]. Therefore, the durability of the developed micron as well as nano-sized topographical features to obtain superhydrophobicity of a surface is one of the major concerns.

3. **Coating stability:** The utilization of a good quality superhydrophobic material such as nano-silica (nano SiO_2) does not pledge that during its chemical or physical bonding with the solid substrate it will not lose its superhydrophobic properties. Because a strong bonding between the superhydrophobic nanoparticle and the substrate leads the detoriation of the superhydrophobicity of the nanomaterial. Such situation signifies that an appropriate balance is required to develop a stable SHC because both the superhydrophobicity and stability of that coating are complementary to each other [52].

4. **Precipitation/condensation problem:** It is well-known that the SHCs and surfaces are water repellent, instead of this feature they are not water vapour repellent. The SHC in such an environment where the temperature is well below the dew point then condensation happen on the coating. Due to the condensation, a significant wetting of SHC happens to force the coating to lose its water-repellent behaviour [53].

5. **Impact problem:** The trapped layer of air generated while fabricating SHSs can be easily decreased and also eradicated by confined high-pressure water jets. The above operation usually performed via two approaches either using a confined

creek of water or using surface erosion underwater. Since the superhydrophobicity of a surface has been simply a surface effect and any crucial surface impingement fabricate faulty superhydrophobicity at the impact site [54].

6. **Emulsifier/oil wetting problem:** Superhydrophobicity of a surface is the outcome of amplified surface tension of a water droplet. When the surface tension of a water droplet is significantly abridged using an emulsifier or oil then the solid surface can be easily wetted because of the eradication of superhydrophobic behaviour of the surface [55].

2.3. SUPERHYDROPHOBIC COATINGS: FABRICATION TECHNIQUES

Usually, water repellent surfaces are recognized by two things, first by micro or nano roughness and second by complicated morphology. The other important feature is repeating of multi-scaled roughness, pin down as nano projections of micro-level morphology. Therefore, for the development of the above mentioned facets on pseudo surfaces, the following fabrication techniques can be utilized. In the following sub-sections, some most commonly used SHS fabrication techniques are described along with their advantages and disadvantages.

2.3.1. ELECTROCHEMICAL DEPOSITION

Various methods were used in the past to tune the roughness and morphology of surfaces. However, the electrochemical deposition method is one of the most promising methods because it purposes a facile control over the surface feature growth-kinetics and provides an easy way to create various morphologies over large size surfaces. Actually, the electrochemical processes are facile, fast and reproducible. Additionally, these processes can be used to produce a variety of morphological objects such as tubes, needles, dendrites, fibres, sheets etc [56]. Numerous processing techniques come under electrochemical deposition such as anodic oxidation, deposition using galvanic cells, polymerization and electrochemical anodization etc. which are commonly utilized for the production of SHSs/coatings [56]. However, such methods are costly and cannot provide

transparent SHCs due to the involvement of metals and generally produce SHCs for corrosion resistance of metals and alloys. A typical schematic diagram based on an electrodeposition process to produce SHC is shown in Fig. 2.7 [57]. Zhang et al. [57] reported the use of one-step electrodeposition process to generate corrosion-resistant SHC on Al metal substrate.
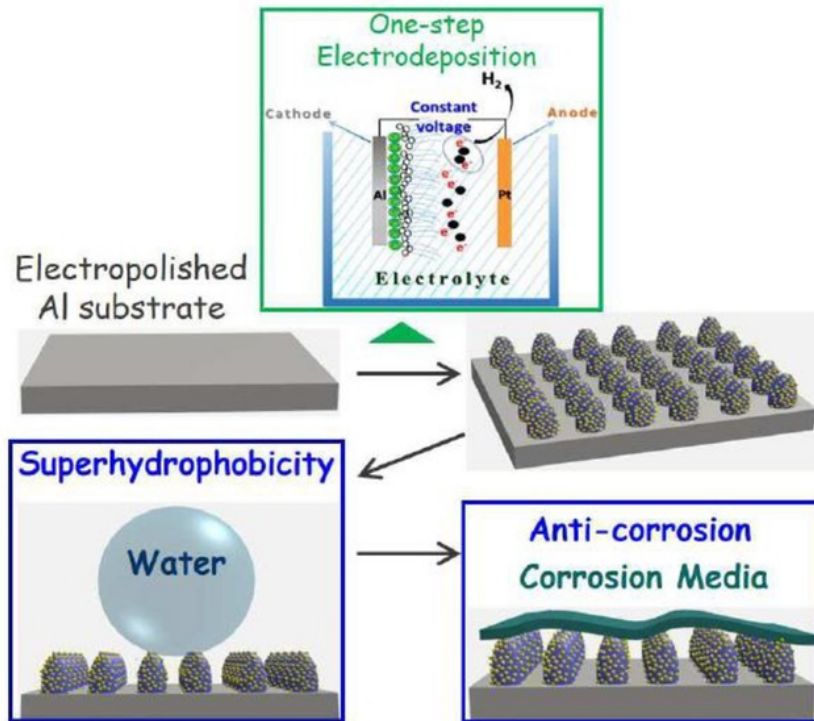
Fig. 2.7 Schematic diagram of an electrodeposition process to produce SHC [57].

He et al. [58] reported a method named as electrochemical anodization route to synthesize different types of ZnO nanostructures on the large area by employing chemicals like methanol electrolyte and the mixed hydrofluoric acid. Within one hour, according to their experimental, they obtained different types of nanostructures like ZnO nanoflowers, nanodots and nanowires. They obtained these nano-structures by having good control on reaction times and also on concentration of the electrolyte. They further reported that after applying the electric field on the fabricated ZnO nano-structure coatings, there will be a change

20

in the wettability of the surface, and this change is responsible for generating surface defective sites on the coating.

Meng et al. [59] succeeded in producing fascinating extremely repellent to water and oil SHSs. They have used metals like aluminium, iron, zinc, and nickel and their alloys like brass and Zn-Fe alloy. They obtained textured rough surface on different substrates via an electrochemical reaction using perfluoro-carboxylic acid solutions. To obtain SHSs of varying roughness, they controlled the concentration, chain length, as well as the reaction process time of perfluoro-carboxylic acid solutions. The developed surfaces reveal superamphiphobicity owing to the synergetic role of surface configuration and morphological features. The SEM micrographs of electrochemical process derived superamphiphobic coatings revealed petal-kind nanosheets spreading all-over the surface (Fig. 2.8a). The petal-kind structures having a thickness varying from 30 nm to a few hundreds of nanometers with micron-level height and length. The inset of Fig. 2.8(a) shows the magnified image of petal-kind structures. Optical images of the CA scenario of water droplets and oil drops sitting on the fabricated coatings (Fig. 2.8b and c) exhibited outstanding water as well as oil repellency.
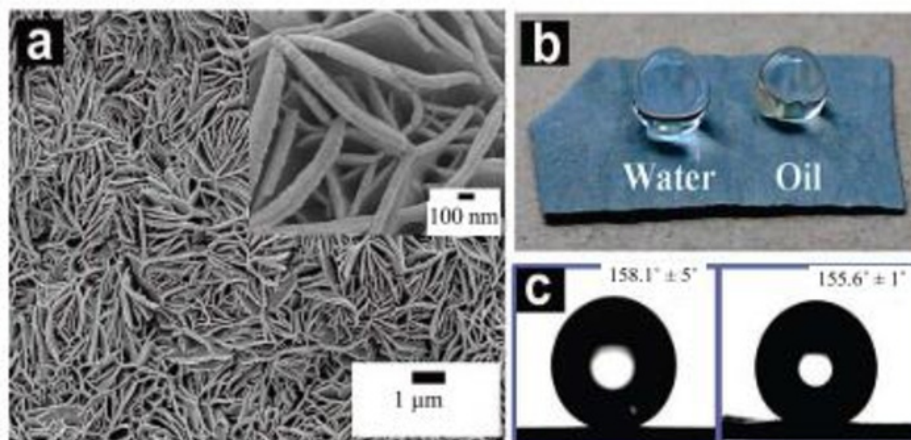
Fig. 2.8 (a) SEM micrograph of the fabricated petal-kind structure surface and the inset is showing a high-magnification micrograph. (b) Optical images of the CA scenario of water droplets and oil drops sitting on the fabricated coatings (c) CA of water drop (left side) and oil drop (right side) [59].

21

2.3.2. ELECTRO-SPINNING AND ELECTRO-SPRAYING

Electro-spinning is one of the simplest and most useful technique to yield continuous polymeric strings with diameters lying in the range of micrometres to nanometers [60] that can be accumulated to develop surfaces having characteristic surface roughness [61]. Electro-spinning is a protrusion technique in which electrical biasing is provided through the protrusion nozzle and a stranded gathering plate. Though electro-spraying technique is analogous to electro-spinning and used to produce films ranging between globules and strings. Usually, electro-spinning is related to fibres and electro-spraying is related to globules [62]. These methods are not very expensive but it is difficult to develop large scale SHCs. However, transparent SHCs can be obtained using electro-spraying route instead of electro-spinning method. The schematic diagrams of electro-spinning and electro-spraying process are shown in Fig. 2.9 and Fig. 2.10 respectively.
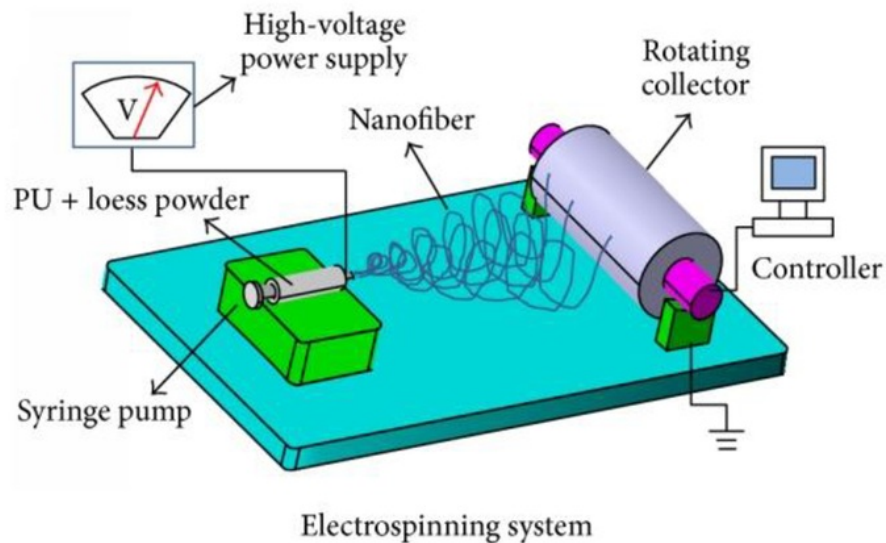
Fig. 2.9 Schematic illustration of an electro-spinning system [63].

22
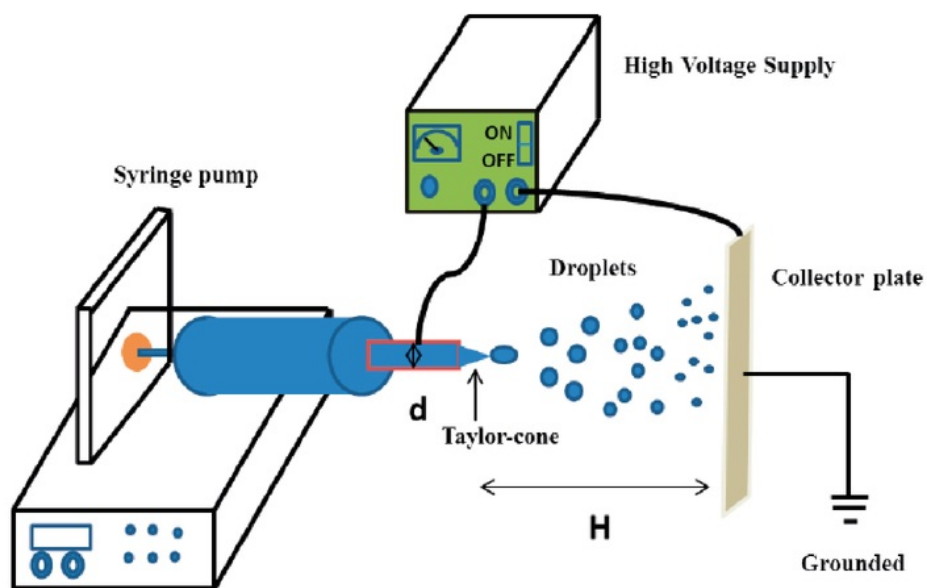
Fig. 2.10 Schematic illustration of an electro-spraying system [64].

Ding et al. described the construction of SHS via electro-spinning technique [65]. They prepared the SHS based on nanofibrous ZnO. They developed the SHS by electro-spinning the poly(vinyl alcohol) and poly(vinyl alcohol)/zinc acetate solutions followed by the calcination process which yields fibrous zinc oxide superhydrophobic films. The wetting properties of the fibrous films were further altered by applying a coating of a low surface energy material fluoroalkylsilane using hexane. They claimed that the super-hydrophilic ZnO fibrous films (CA ~ 0°) were transformed into super-hydrophobic films (CA ~ 165°) due to the surface functionalizing agent coating onto the fibrous films. Fig. 2.11 shows the FESEM micrographs of the super-hydrophilic ZnO fibrous films with CA ~ 0° and super-hydrophobic ZnO fibrous films with CA ~ 165°.
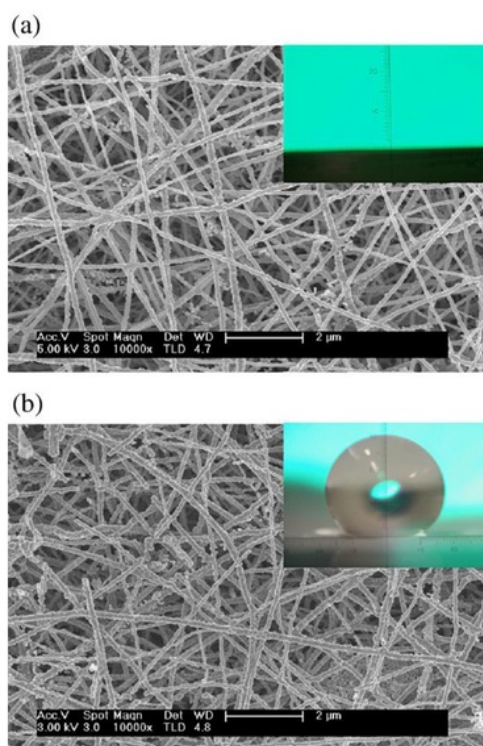
Fig. 2.11 FESEM micrographs of (a) the super-hydrophilic ZnO fibrous films with CA ~ 0° and (b) super-hydrophobic films ZnO fibrous films with CA ~ 165° [65].

Burkarter et al. [7] reported the preparation of polytetrafluoroethylene based SHCs on F-doped tin oxide deposited glass substrate via an electro-spraying method. The results indicate that during the heating of the glass substrate up to 150 °C, the solvent used for the synthesis of SHC assist the evaporation of water when it comes in close contact with the substrate. Different times varying from 30 s to 20 min were tried for the coating deposition based on a specific configuration. The polytetrafluoroethylene based coating on the F-doped tin oxide deposited glass substrates reveal hydrophilicity. Due to the hydrophilic character, the substrates can wet effortlessly and leads the floating of the coating on substrate because of the wetting. The heating of the coated substrates in open atmosphere at 265 °C removed all the wetting agents and finally results in the highest CA of ~160° with a sliding/rolling off angle about ~ 2°. Fig. 2.12 shows the SEM image of electro-

sprayed polytetrafluoroethylene with a deposition time of 20 min and the inset on the top left of the image is showing the optical image of water droplet on the SHC.
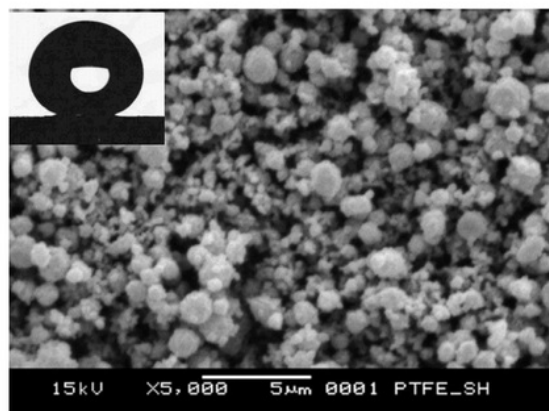
Fig. 2.12 SEM image of electro-sprayed polytetrafluoroethylene with a deposition time of 20 min and the inset on the top left of the image is showing the optical image of the water droplet on the SHC [7].

2.3.3. CHEMICAL VAPOR DEPOSITION (CVD)

CVD is a well-known highly effective technique to fabricate SHCs. In this technique, gaseous substances or elements usually deposited onto a solid substrate to fabricate non-volatile solid coatings/films. CVD is a highly competent and frequently used method to grow variety of nanostructures such nanotubes, nanoparticles, nanofibers, nanocombs, nanorods, nanobeads etc. But, the major problem with CVD is that large size samples difficult to obtain and also it is an expensive synthesis process.

Cai et al. [66] demonstrated the fabrication of transparent and hollow superhydrophobic films/coatings with advantageous features such as excellent thermal stability and good moisture inhibition. They prepared superhydrophobic films utilizing a template (candle soot) and CVD of methyltrimethoxysilane followed by calcination at 450 ℃. They optimized the deposition time with respect to the transparency and superhydrophobicity of the films. They obtained the high transmittance about 90% with CA more than 165º and SA about 2º for the developed superhydrophobic films. Additionally, the films demonstrated excellent

25

thermal stability and good moisture inhibition even after calcination up to 500 °C. The schematic diagram for the synthesis of transparent superhydrophobic hollow films by CVD is shown in Fig. 2.13.
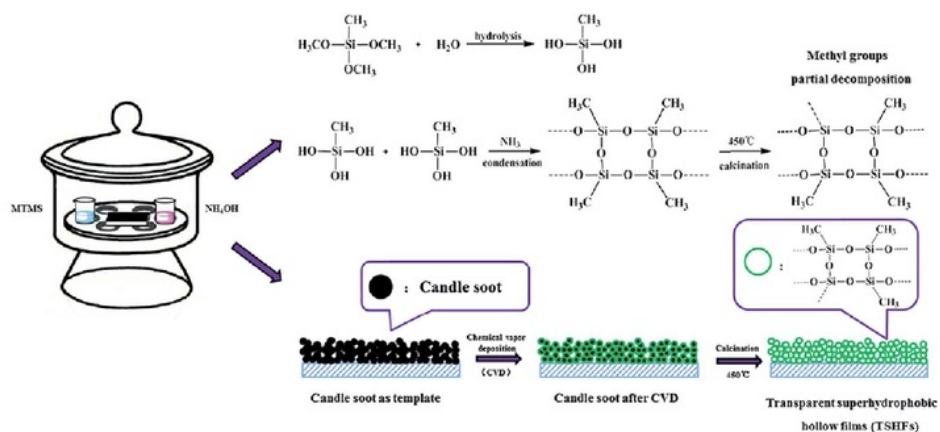
Fig. 2.13 The schematic illustration of the synthesis of transparent superhydrophobic hollow films by CVD [66].

Hozumi et al. [67] reported the modification of active wetting behaviour of an oxidized Al and Ti surface via CVD of 1,3,5,7-tetramethylcyclotetrasiloxane. By changing the control temperature of CVD process, the hydrophilic Al and Ti surfaces were converted to the SHSs. Water droplets on the developed superhydrophobic surfaces roll off quite easily when the specimen surfaces were tilted gently.

Hsieh et al. [68] synthesized fabricated a highly water repellant carbon fabric containing micro and nano-scaled roughness. To synthesize superhydrophobic carbon fabric, carbon nanotubes were deposited onto micron-sized carbon fibres via a catalyst based CVD method followed by fluorination of the surface. The average size of carbon nanotubes about 20-40 nm was deposited onto arranged carbon fibres having diameter in the range of 8-10 μm. The water CA considerably enhanced from ~ 148° to ~ 170° due to the presence of carbon nanotubes over the arranged carbon fibres. Fig. 2.14 shows the optical images of water drops scenario

26

for (a) the pristine carbon fabric, (b) fluorine treated fabric and (c) fluorine treated fabric consisting combination of micro and nano-scale roughness.

Fig. 2.14 Optical images of water drop scenario for (a) the pristine carbon fabric, (b) fluorine treated fabric and (c) fluorine treated fabric consisting combination of micro and nano-scale roughness.

2.3.4. LAYER-BY-LAYER (LBL) DEPOSITION

The LBL method is one of the preferred methods to produce a variety of micro-scale, nano-scale structures and SHCs [56]. The LBL is a periodic technique that creates a fine layer of a charged material by adsorbing it onto a solid/semi-solid substrate. Successive layers can be deposited on the top of another layer consisting opposite charge material and lead to the formation of a multilayer consisting single structure having thickness of the nano-level. The repetition of layer-by-layer deposition can be done periodically to obtain the anticipated thickness of the coating. To control the wetting behaviour of LBL deposited coatings, nanostructures can be introduced during the deposition to enhance the roughness of the coatings. The main merit of LBL technique is the perfect thickness control of the film/coating as well as its perfectness over the synthesis of highly transparent

coatings/films especially on odd/complex surfaces [56]. The major disadvantage of this technique is time-consuming and applicable for limited materials.

Syed et al. [69] reported the fabrication of corrosion-resistant SHCs by LBL deposition technique. They used an LBL and spin coating method jointly to produce polyaniline-tetramethylsilane modified silica nanoparticles based superhydrophobic corrosion-resistant coating. The specimens with odd surface were found hydrophobic whereas, the specimens with even surface revealed hydrophilicity. The maximum water CA was about 153° with a SA about 6° with a variation about ± 2°. The anti-corrosion status of the fabricated coatings was found stable up to 240 h. Fig. 2.15 illustrates the schematic diagram of the fabrication of polyaniline-silica composite (PSC) and functionalization of silica nanoparticles by tetramethylsilane (TMS-SiO$_2$) and the synthesis of Poly-diallyl-dimethyl-ammoniumchloride (PDDA)/PSC and PSC/ TMS-SiO$_2$ composite multi-layers.
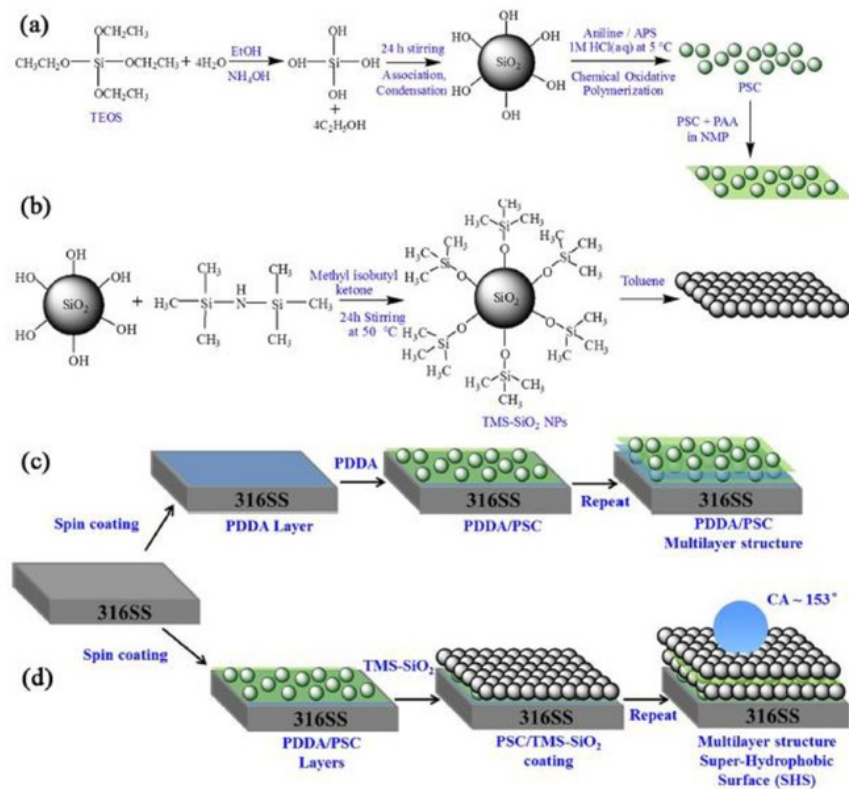
Fig. 2.15 Schematic diagram of the fabrication of polyaniline-silica composite (PSC) and functionalization of silica nanoparticles by tetramethylsilane (TMS-SiO_2) and the synthesis of Poly-diallyl-dimethyl-ammoniumchloride (PDDA)/PSC and PSC/ TMS-SiO_2 composite multi-layers [69].

Zao et al. [70] produced superhydrophobic cotton fabrics using electro-static LBL approach by assembling polyelectrolyte and nano-size SiO_2 particle multi-layers onto cotton fabrics and later on treated the fibres with fluoroalkylsilane (Fig. 2.16). The morphological features of coated fabrics were modified by varying the multi-layers number during LBL deposition. Though a high CA about more than 150˚ was achieved using 1-3 multi-layers, the coated fabrics revealed tacky behaviour due to the SA more than 45˚. However, the 5 multi-layers of polyelectrolyte and nano-size SiO_2 particle on cotton fabrics exhibit smooth superhydrophobic character with a SA < 10˚.
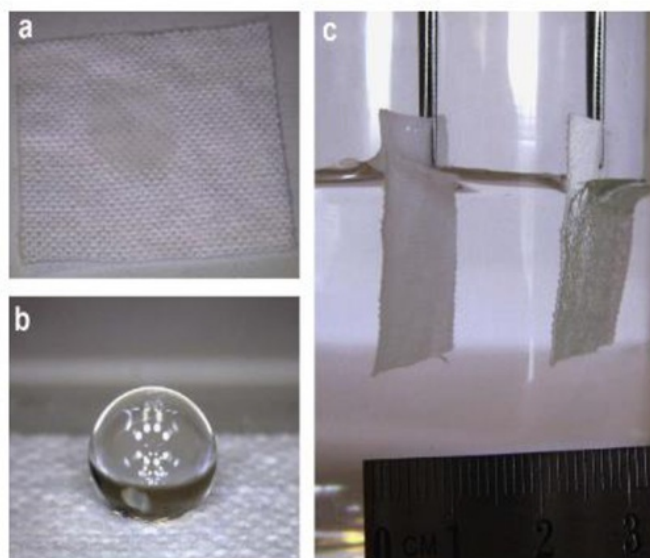
Fig. 2.16 Optical images of water droplets on (a) pristine cotton fabrics, (b) superhydrophobic fabrics coated with nanoparticles consisting multi-layers and (c) pristine (left side) and superhydrophobic (right side) cotton-fabric engrossed in water [70].

2.3.5. WET-CHEMICAL METHOD

Wet-chemical coating is one of the simplest industrially espousal method because it offers the use of multiple materials for large-level production of ordered SHCs. But, the major issue with this method is the use of harmful surface etching chemicals.

Qi et al. [71] reported the fabrication of a wafer-level chemical etching assisted superhydrophobic and anti-reflective silicon-based surface. They used KOH and silver-catalytic etching to fabricate pyramid-like ordered nanostructures on a silicon wafer followed by fluorination of the surface that presents superhydrophobicity along with anti-reflection character. Maximum water CA of 169° with a roll-off angle < 3° was obtained. On similar track, monoalkyl-phosphonic acid was utilized to generate reliable SHS on Ni metal using a wet chemical route [72]. Flower-like micron-level structures were steadily generated owing to a chemical reaction leading to an incessant slipcover. Fig. 2.17 shows the cross-sectional view of SEM image of (a) silicon wafer revealing pyramid-like structure due to etching by KOH and (b) ordered structures on silicon wafer created by Ag-derived etching.
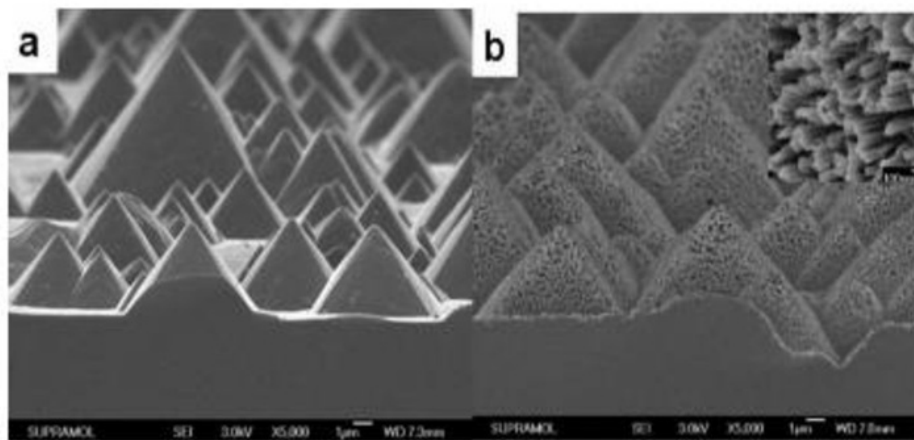
Fig. 2.17 Cross-sectional view of SEM image of (a) silicon wafer revealing pyramid-like structure due to etching by KOH and (b) ordered structures on silicon wafer created by Ag-derived etching [71].

30

Wang et al. [73] produced a flower-kind SHC on pristine Mg metal via chemical etching using H_2O_2, H_2SO_4, ethanol and stearic acid. They obtained the highest CA of 154° with a roll-off angle of 3°. The developed coating also exhibits 4 times enhancement in the resistance of SHS compared to pristine Mg when immersed for 1 h in sodium chloride solution.

Pan et al. [74] fabricated a stable superhydrophobic rough surface by HNO_3 and cetyltrimethyl ammonium bromide etching of copper wafer followed by ultrasonication functionalization of the surface by 1H,1H,2H,2H-perfluorodecyltriethoxysilane. Etching action caused the generation of spherical micro-pits on the surface due which the rough surface not only showed the superhydrophobicity towards water but also for corrosive liquid.

2.3.6. PHASE SEPARATION TECHNIQUE

Phase separation technique is one of the facile and cheap routes to fabricate superhydrophobic mesoporous polymer membranes. It is useful for only limited materials. Khoo et al. [75] reported the fabrication of nanostructures of different shape, size and morphology via phase separation technique. They used methyltrichlorosilane for phase separation and created nanostructures on silica and glass substrates. Morphological features of the synthesized nanostructures mainly governed by the concentration of methyltrichlorosilane, humidity, temperature and reaction time. Because of the controlled reaction conditions the nano-architectures in form of nano-fibres and nano-spheres of varying diameter evolved, which exhibits superhydrophobicity.

Yang et al. [76] reported a facile phase separation route to produce anti-corrosion superhydrophobic polyvinyl-chloride coatings for an Mg alloy (AZ91D). They obtained a low surface energy rough surface using simple phase separation route. Maximum CA > 150° with outstanding corrosion resistance as well as good adhesion of the coating was obtained. A schematic illustration of synthesis of superhydrophobic polyvinyl-chloride coatings for Mg alloy (AZ91D) is shown in Fig. 2.18. Ethanol content was varied in polyvinyl-chloride and tetrahydrofuran

solution mixture in order to control roughness, structure and superhydrophobicity of the coating. In the final stage of processing, ethanol and tetrahydrofuran were evaporated and resulted in the creation of pores into the coating and it was realized that the pore size and their distribution changed the surface roughness and hydrophobicity of the developed surface.
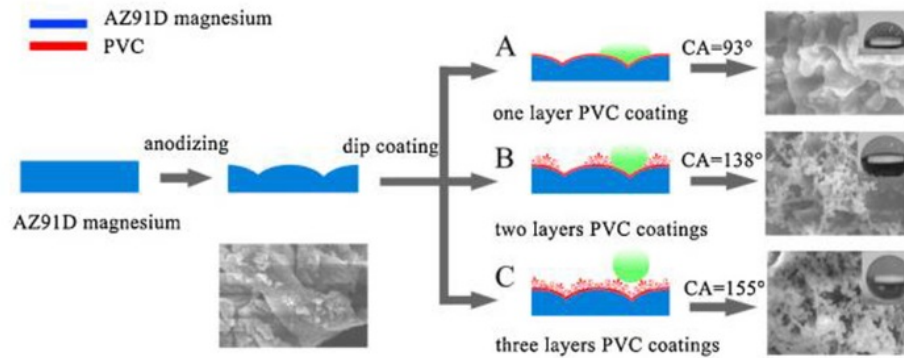
Fig. 2.18 Schematic illustration of the synthesis of superhydrophobic polyvinyl-chloride coatings for Mg alloy (AZ91D) [76].

Song et al. [77] reported the advanced method of fabrication 3,6-O- ditertbutyldimethyl silyl chitosan polymer. Additionally, they used the same polymer to synthesize robust SHCs via a facile and cost-effective phase separation technique. They produced excellent hydrophobicity for the complete range of pH by generating three-level arranged roughness on the surface of the films.

2.3.7. IMPRINTING TECHNIQUE

Traditional imprinting method can be utilized to generate SHSs that generally consists of a master and a replica as is the case of lithography as well as templating techniques. These techniques can be used in two ways, one as an individual and another including some other processing technique to reduce the intricacy of the synthesis technique. Pozzato et al. [78] reported the synthesis of SHSs on silicon via a nano-imprint lithography technique followed by wet chemical etching. Glass made shapes were utilized to imprint a photoresist coating. The remaining

unwanted portion of the coating after imprinting was detached via exposing it to UV-light and following the fabrication of the photoresist. Then protected hydrofluoric acid etching was performed on the synthesized pattern to shift it to a reedy SiO_2 layer followed by anisotropic etching by wet chemical method using KOH and shifting the layer to silicon. Subsequently, hydrophobic octadecyltriclorosilane coating was deposited to obtain the superhydrophobic properties. They achieved a maximum CA of 167°. The synthesis of SHSs on silicon via a nano-imprint lithography technique followed by wet chemical etching is schematically shown in Fig. 2.19.
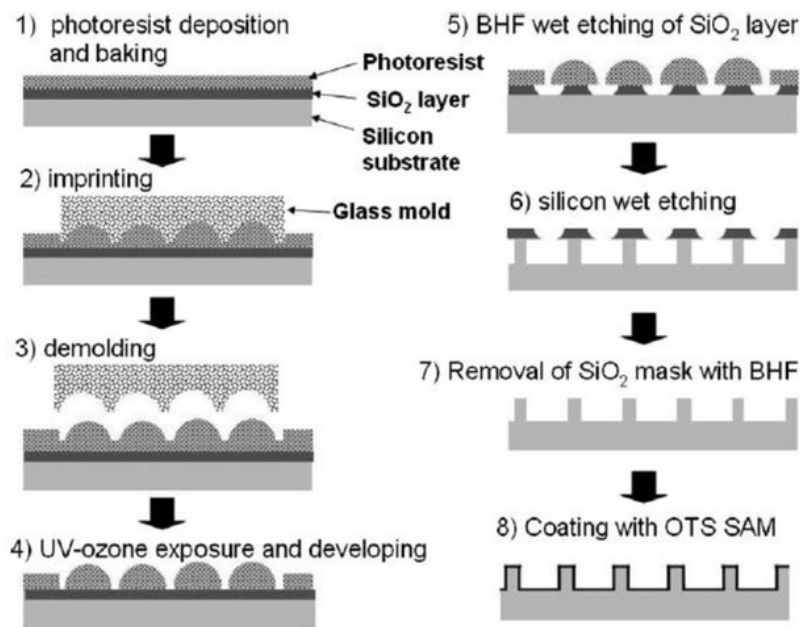
Fig. 2.19 The schematic diagram of the synthesis of SHSs on silicon via a nano-imprint lithography technique followed by wet chemical etching [78].

2.3.8. LITHOGRAPHY TECHNIQUE

Lithography technique is based on the replication of master information. This technique can provide a precise replica contingent on the desired product. Such techniques basically classified into subclasses based on the type of the system utilized such as type of substrate and power source etc. The main types of

lithography techniques are photolithography or optical lithography, soft lithography, X-rays lithography, electron-beam lithography and nano lithography etc. Each lithography technique has certain merits and demerits.

Yang et al. [79] reported the fabrication a strong, light and flexible superhydrophobic polyvinyl butyral/SiO$_2$ coatings for a wood substrate including the concept of petals of a red rose. SHCs were prepared using a combination of nanoimprint lithography and solvothermal routes. The fabricated coatings revealed vigorous superhydrophobicity with a high water CA of about 160° including outstanding thermal stability and durability. Moreover, the fabricated coating exhibited high buoyancy. Fig. 2.20 shows the schematic diagram of the reproduction route of polydimethylsiloxane impression of petals of a red rose and synthesis method of superhydrophobic polyvinyl butyral/SiO$_2$ coatings for wood.
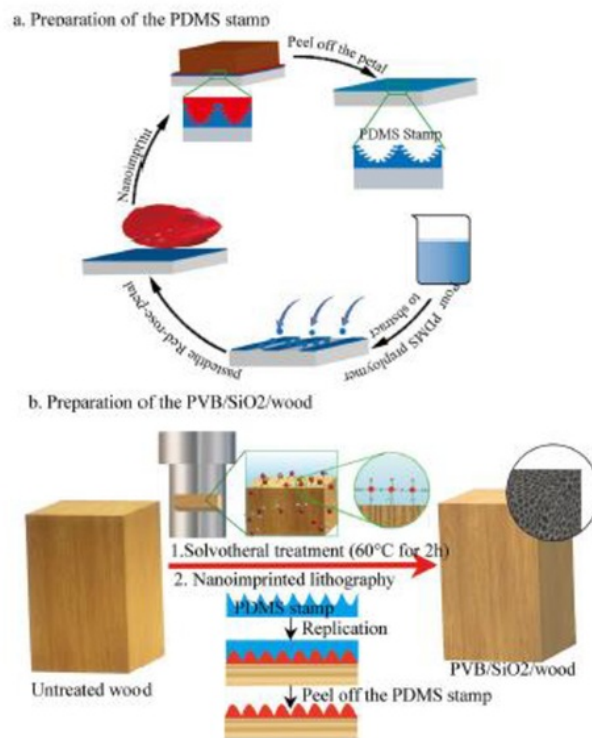
Fig. 2.20 Schematic diagram of (a) the reproduction route of polydimethylsiloxane impression of petals of a red rose and (b) synthesis method of superhydrophobic polyvinyl butyral/SiO$_2$ coatings for wood [79].

2.3.9. TEMPLATING TECHNIQUE

Fundamentally, the templating method is analogous to the moulding method of fabrication. This method uses a master template then using molds, a replica can be prepared and later on it can be detached from the molds to obtain the desired surfaces. This technique is economical but time-consuming and applicable for limited materials.

Chen et al. [80] reported the synthesis of transparent SHC consisting of hollow SiO_2 spherical particles via carbon templating method. The schematic diagram of the synthesis route of transparent SHC is shown in Fig. 2.21. The developed coating was further treated by 3-aminopropyldiethoxymethylsilane to lower down the surface energy of the coating. The raspberry kind structure of silica porous capsules leads to the superhydrophobic character of the coating and further calcination of that coating results in the high transparency.
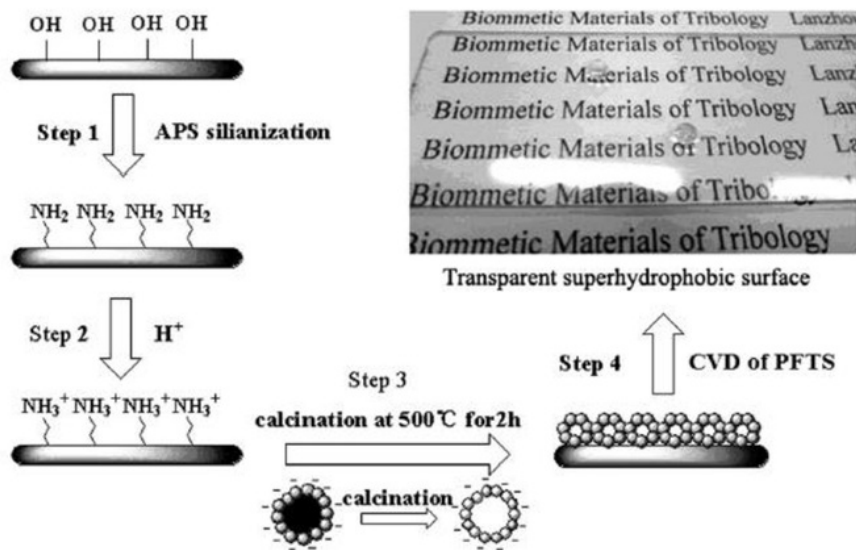
Fig. 2.21 The schematic diagram of the synthesis route of transparent SHC [80].

2.3.10. HYDROTHERMAL METHOD

Hydrothermal technique is a cost-effective, reproducible and eco-friendly technique for the production of nonstructural feature on variety of metal substrates via in-situ synthesis process. The growth of nanostructures on metal substrates via

such method is very effective for trapping the air by increasing the surface roughness at nano-level.

Yuan et al. [81] reported the synthesis of an SHC on electroless Ni–P coated AZ61 Mg-alloy using hydrothermal technique followed by immersion of the coating in stearic acid to enhance self-cleaning and corrosion-resistant properties of it. The coated Ni-P substrate alone was hydrophilic in nature, however, the substrate was transformed into superhydrophobic one via hydrothermal method. The control parameters of hydrothermal technique such as time and temperature significantly affected the surface morphology and superhydrophobicity of the substrates. At high temperature during hydrothermal process created the petal-like nanofilms which exhibited better wetting properties than the lemongrass-kind nanofilms at low temperature during the processing. The maximum water CA of ~ 155.6º with a roll-off angle of 2º were obtained for the developed SHCs at controlled temperature for a specific time-oriented hydrothermal reaction. Additionally, the coatings exhibited superior corrosion-resistant performance. The schematic illustration of synthesis of an SHC on electroless Ni–P coated AZ61 Mg-alloy using hydrothermal technique is shown in Fig. 2.22.
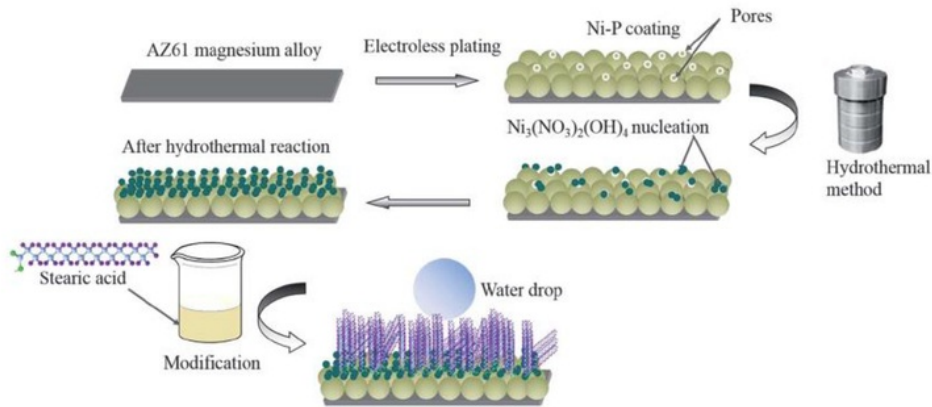
Fig. 2.22 The schematic illustration of the synthesis of an SHC on electroless Ni–P coated AZ61 Mg-alloy using hydrothermal technique [81].

2.3.11. SOL-GEL ROUTE

The sol-gel route is a facile, cost-effective, commercially acceptable, fast, low temperature operated and eco-friendly technique for the production of a variety of nanostructure with numerous morphological features, bulk nanomaterials and SHCs/films. It is one of the most preferred methods to develop good quality coatings/films with thickness of the order of few microns and it is analogous to the physical-deposition routes up to certain extent. The sol-gel route have some demerits like precise thickness control and cracking issue with the deposited films due to heat-treatments of the films. To deposit a film or coating of a sol-gel processed material on various substrates, generally three routes have been followed such as spray-coating, spin-coating and dip-coating.

Singh et al. [82] reported the synthesis of superhydrophobic and photocatalytic active coating on cotton fabrics using a sol-gel route followed by dip-coating. The SHCs were synthesized using in-situ prepared poly-triethoxyvinylsilane and polydimethylsiloxane followed by AgBr coating/film to obtain the photocatalytic activity. The coated fabrics revealed self-cleaning, superhydrophobicity and superoleophilicity respectively. The maximum water CA about 154° with a water roll-off angle of about 8° along with lubricant CA of about 0° were obtained for the coated fabrics. Additionally, the coated fabrics revealed its effectiveness for the separation of mixtures of oil and water even up to ten filtration cycles. Furthermore, the coated fabrics revealed its durability in various acids, alkalines, salt-solutions, etc. Fig. 2.23 shows the schematic diagram of the synthesis of superhydrophobic fabrics by sol-gel route.

Zhang et al. [83] reported the use of a sol-gel technique to fabricate thin coatings/films of organically altered silicates (SiO_2 nanoparticles with an average size of 24 nm). The condensation of tetraethylorthosilicate and dimethyldiethoxysilane leads the attachment of methyl groups of hydrophobic nature with the deposited films followed by further treatment of the surface with variety of silane groups to obtain the superhydrophobicity. The small size of nanoparticles found quite useful for developing anti-reflective coatings because of
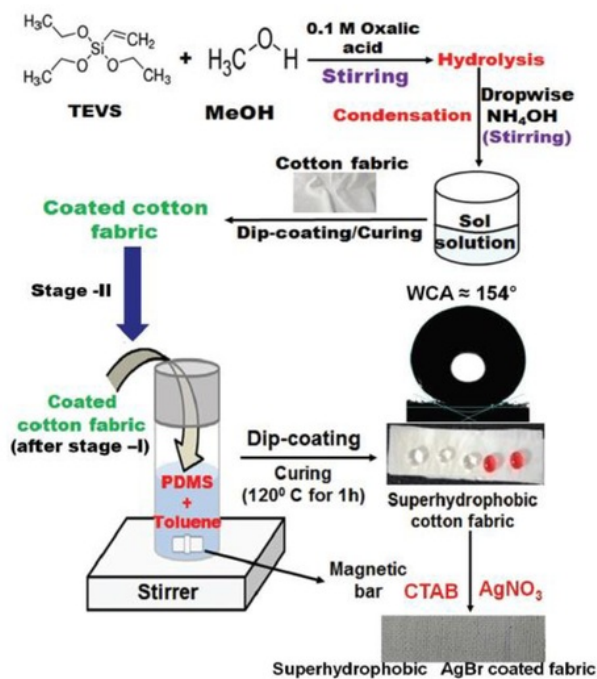
Fig. 2.23 Schematic diagram of the synthesis of superhydrophobic fabrics by sol-gel route [82].
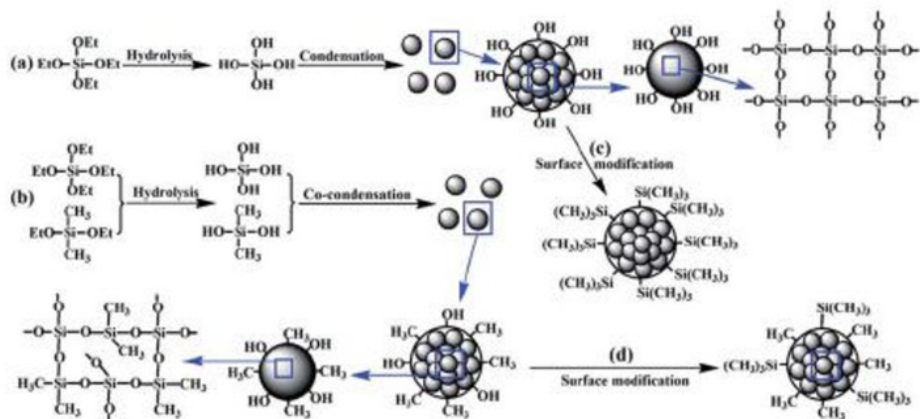
Fig. 2.24 A graphic illustration of (a) synthesis method of SiO_2 nanoparticles (b) organically altered silicates nanoparticles from tetraethylorthosilicate and dimethyldiethoxysilane and (c and d) hexamethylisilazane altered nanoparticles [83].

negligible light scattering. Additionally, the developed SHCs exhibited a high transmittance of about 99.5% with outstanding environmental resistance. Fig. 2.24 shows a graphic illustration of (a) synthesis method of SiO_2 nanoparticles (b) organically altered silicates nanoparticles from tetraethylorthosilicate and dimethyldiethoxysilane and (c and d) hexamethylisilazane altered nanoparticles.

2.4. APPLICATIONS OF SUPERHYDROPHOBIC COATINGS

The SHCs/films/surfaces exhibit tremendous applications in different sectors, especially in energy-related fields. Some potential applications of SHSs such as anti-corrosion, anti-freezing, anti-frosting, anti-icing for photovoltaic cells, aeroplanes, ships, power lines, anti-friction for submarines, self-cleaning of solar panels, glass windows etc. are shown in Fig. 2.25 [84].

Fig. 2.25 The potential applications of SHCs/films/surfaces [84].

2.5. DIGITAL IMAGE PROCESSING

Digital image processing practices commenced at the starting of 1970. Image processing in its starting was found useful in various sectors such as astronomy, remote Earth resources interpretations and medical imaging. It is a way to transform an image into digital information that can be operated according to the requirement such as to obtain an improved image and extraction of valuable information. In this technique, the image act as the input and image characteristics acts as an output [85]. It treats images as 2D (2-dimensional) signals or inputs to process them using well-known signal dispensing routes. An arithmetical tactic designates a surface through image-statistics that reveal non-deterministic characteristics of three-dimensional dissemination of image signal. The features of an image are denoted as pixels. Even a grey colour image is not just black and white image but it consists of various shades of a gray colour. MATLAB is a powerful tool for image processing because it consists of an image processing toolbox that encompasses a broad range of customary algorithms. Using MATLAB, one can easily perform various things such as image segmentation, image enhancement, image analysis, geometric transformations noise reduction, and image registration, etc. Pattern analysis is a sub-domain of image processing technique [85]. The basic stages of an image processing method are shown in Fig.2.26.
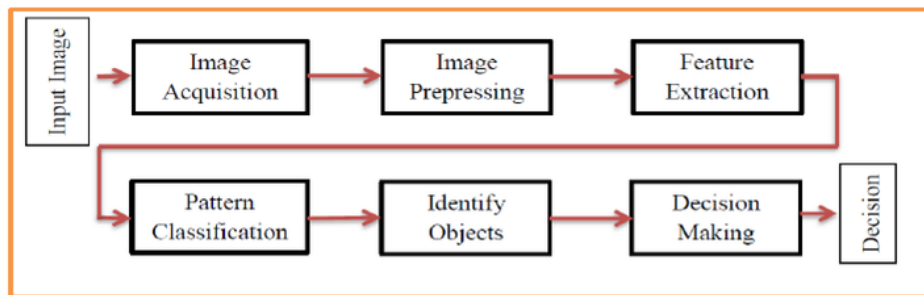
Fig. 2.26 Image processing method [85].

2.6. PATTERN ANALYSIS

Pattern recognition (or analysis) is a division of machine learning applied directly to recognize the regularities and pattern of the data. The idea of machine learning

is employed for statistical pattern recognition and regulates in the data. The machine learning approach is classified in two approaches: (1) supervised learning, which trains a model on identified input and output data so that it can expect future outputs, and (2) unsupervised learning, which finds hidden patterns to develop predictive model based on input and output data or intrinsic structures in input data [86], [87].

2.6.1. SUPERVISED LEARNING

In supervised learning, the prior information is available about the class of subset of data. The pattern recognition systems are trained from labelled training data. It builds the model to make the predictions based on the evidence available for uncertainty. The supervised learning algorithms are applied for known set of input-output data, which we are trying to predict and get the response of new data. Supervised learning follows classification and regression methods to develop predictive models.

2.6.2. UNSUPERVISED LEARNING

The unsupervised learning is based on the unlabeled instances, and all the classes are inferred from the unstructured input dataset. The learning technique is applicable to find out hidden patterns in data of unlabeled input data and draw the inferences from datasets consisting of unknown values. The method follows the clustering technique to set the unlabeled samples constructed on similar distance measurement. This technique is explicitly for data analysis to get groupings or hidden patterns in data. The general algorithms for clustering methods are K-means or K- Medoids, Fuzzy C means Gaussian Matrix Model, Neural networks, Hidden Markov models and self-organizing maps etc [88], [89].

2.7. K-MEANS CLUSTERING

K-means clustering is known to the society since 1970 and works much better compared to other well-known clustering-algorithms such as expectation-

41

maximization based on density algorithm. K-means clustering is facile route for image processing including image-segmentation as well as image-annotation. K-means clustering is used for clustering of minor pixel spots of images and then epitomize those images in form of cluster-centres and replicate this process much time to create a "deep" linkage of image-features. Based on this concept, it provides much better results compared to other clustering algorithms. It is at present the inbuilt part of various standard software's. It needs the fixing of cluster number prior to the analysis and it depends on the starting parameters including the selected distance. It can be started by selecting random K values of the images.

In a very recent study, Maw et al. [90] reported the image grouping by uniting K-means clustering algorithm plus deep learning method. Initially, the K-means clustering algorithm was applied for the image processing to deal with numerous disparities in forefront as well as background images acting as inputs. This preprocessing of the images promotes the accomplishment of better accuracy. Then to categorize, colour, size, shape and image location in the standard database, 2D (2-dimensional) deep learning method was applied to obtain outstanding outputs.

Hameed et al. [91] reported the estimation of surface roughness utilizing large scale SEM (scanning electron microscopy) images via image processing route. The surface roughness study based on SEM images (large scale) was performed with the help of AFM (atomic force microscopy) images (small scale) of Tin oxide (SnO_2) coatings of different thickness such as 450 nm, 525 nm and 600 nm deposited onto glass slides prepared by a thermal evaporation method. Various scales 1 to 50 μm zoomed SEM images of the coatings were selected for the analysis. First the surface roughness of the coatings was determined using AFM images and then SEM images were used for the determination of the surface roughness which was validated with the AFM data.

Similarly, many other researchers reported the importance of image processing for analyzing various parameters or features of different materials by utilizing SEM and AFM images. Arzate-Vázquez et al. [92] described the estimation of porosity of calcified chicken-eggshells utilizing AFM images via an image processing

technique. Zhao et al. [93] in a very recent study described the study of coal as well as shale pore structure including surface roughness utilizing AFM images via image processing method. In another study Zhang et al. [94] reported the image processing of SEM images of PP/rice-husk composite via MATLAB. Fig. 2.27 shows the SEM image of PP/rice-husk composite (left image) and MATLAB processed image of the same composite (right image).
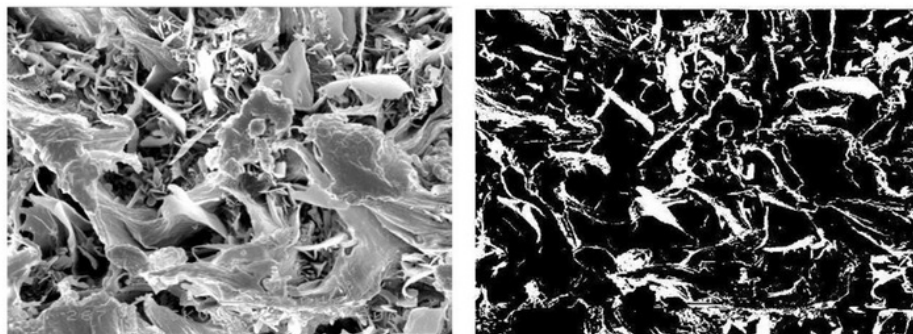
Fig. 2.27 SEM image of PP/rice-husk composite (left image) and MATLAB processed image of the same composite (right image) [94].

2.8. SUMMARY

In this work, the fundamentals of superhydrophobicity are described in detail. Surface tension and surface free energy are the key parameters to control the wetting properties of a material. To develop transparent SHCs or films nano-roughness due to the introduction of nanoparticles must lie in the range of 1-100 nm to avoid the scattering of the incident light. For SHCs, the water CA must lie in the range of 150-180° with a sliding or roll off angle as small as possible up to 0°. All over the world, plenty of methods by choosing a variety of nanomaterials have been tried out to obtain SHCs due to their tremendous applications in various industrial sectors. The major constraints to the development of SHCs have been also described in detail. Further, the SHCs are highly desired for energy applications such as self-cleaning, anti-icing, anti-fogging applications for solar panels. The best-identified practices for the development of transparent SHCs are based on nanoparticles (e.g., ZnO, SiO_2, TiO_2, etc.) embedded polymer coatings

prepared via an industrial scale acceptable techniques such as sol-gel method. Additionally, digital image processing can assist in a great manner to understand the important features of SHCs. In image processing, the pattern analysis approach via unsupervised learning using K-means clustering technique is a powerful method to study the surface features of SHCs. MATLAB is a powerful tool to apply the K-means clustering on SEM or AFM images to determine the various parameters of the SHSs more precisely and quite helpful for understanding the basic mechanisms of the superhydrophobicity.

CHAPTER 3. EXPERIMENTAL

3.1. RESEARCH METHODOLOGY

3.1.1. SOL-GEL

Sol-gel route was employed to synthesize nanoparticles that consist of transformation of precursors (starting material) into a sol (colloidal suspension). The sol then after slow heating at low temperature converted into a gel-like network comprising particles and polymer networks. This route mainly consists of four steps such as hydrolysis, condensation, nucleation (or growth) and gel formation. The key benefits of this method are low-temperature processing, precise control overgrown nanoparticle size, easy to cast in complex forms of specimens , easy to control quality of the final product with minimal impurities. The sol-gel route is a facile, robust, cost-effective, less toxic and eco-friendly technique to produce various nanostructures as well as SHCs.

The surface of the synthesized nanoparticles was then modified using various functionalizing agents and then introduced in the host matrix to develop transparent SHCs. The transparency and superhydrophobicity of the prepared coatings were optimized by controlling the various parameters including nanoparticle concentration, size and type as well as process control parameters.

For the preparation of SHCs on glass substrates (or slides), two well-known routes were employed such as spin-coating and dip-coating.

3.1.2. SPIN-COATING

In the spin-coating method, surface-functionalized nanoparticle embedded host polymer was dissolved in a solution.

Only a few drops of that solution was deliberately poured on the vacuum stuck glass substrate for its rotation at high speed for a specified time to uniformly spread the solution by centrifugal force as shown in Fig. 3.1. By keeping the sample at room temperature for few minutes the evaporation of the solvent can be accomplished so that a thin and uniform coating is obtained. The control parameters of the spin-coating route such as rotation speed, viscosity of the solvent, rotation time, etc. were optimized prior to the preparation of transparent SHCs.

3.1.3. DIP-COATING

In the dip-coating method, surface-functionalized nanoparticle embedded host polymer was dissolved in a solution. Then the glass substrate on which coating is desired gradually dipped into the solution and removed from the solution at a controlled rate as shown in Fig. 3.2. Then the coated substrate was allowed to dry at room temperature by solvent evaporation and a thin and uniform coating was obtained. These steps can be repeated several times to increase the thickness of the coating. Again the transparency and superhydrophobicity of the coatings were optimized by controlling the thickness of deposited coatings, nanoparticle concentration, type and functionalizing agent type and concentration including the dipping and withdrawal speed of the substrate from the solution. Generally, dip-coating method based coating thickness is higher than the thickness of the coating obtained by spin-coating method with same solution.
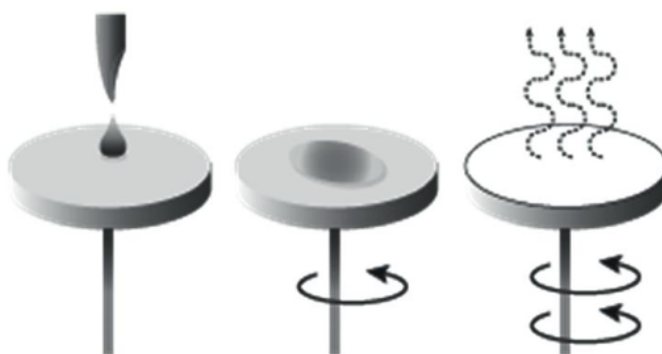
Fig. 3.1 Schematic diagram of the spin-coating method.
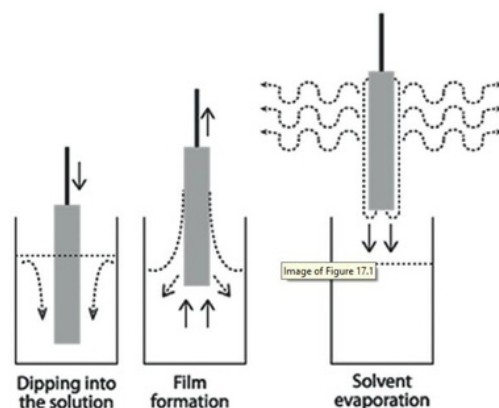
Fig. 3.2 Schematic diagram of the dip-coating method.

3.2. MATERIALS

The following materials were used for the preparation of transparent SHCs.

- Polystyrene (PS, Mw ~ 35,000)

- Chlorotrimethylsilane (TMCS, molecular weight, Mw ~ 108.64)

- 3-mercaptopropyltrimethoxysilane (MPMS, Mw ~ 196.34)

- Triethoxyoctylsilane (TEOS)

- SiO2 nanoparticles (APS ~ 25 nm)*

- ZnO nanoparticles (APS ~ 50 nm) synthesized by Zinc acetate $(Zn(O_2CCH_3)_2)$.

- Ethanol

- Tetrahydrofuran (THF, Mw ~ 72.11)

- Glass substrate

All the chemicals were obtained from Sigma Aldrich Company Branch, India.

*Procured from Reinste Nano Ventures, Pvt. Ltd., India.

3.3. CHARACTERIZATION TECHNIQUES

3.3.1. XRD

X-ray diffraction (XRD) is a powerful advanced instrument that uses characteristics X-rays to obtain the diffraction pattern of a material that can be interpreted to identify a particular phase of a material that is based on the crystallography of the material. XRD can reveal the difference between amorphous and crystalline materials, but meaningful information can be extracted from the crystalline materials. The XRD spectra of the crystalline materials generate sharp peaks, the peak position against 2 theta angle and their intensity are used to extract the data of the materials. The X-ray diffraction follows on the well-known principle of Bragg's law. Phase identification of the nano-powders can be made easily using Cu-Kα radiation source having wavelength of 1.54 Å. Usually, slow scanning of the samples performed for the accuracy in results. A typical XRD instrument is shown in Fig. 3.3.

Fig. 3.3 A typical XRD instrument

3.3.2. FESEM

FESEM is abbreviated as Field Emission Scanning Electron Microscope. It works with electrons which are liberated by a field emission source as compared to light. Finally, the desired Object scanned by electrons in a zig-zag pattern. It visualizes extremely small (nearly 1 nanometer or 1 billion of a millimetre) topographic details on the surface. It can be used for studying like nanostructures, synthetic polymers, thin-film or coating on microchips and organelles and many more. FESEM employs a focused beam of electrons to produce an image and also to analyze the specimen. A typical FESEM instrument with accessories is shown in Fig. 3.4.

Fig. 3.4 A typical FESEM instrument with accessories.

The principle of electron microscope is similar to light microscope but the difference is light microscope using visible light as a source and electron microscope using very energetic electrons as a source. Nevertheless, in optical microscope, the resolution is limited by its wavelength as compared to energetic or accelerated electrons having very short wavelength. Due to this reason it's possible to see very small features at very high magnification with a great resolution.

3.3.3. FTIR

FTIR abbreviated as Fourier Transform Infra-Red, preferable technique of IR spectroscopy (infrared spectroscopy). Since seven decades Infrared spectroscopy has been a magnificent method to analyze materials in laboratory. Infrared spectroscopy technique represents a fingerprint or distinguished identifying characteristic of a sample in the form of absorption peaks. The IR peaks appear because of the vibrational frequencies of typical bonds of atoms or molecules of a material. As every material is made up of atoms/molecules so no two compounds generate exactly similar IR spectrum. Hence, IR results qualitative identification or analysis of any type of material and the size of the peak demonstrates the amount of material present. In present software algorithm, IR becomes a high-quality tool for positive identification or quantitative analysis. A typical FTIR instrument with accessories is shown in Fig. 3.5.
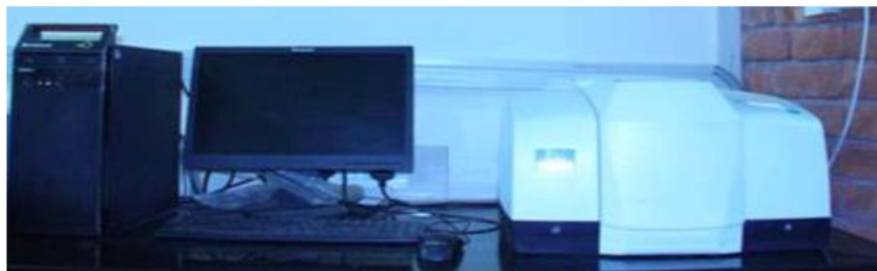
Fig. 3.5 A typical FTIR instrument with accessories.

3.3.4. ZETA SIZER

Zeta sizer is an advanced instrument that can characterize a broad range of particles from nano-level to micron-level. The condition is the particles must be in almost spherical in shape. For the characterization of particles, initially particles are dispersed in aqueous or non-aqueous solutions and then using dynamic light scattering concept the average size of the particles can be estimated.

The Zetasizer instrument is capable to measure some important attributes of molecules or particles in liquid medium such as molecular weight, Zeta potential and particle size. These parameters can be measured over a wide range of

concentration by employing the technology within Zeta-sizer system. A typical Nano-Zeta sizer or particle sizer is shown Fig. 3.6.

Fig. 3.6 A typical Nano-Zeta sizer or particle sizer.

3.3.5. AFM

It is abbreviated as Atomic force microscope (AFM). It is one kind of scanning probe microscope. Scanning probe microscopes are designed for measuring properties like friction, height as well as magnetism with the help of a probe. For acquiring topographical images of samples, the SPM raster scans the probe over the sample and simultaneously measure its properties. Resolution of a typical AFM is of the order few nanometers. The advantage of AFM is it can take images of various surfaces like polymers, composites, ceramics, biological samples, glass and many more. The AFM broadly works in three modes such as contact mode, non-contact mode and tapping mode. Van der Wall's forces play a major role in the working of an AFM. For delicate materials such as polymers or polymer coatings, the most preferred operating mode of AFM is the tapping mode in which the AFM tip vibrates close to the sample surface or taps the sample surface gently without

degrading it and helps in acquiring the images using standard image processing tools. AFM provides 3 D topographical images of the samples with a high resolution via raster scanning of the sample surface. A table-top AFM instrument is shown in Fig. 3.7.
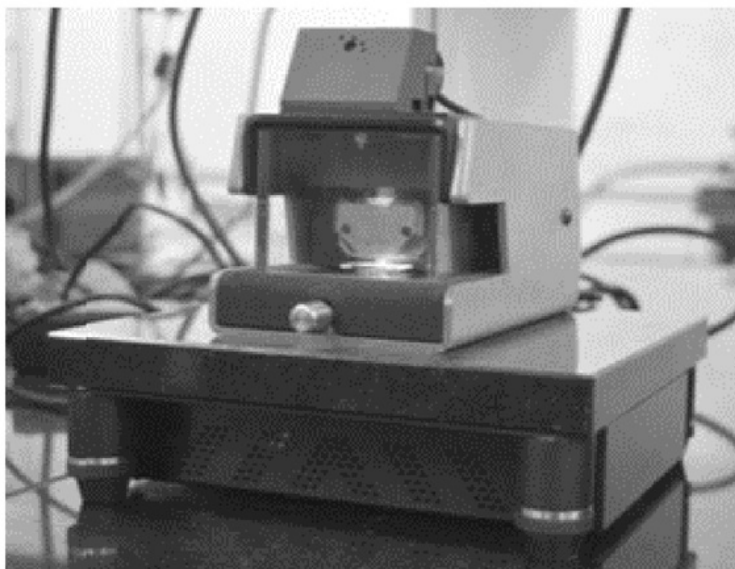
Fig. 3.7 A table-top AFM instrument.

3.3.6. DROP SHAPE ANALYZER

The wetting properties of a material can be studied using CA goniometry or drop shape analyzer. Drop shape analyzer can measure the following important parameters such as wettability of any solid materials (e.g., plastic, glass, ceramic, paper, wood, etc.). The drop shape analyzer can measure the static, advancing and receding CAs, roll-off angles on hydrophobic and SHSs. It can measure the surface tension and liquid-liquid interfacial tension using the Pendant drop method. The wetting properties depends on the CA between the solid surface and the liquid droplet. Along with the CA, CA hysteresis study is also required due to the presence of physical and chemical inhomogeneity on the surface for the complete understanding of the wetting properties of a material. A typical drop shape analyzer instrument is shown in Fig. 3.8.

52

Fig. 3.8 A typical drop shape analyzer instrument.

3.3.7. UV/VIS SPECTROMETER

Ultraviolet-visible (UV/VIS) spectroscopy is an absorption or transmission spectroscopy in the ultraviolet partial and the complete visible-light regions. It implies that light is used in the visible as well as in adjacent ranges. In recognition of the colour of the chemicals involved in the process are greatly affected by the absorption or reflectance. In this range of the electromagnetic spectrum, molecules and atoms go through electronic transitions. Absorption spectroscopy and fluorescence spectroscopy are complementary to each other. The absorption spectroscopy determines ground-state to the excited-state transitions whereas fluorescence spectroscopy estimates excited-state to ground-state transitions. The UV/VIS spectroscopy needs an excitation wavelength to characterize a material. It can characterize the materials in liquid form as well as solid form such as coatings. This is very useful technique for determination of the transmittance of the coatings. A UV/VIS spectroscopy instrument is shown in Fig. 3.9.

Fig. 3.9 An UV/VIS spectroscopy instrument.

3.4. PATTERN ANALYSIS

FESEM images were used for extracting the surface roughness information using pattern analysis via machine learning tools. Various FESEM images of the SHCs were selected for the pattern analysis. The average surface roughness and exact surface roughness of the FESEM images were estimated using supervised and unsupervised machine learning methods. The methodology of the pattern analysis was based on the steps starting process of the FESEM images, image pre-processing, image segmentation, image feature extraction, image analysis and score prediction via machine learning approach. The image analysis was performed using K-means clustering approach. The FESEM images provided exaggeration in three dimensions: x, y and z. The FESEM images always need image processing before optimal inspection of the surface structures. The inbuilt libraries of MATLAB tool were used to process the FESEM images and different constructs of all levels of image processing to score prediction. The image segmentation was performed using inbuilt 2D and 3D HAAR (square-shaped function) Discrete Wavelet Transform (DWT) processing tools. Initially, the images were loaded into the library, changed to a grey level image, resized, segmented and processed using wavelets. The MATLAB mathematical morphology-based algorithm was applied

54

for carrying the image sub-operations like closing, opening, erosion and dilation. The MATLAB tool predicted the roughness of the SHSs via K-means algorithm including % error, simulation time and total simulation time parameters, etc.

CHAPTER 4. SYNTHESIS OF NANO-TEXTURED POLYSTYRENE/ZNO COATINGS WITH EXCELLENT TRANSPARENCY AND SUPERHYDROPHOBICITY

4.1. ABSTRACT

Transparent superhydrophobic polystyrene/ZnO nanocoating, possessing an average roughness of 28 nm and high CA (> 150º) has been synthesized through a modified facile sol-gel route. The anticipated hierarchical roughness of the coating was obtained using dual functionalized ZnO nanoparticles. Chlorotrimethylsilane and 3-mercaptopropyltrimethoxy silane were espoused as nanoparticle surface functionalizing agents to generate SHC. The effect of experimental parameters on transparency and superhydrophobicity of developed coatings was examined to obtain optimum conditions. Such developed coatings can prove to have substantial industrial applications.

4.2. INTRODUCTION

Transparency of a substrate is a vital feature for coating in industrial applications. Transparent substrates with numerous surface characteristics like superhydrophilic (CA, CA $\leq 5°$), hydrophilic ($5º < $ CA $\leq 90°$), hydrophobic ($90° < $ CA $< 150º$) and superhydrophobic (CA $\geq 150°$), surfaces have been fabricated by organic and inorganic hybrid materials [95]. These substrates have been used extensively for various applications like solar cells, self-cleaning, anti-icing and anti-fogging coatings [23], [95], [96]. Various coating methods like spraying, spin coating, dip-coating, physical/chemical vapour deposition, etc. have been used for the preparation of transparent substrates [95], [97]–[99].

As the transparency and surface roughness of thin films are competitive, it is quite difficult to simultaneously synthesize superhydrophobic and transparent surfaces. Surface roughness is obligatory for SHSs which results in the scattering of light [100]. This scattering of light is responsible for blurring of SHSs [100]. Recent research on nanostructures filled polymer composites shows momentous potential in fabricating transparent and SHSs [101], [102]. Karunakaran et al. reported the synthesis of transparent superhydrophobic thin films SiO_2 nanoparticles [100]. Budunoglu et al. reported fabrication of highly transparent, flexible and thermally stable superhydrophobic films using functionalized silica aerogel materials [103]. Nakajima et al. fabricated transparent SHSs using titanium acetylacetonate and fluoro silane [104]. Xu et al. reported 95% of transparency with superhydrophobicity using fluorinated SiO_2 nanoparticles on silica wafer [105]. Fluorine based silane precursors have been extensively used to produce SHSs [106], [107]. As the polymers have better thermal and mechanical properties than the small molecule surfactants or functionalizing agents, thus they are generally chosen for SHS applications [108]. Polystyrene is a well-known commercially available transparent and hydrophobic polymer (water CA ~ 93º) [108], [109] with a glass transition temperature of ~ 100 ºC.

ZnO nanomaterial has gained significant research interest due to its low cost, abundance, wide bandgap semiconductor, eco-friendliness, chemical stability and thermal stability properties, which are used substantially for its catalytic, photo-electrochemical, optoelectronic properties etc. [110]. Recent reports indicate the possibility of conversion of intrinsically hydrophilic ZnO [111] surface into SHS [112]. Gongping et al. reported synthesis of hydrophobic nanoneedles and nanonails using hierarchical nanostructures of ZnO [113]. Fabrication of SHSs using ZnO nanomaterial is also reported from researches conducted by other groups [114].

The high cost of deposition techniques and various complex processing factors makes the fabrication of SHSs challenging. In the current study, a facile, low cost, modified sol-gel method has been employed to produce highly transparent

57

and superhydrophobic polystyrene/ZnO coating. This approach significantly reduces the processing parameters and deposition complexities compared to other deposition methods.

4.3. EXPERIMENTAL

ZnO nanoparticles were synthesized by sol-gel route. The detailed process has been described and discussed in our previously reported work [110]. The nanoparticles were initially functionalized by chlorotrimethylsilane (TMCS, molecular weight, Mw ~108.64) and later on functionalized using 3-mercaptopropyltrimethoxy silane (MPMS, Mw ~196.34). ZnO (1 g) was mixed with TMCS (0.025 mol) and then added to Ethanol (100 ml). The mixture was stirred with glass rod for five min followed by magnetic stirring for 15 min at 60 °C. The mixture was filtered and dried in vacuum at 30 °C for 24 h to obtain TMCS functionalized ZnO. The functionalized ZnO was further modified using 3-mercaptopropyltrimethoxy silane (MPMS) by following the work of Bach et. al [115]. The amount of MPMS was varied from 49 to 25 wt% for modification of TMCS functionalized ZnO as shown in Table 4.2. The resulting dual functionalized ZnO (1 to 25 wt%) was added to PS (50 wt%, Mw ~35,000) and tetrahydrofuran (THF, Mw ~72.11) followed by stirring of 30 min. The final mixture was spin-coated on glass substrate using 4000 rpm for 1 min to produce transparent and SHCs. All the reagents and chemicals were procured from Sigma Aldrich, India. The detailed procedure for dual functionalization of ZnO nanoparticles and fabrication of transparent and SHCs is illustrated in Fig. 4.1.

The morphology of nanopowder and deposited coatings was characterized by high-resolution scanning electron microscopy (FESEM, Quanta 200F, FEI, USA). X-ray diffraction (XRD) analysis was performed by Bruker D8 Advance Diffractometer (Germany) with Cu-Kα radiation. The size of nanoparticles before and after functionalization was measured by Zeta Sizer, (Nano-ZS, Malvern Inst. Inc., UK). Perkin Elmer Lambda 35 UV/VIS spectrometer was used to determine the transparency of coated substrates. Fourier transform infrared (FTIR) spectra of ZnO

and TMCS coated ZnO nanoparticles were recorded on Thermonicolet (Anexus) 1600 series. The morphology and root-mean-square (R_{rms}) roughness of ZnO/Polystyrene nanocomposite coatings were characterized by atomic force microscopy (AFM, NT-MDT, Ntegra) with tapping mode. The surface wettability of the coatings was investigated by drop shape analyzer (DSA 100, Krüss GmbH, Germany) at ambient conditions.
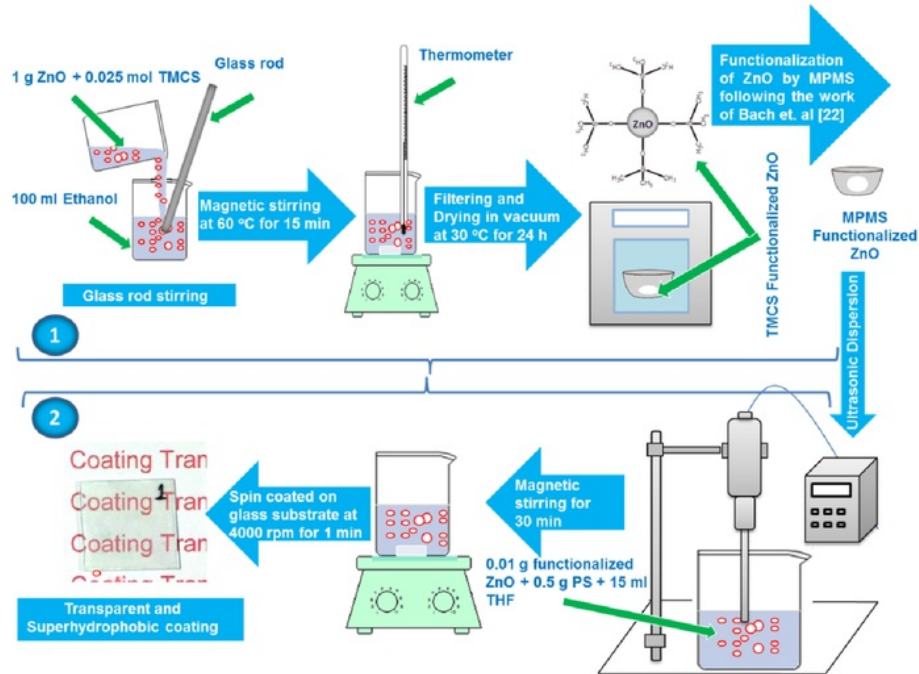
Fig. 4.1 (1) TMCS and MPMS-functionalization of ZnO nanoparticles and (2) fabrication of transparent and SHC.

4.4. RESULTS AND DISCUSSION

X-ray diffraction pattern of the ZnO nanopowder revealed the wurtzite structure (JCPDS: 21-1486) as shown in Fig. 4.2(a). The planes (hkil) were designated on intense diffraction peaks. The average size of ZnO nanoparticle was determined using the Scherrer formula [110]. The Scherrer formula is given in equation (4.1).

$$D= (K\lambda)/\beta' \times COS(\theta) \times 10 \qquad\qquad (4.1)$$

59

where β is the FWHM, K is a constant having value 0.9 & λ is the wavelength of radiation which is equal to 1.5418 Angstrom and D is the particle size in nanometer. The calculation of particle size along with (hkil) planes for the ZnO is illustrated in Table 4.1. It is noticed from Table 4.1 that there is not much variation in the particle size. The average ZnO particle size measured using Scherrer formula was about 36 nm.

Table 4.1. Calculation of ZnO particle size using Scherrer relation

S. No.	2θ (Deg.)	θ (Deg.)	θ (Rad.)	COS (θ)	β in (Deg.)	β' (Rad.)	D (nm)	d (hkil)
1.	31.695	15.848	0.277	0.962	0.224	0.0039	37	$10\bar{1}0$
2.	34.309	17.155	0.299	0.955	0.202	0.0035	41	0002
3.	36.302	18.151	0.317	0.950	0.228	0.0039	37	$10\bar{1}1$
4.	47.519	23.759	0.418	0.915	0.239	0.0042	36	$10\bar{1}2$
5.	55.577	27.789	0.485	0.885	0.279	0.0049	32	$11\bar{1}0$
6.	62.834	31.417	0.549	0.853	0.271	0.0047	34	$10\bar{1}3$
7.	66.351	33.176	0.579	0.837	0.191	0.0033	50	$20\bar{2}0$
8.	67.928	33.964	0.593	0.829	0.315	0.0055	30	$11\bar{2}2$
9.	69.058	34.529	0.603	0.824	0.321	0.0056	30	$20\bar{2}1$
10.	76.931	38.466	0.672	0.783	0.334	0.0058	30	$20\bar{2}0$

Zeta sizer analysis indicated 50 nm for pristine, 65 nm for TMCS-functionalized and 48 nm for MPMS-functionalized ZnO particles (Fig. 4.2b). Generally, the functionalization of the nanoparticle by any silane agent leads to increase in particle size few to tens of nanometer depending on the grafting density and molecular weight of the employed silane molecules [116], [117]. The increased size of functionalized nanoparticles is attributed to the adsorption of silane groups on the surface of ZnO nanoparticles. However, the size of MPMS-functionalized ZnO particles is less than the pristine nanoparticles. This may be because of significant

breaking of the clusters of nanoparticles due to dual functionalization. FESEM images of pristine ZnO and TMCS functionalized ZnO nanoparticles are shown in Fig. 4.2(c) and 4.2(d). FESEM images demonstrated the smooth surface of wheat like and round-shaped highly clustered nanoparticles. The average size of pristine ZnO nanoparticles estimated by FESEM images was about 45 nm. However, the TMCS functionalization reduced the degree of clustering of nanoparticles. The average size of functionalized nanoparticles estimated by FESEM images was about 62 nm. The average size of pristine and functionalized ZnO nanoparticles measured by FESEM and Zeta sizer found in good agreement.
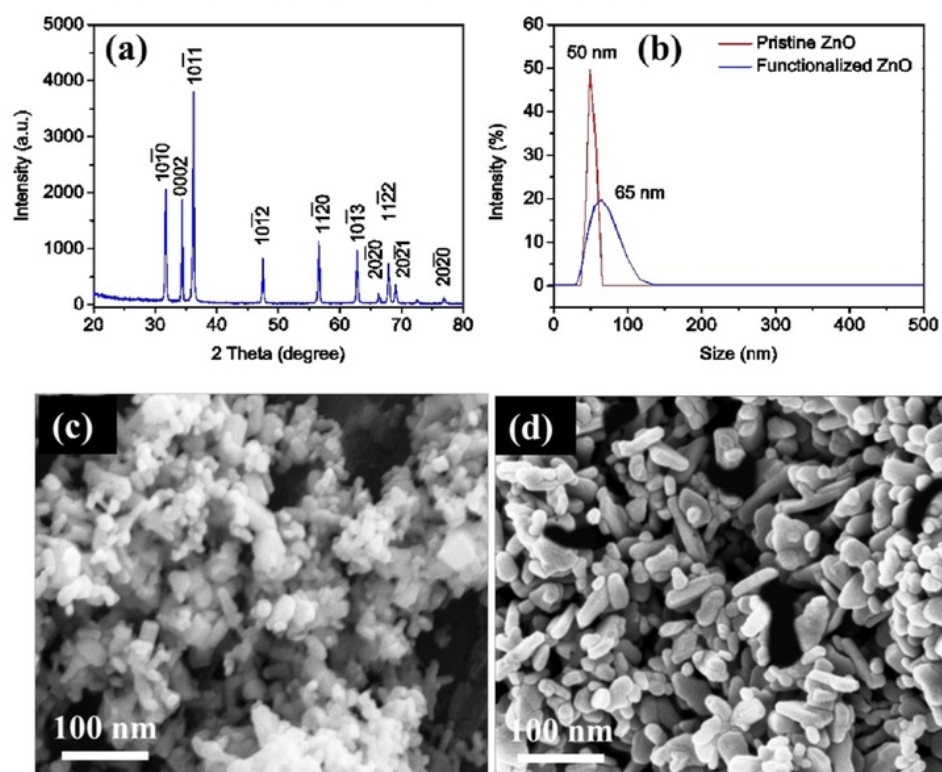
Fig. 4.2(a) X-ray diffraction pattern of pristine ZnO, (b) Zeta sizer curves of pristine and functionalized ZnO. FESEM images of (c) pristine ZnO and (d) TMCS functionalized ZnO.

61

In the present study, ZnO nanoparticles were reacted with TMCS in ethanol to replace hydroxyl groups on the nanoparticle surface by hydrophobic hydrocarbon chains. The surface modifying layer can efficiently avoid the uncontrolled agglomeration of particles [116], [117]. Additionally, the chances of enhancement in surface hydrophobicity of nanocomposites can be promoted [114]. Fig. 4.3 shows the FTIR spectra of chlorotrimethylsilane, pristine ZnO and TMCS modified ZnO nanoparticles. The small peak at 1611 cm^{-1} and the broadband at 3423 cm^{-1} are because of the ZnO–OH groups [118]. But, after the reaction with TMCS, very small peak at 2951 cm^{-1} appear, representing the existence of CH_2 groups [118], [119], Another absorption peak at 848 cm^{-1} is attributed to the Si-O vibration [120], which is found slightly shifted in case of TMCS functionalized nanoparticles. Thus, it confirms the presence of TMCS on the surface of modified ZnO nanoparticles. The appearance of an absorption peak around 2330 cm^{-1} corresponds to the CO_2. While a significant characteristic peak around 510 cm^{-1} corresponds to the ZnO structure.
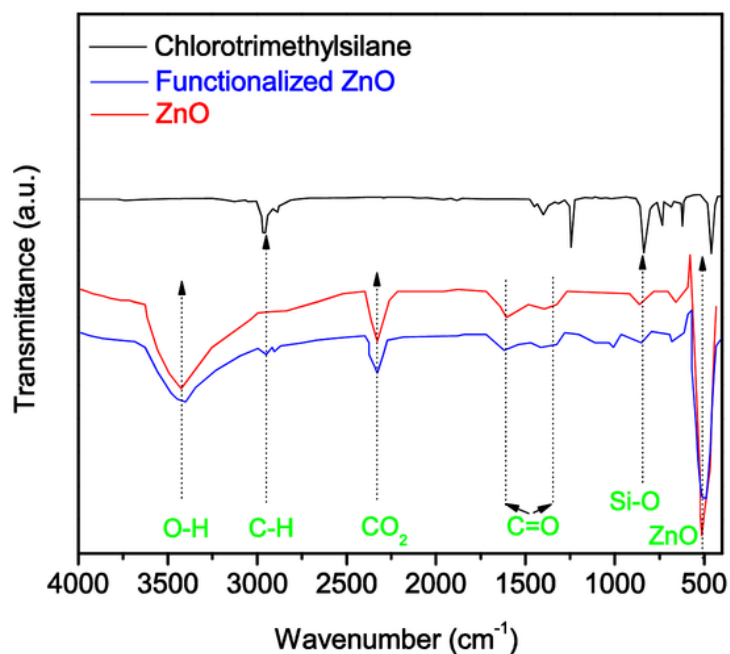
Fig. 4.3 FTIR spectra of pristine ZnO nanoparticles and TMCS functionalized ZnO nanoparticles.

62

Optimization of water CA with dual functionalized ZnO nanoparticles is summarized in Table 4.2.

Table 4.2 Optimization of water CA with ZnO and MPMS.

Sample Name	PS (wt%)	ZnO (wt%)	MPMS (wt%)	CA (°)		SA (°)
PS/ZnO-1	50	1	49	123		20
PS/ZnO-5	50	5	45	129		18
PS/ZnO-10	50	10	40	137		15
PS/ZnO-15	50	15	35	148		8
PS/ZnO-20	50	20	30	152		3
PS/ZnO-25	50	25	25	150		5

Initially, the concentration of MPMS was varied with respect to the nanoparticle content and then dual functionalized nanoparticle content was varied to yield polystyrene/ZnO coatings. The idea behind the selection of another surface functionalizing agent MPMS was to stop the further agglomeration of some unmodified ZnO nanoparticles. Because the FESEM images show that even after the functionalization of ZnO by TMCS, some clusters are still present (Fig. 4.2d). With the increase in chain length of the MPMS compared to TMCS, the possibility of the functionalization of unmodified ZnO nanoparticles can be increased. The more reactive Sulphur atom in the MPMS can further modify the surface of unmodified nanoparticles [121], which is also supported by the Zeta sizer results (Fig. 4.2b). A monotonic increase in CA was realized for the increase in

concentration of nanoparticles up to 20 wt.%. That is attributed to the uniform increase in surface roughness of coating with the increase in nanoparticle content. Furthermore, the increase in nanoparticle content beyond 20 wt.% reduced the CA, which may be attributed to non-uniform increase in the surface roughness of the coating.

FESEM images of synthesized coatings including nanoparticle content 1, 20 and 25 wt.% revealed reasonably different morphologies (Fig. 4.4a-c). Sample PS/ZnO-1 revealed smooth nanoporous morphology with uniform particle distribution throughout the surface. The presence of nanopores with nanoparticles acts as secondary texture and thus helps to construct the micro-nano structure. The main cause of this is the evaporation of THF [108]. Parts of air can be entrapped in the nanopores and generate a layer of air pad to reduce liquid-solid contact area between water droplet and the coating, which can increase the hydrophobicity [23]. Moreover, PS/ZnO-20 showed quite rough morphology with uniform distribution of tightly packed small agglomerates of the nanoparticles. However, PS/ZnO-25 revealed the combination of rough and smooth morphology due to significant clustering and non-uniform distribution of the nanoparticles.
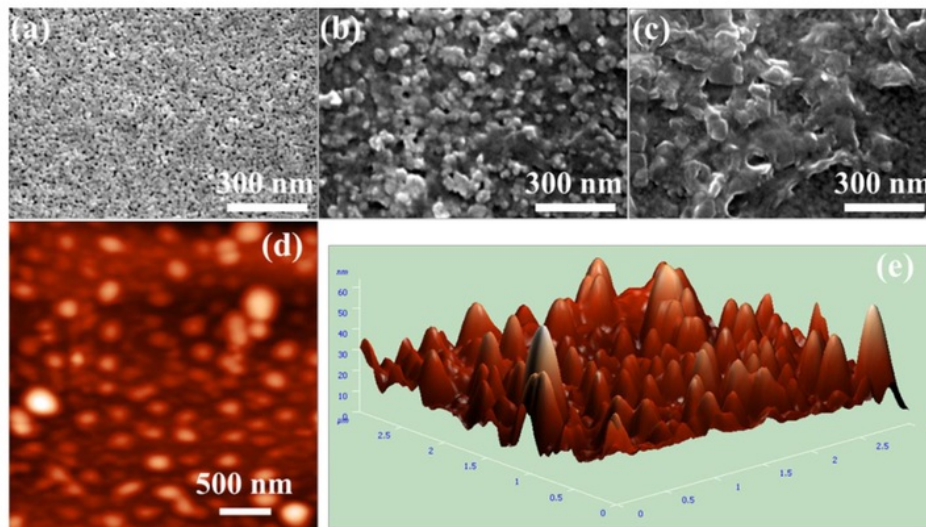
Fig. 4.4 FESEM images of nanocoatings: (a) PS/ZnO-1, (b) PS/ZnO-20 and (c) PS/ZnO-25. (d) 2D and (e) 3D AFM images of PS/ZnO-20 coating.

AFM image of PS/ZnO-20 (Fig. 4.4d) confirmed the formation of nanostructure coating comprising the uniform distribution of tightly packed small agglomerates of the nanoparticles. 3D AFM image revealed an adequate rough surface with a large number of sharp bumps stand on the coating (Fig. 4.4e), indicating the hierarchical roughness of PS/ZnO-20 coating. Fig. 4.5 exhibited the variation in roughness and CA with respect to the nanoparticle concentration. The R_{rms} roughness and CA monotonically increase with the increase in nanoparticle concentration up to 20 wt.% and beyond this limit, they slightly decline. The surface properties mainly rely on the R_{rms} roughness of a coated surface. The rough surfaces can be either hydrophobic or hydrophilic until the surface is not properly treated with a low surface energy material. Thus, the increase in R_{rms} value of a low surface energy treated surface can increase the CA but up to a certain limit [122]. The high hydrophobicity was also observed by Perkas et al. for layered deposition of ZnO nanoparticles (70–90 nm) on glass substrate. However, the maximum CA obtained by the sol-gel method followed by thermal decomposition was only 141° [22]. Thus, it can be inferred that the dual-functionalized nanoparticles reinforced PS coatings are accountable for the hierarchical roughness, and the superhydrophobicity.
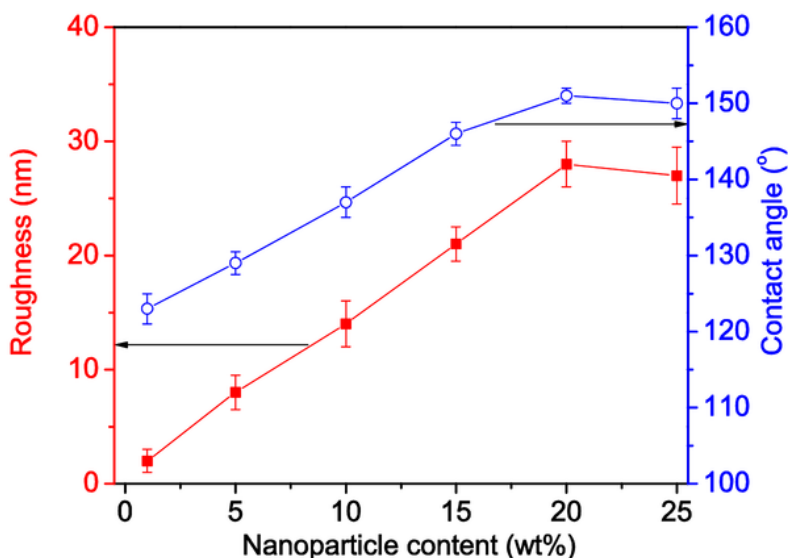
Fig. 4.5 Variation of Roughness and CA with respect to nanoparticle concentration.

The transmittance of PS/ZnO-20 nanocomposite coated glass and bare glass were investigated and shown in Fig. 4.6. It was observed that the transparency of coated glass slightly lower than that of the bare glass. The transparency in case of bare glass was 93.8% to 91.4% from 400 nm to 800 nm. However, the transparency in the case of nanocomposite coated glass was 91.9% to 89.8% from 400 nm to 800 nm. Thus, the transmittance of coated sample is close to the transmittance of bare glass, which shows that the dual-functionalized nanoparticles reinforced PS coatings are responsible for the hierarchical roughness, transparency and the superhydrophobicity.
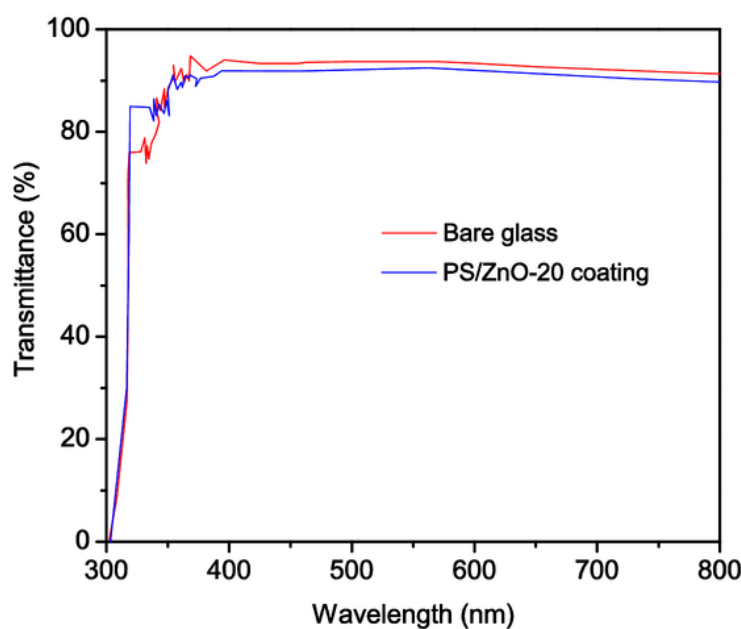
Fig. 4.6 The transmittance % versus wavelength for bare glass and PS/ZnO-20 nanocomposite coated glass.

4.5. CONCLUSIONS

Transparent superhydrophobic polystyrene/ZnO nanocoating, possessing average roughness of 28 nm, a high CA > 150° has been successfully synthesized by a modified facile sol-gel route. The transparency close to transmittance of bare glass

66

has been obtained for the nanocoating. Thus, the reported method has inordinate potential to develop transparent and SHSs for various industrial applications.

CHAPTER 5. A FACILE APPROACH TO DEVELOP MODIFIED NANO-SILICA EMBEDDED POLYSTYRENE BASED TRANSPARENT SUPERHYDROPHOBIC COATING

5.1. ABSTRACT

Triethoxyoctylsilane modified nano-silica (TOS-SiO$_2$) embedded polystyrene (PS) based transparent SHC has been synthesized on a glass substrate via a facile sol-gel method. A dip-pulling process was employed to synthesize the coating. The morphology of the PS/TOS-SiO$_2$ coating revealed V-shape dyads like porous structure. The static water CA of 162 ± 2° with a SA of 3 ± 1° was obtained for the synthesized coating. The thin coating showed a high average transmittance of 91.8 ± 0.5% close to the average transmittance of bare glass (92.6 ± 0.2%). An appropriate amount of TOS-SiO$_2$ embedded PS with unique morphology and average roughness of 65.39 ± 6.7 nm provided a transparent SHC. The transparency and roughness of the SHC were optimized by controlling the dip/pull speed and time. The developed transparent SHC can be utilized for self-cleaning application of the cover glass of solar panels.

5.2. INTRODUCTION

An SHS with a water droplet must show a CA > 150° and SA < 10° [123]. An SHS can be developed using low surface energy base materials and by generating nanoroughness on it [124]. Nanoroughness on a surface plays a vital role in developing SHSs. Slight tilting of the SHS make the water droplet to roll-off thereby collecting and confiscating the dust particles on it due to the small contact area between the SHS and the water droplet and thus

representing the self-cleaning effect. To utilize the self-cleaning effect of SHSs for solar panels, their optical transparency is highly desired. However, for an SHS, transparency and roughness are competitive properties [124]. If the roughness increases, transparency decreases and vice-versa [125]. Hence, the synthesis of transparent SHSs is a challenging task. Thus, it is obligatory to optimize the roughness to maintain the desired transparency of the SHCs (SHCs) for solar panels. Nakajima et al. [126] reported that the scattering of light is negligible for surface roughness < 100 nm. Worldwide, several techniques such as sol-gel, spin-coating, dip coating, spray coating, chemical vapour deposition (CVD), etc. have been employed for the synthesis of transparent SHCs [95], [97], [98]. Numerous nanoparticles such as nano-silica, alumina, titania, zinc oxide etc. have been widely deposited on the glass substrates for the development of SHCs [123], [127]–[129]. Silica nanoparticles are one of the most commonly used oxides in developing SHCs due to their low cost, minimal toxicity, thermal and mechanical stability, etc. [124], [130].

In the present study, a simplistic economical sol-gel route has been used to synthesize a transparent superhydrophobic TOS-SiO_2 embedded PS coating on a glass substrate. An economical, transparent hydrophobic polymer PS is chosen as the base material for the coating due to its superior thermal and mechanical stability compared to the silane-based functionalizing agents [108]. The dip-pulling process has been optimized to set up the balance between competitive superhydrophobicity and transparency of the PS/TOS-SiO_2 coatings.

5.3. EXPERIMENTAL

SiO_2 nanoparticles (size ~ 25 nm, Reinste Nano Ventures, Pvt. Ltd., India) were functionalized by a facile hydrothermal reaction [131]. Initially, 1 g TOS was added into 100 ml ethanol and continuously stirred for 3 h at 55 °C to hydrolyze the silane completely. Then 5 g SiO_2 nanoparticles added into the hydrolyzed silane solution and stirred for 3 h under ambient conditions. Then, the nanoparticle consisting solution dried at 110 °C for 3 h to obtain TOS functionalized superhydrophobic

nanoparticles. The PS with average $M_w \sim 35,000$ was used to provide good adhesion between the glass substrate and the nanoparticles [123]. The functionalized 5 g SiO_2 nanoparticles added to 1 g PS containing 50 ml tetrahydrofuran (THF, $M_w \sim 72.11$) and continuously stirred for 1 h. The transparent SHC was prepared on a glass substrate by dip-pulling method followed by heating at 70 °C for 2 h. The sequential steps for the preparation of transparent SHC and the possible mechanism of synthesis of superhydrophobic SiO_2 nanoparticles are illustrated in Fig. 5.1.
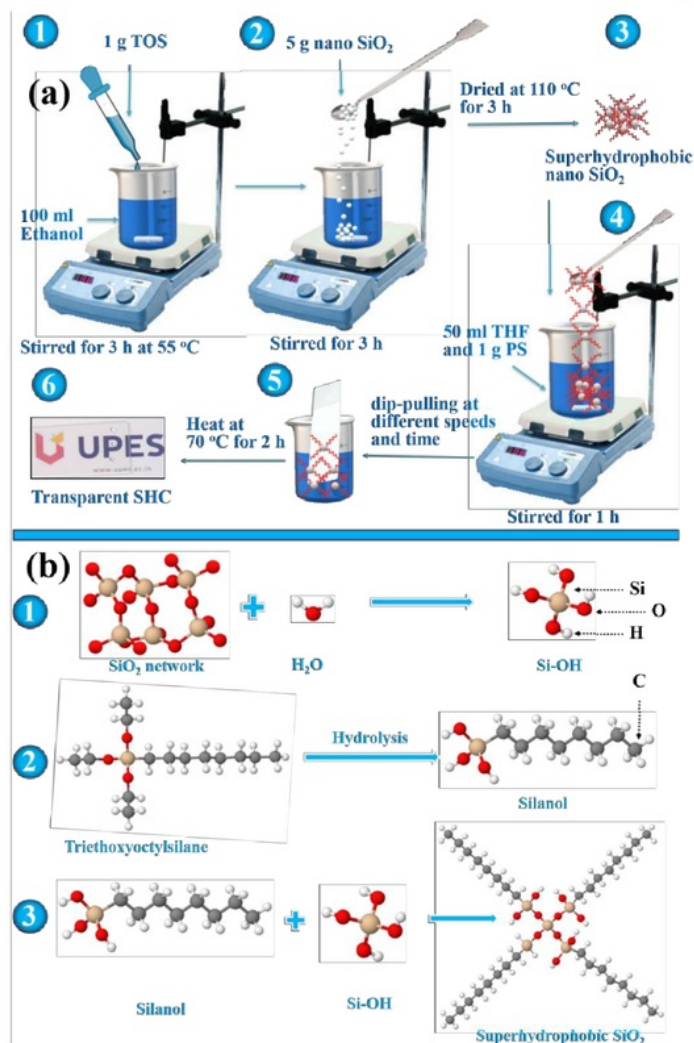
Fig. 5.1 (a) Sequential steps for the preparation of transparent SHC, and (b) the possible mechanism of synthesis of superhydrophobic SiO_2 nanoparticles.

The transparency and superhydrophobicity of the coating were optimized by varying the dip/pull speed and time as mentioned in Table 5.1. All the chemicals were purchased from Sigma Aldrich, USA. The surface functionalization of the nanoparticles was characterized by a Fourier transform infrared (FTIR) spectroscopy (Perkin Elmer FTIR/FIR Frontier, Spectrometer, USA). A 5 MP digital camera was used to capture the optical images of the coatings. The morphology, CA and transmittance of the coatings were characterized by a field emission scanning electron microscope (FESEM, Quanta 200F, FEI, USA), drop shape analyzer (DSA 100, Krüss GmbH, Germany) and UV-Visible spectrometer (Perkin Elmer Lambda 35 UV/VIS, USA), respectively. The roughness of the coating was determined using an atomic force microscope (AFM, NaioAFM, Nanosurf, Switzerland).

Table 5.1 Optimization of transparency and roughness of the SHC by changing the dip/pull speed and time.

Sample No.	Dip/Pull Speed (mm/s)	Dipping Time (s)	Transparency (%)	Roughness, R (nm)		CA (°)	SA (°)
				$R_{avg.}$	R_{rms}		
1	10	30	92.4	27.11	39.34	132 ± 3	12 ± 1
2	20	60	92.1	56.54	77.68	145 ± 3	7 ± 2
3	30	90	91.8	65.39	84.96	162 ± 2	3 ± 1
4	40	120	90.5	77.89	102.06	159 ± 1	4 ± 2
5	50	180	88.2	95.76	113.19	153 ± 2	4 ± 1

5.4. RESULTS AND DISCUSSION

FTIR spectra of pristine and functionalized SiO_2 nanoparticles is shown in Fig. 5.2. The strong absorption peaks at 799 and 1106 cm^{-1} correspond to Si-O-Si symmetric and asymmetric bands, respectively [132]. The peaks around 620 and 473 cm^{-1} also belongs to the Si-O-Si network [133]. The absorption peaks around 1634 and 3454 cm^{-1} corresponds to carboxyl and hydroxyl groups respectively [133]. The weak peaks at 2850 and 2919 cm^{-1} corresponds to the stretching vibrations of C-H bonds [132]. The adsorption peak at 965 cm^{-1} corresponds to Si-O stretching vibration of Si-OH bond [133]. After the modification of SiO_2 nanoparticles by TOS, the increase in the transmittance of weak peaks at 2850 and 2919 cm^{-1} and the disappearance of the peak at 965 cm^{-1} along with the shifting of a strong peak position from 799 cm^{-1} to 808 cm^{-1} indicate the successful surface modification of the SiO_2 nanoparticles.
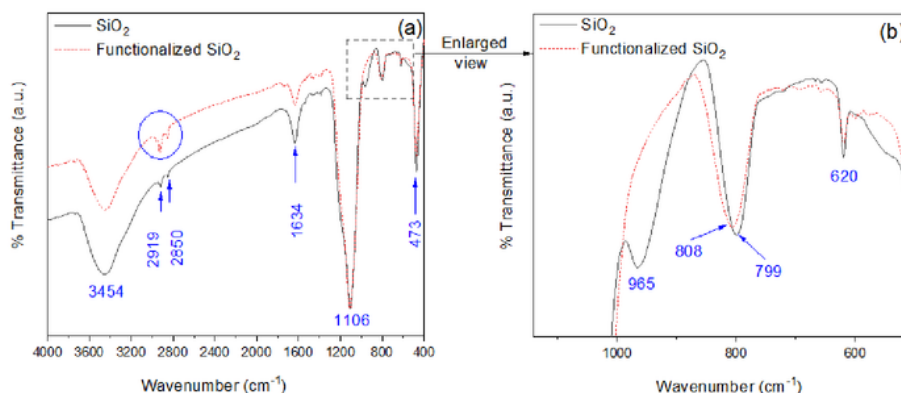
Fig. 5.2 (a) FTIR spectra of pristine and functionalized SiO_2 nanoparticles with (b) enlarged view.

The optical images of the front view (Fig. 5.3a) and side view (Fig. 5.3b) of the developed coatings with water droplets clearly revealing their high transparency and superhydrophobicity. Fig. 5.3(c) shows the static water CA of $162 \pm 2°$ with a SA of $3 \pm 1°$ for PS/TOS-SiO$_2$ coating (leftmost water droplet). The CA for three droplets in a row appears different because of change in the viewing angle. FESEM image of PS/TOS-SiO$_2$ coating revealed V-shape dyads (indicated by dotted white

72

lines) like porous structure (Fig. 5.3d). It seems that the V-shape dyads grew on the surface. It may have happened because of the dip/pulling of the glass slides in the resulting solution at an optimized speed of 30 mm/s and dipping time of 90 s. The grown structure makes the surface quite rough ($R_{avg} \sim 65.39$ nm and $R_{rms} \sim 84.96$) as confirmed by the AFM image of the coating (Fig. 5.3e), which is crucial for the SHSs. The presence of nanopores in the microstructure of the coating is due to the evaporation of THF [108]. Air can trap easily in such a structure and can create a film of air pad to decrease the contact area between water drops and the coated surface. The reduced contact area can improve the hydrophobicity of the coating [23]. A very thin coating showed a high average transmittance of $91.8 \pm 0.5\%$ close to the average transmittance of bare glass $92.6 \pm 0.2\%$ (Fig. 5.3f). An appropriate amount of TOS-SiO$_2$ embedded PS with unique morphology is responsible for transparent SHC.
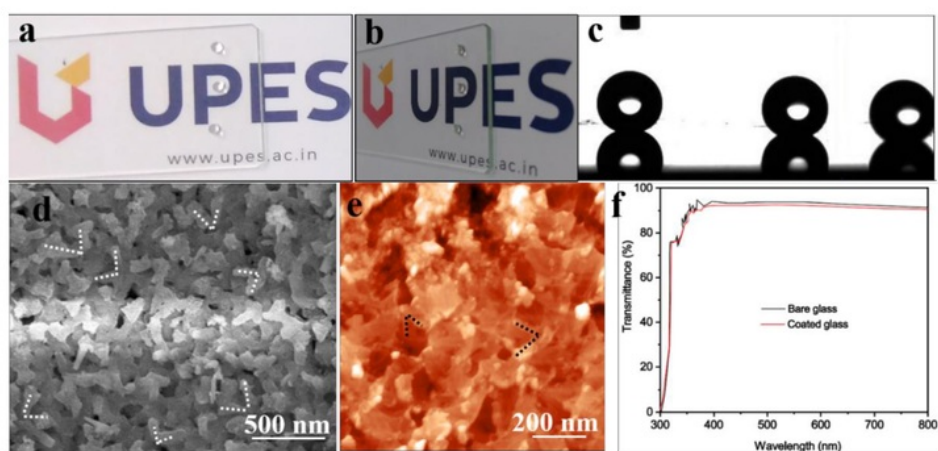
Fig. 5.3 The optical images of the (a) front view, (b) side view of the coatings with water droplets, (c) static water CA, (d) FESEM image and (e) AFM image of the coating. (f) The transmittance % versus wavelength curves for a bare glass and coated glass.

5.5. CONCLUSIONS

TOS-SiO_2 embedded PS based transparent SHC was obtained via a facile sol-gel method. Dip/pull speed of 30 mm/s and dipping time of 90 s found responsible for unique morphology with an average roughness of 65.39 ± 6.7 nm of the transparent SHC. The static water CA of $162 \pm 2°$ with a SA of $3 \pm 1°$ and high average transmittance of $91.8 \pm 0.5\%$ which is close to the average transmittance of bare glass ($92.6 \pm 0.2\%$) was achieved for the developed coating. The developed transparent SHC can be utilized for self-cleaning application of the cover glass of solar panels.

CHAPTER 6. PATTERN ANALYSIS AND MACHINE LEARNING

This chapter details the pattern analysis and machine learning approach used on FESEM images to predict the score as outcome of the MATLAB image processing tool [86], [134], [135]. The K-means clustering approach is used for the same and MATLAB simulation time is also estimated [136]–[138].

6.1. PATTERN ANALYSIS

Pattern recognition is a division of machine learning applied directly to recognize the regularities and pattern of the data. Pattern recognition is one of the important attributes of living things and human beings. It is the method to identify the objects in our daily routine. The objects are recognized using different patterns. The pattern distinguishes one object from others of several types. The pattern is defined as the attribute to distinguish interrelation of events, concepts or data. Human follows the pattern recognition task in our daily life. We recognize our known person by hearing his/her voice, recognition of face handwriting, signature, questers etc. After recognition human takes, some decision based on the experience and observations with the recognized object.

The greater number of experiences and operations help the human to make better decisions. In the same way, the computer takes the decision about pattern recognition. The human brain is considered as the supercomputer has the superior ability to recognize patterns. The human does not have this ability right from birth. A newly born baby learns solely to recognize his mother, father and other objects and patterns available in surroundings.

The fundamental step is to get the ability to make a difference in objects. This ability comes by psychophysiological processes that stores patterns in memory cells. As the age grows of child, he tries to identify some of them as different entity and by experience, he comes to know that different objects belong to different category called class. The child refines the recognition methods by storing the replica of each category. This ability is called learning process. Every individual new object is associated with existing statistical populations of the brain.

The objective of the pattern recognition is regarded as one of discriminating the input data and populations. All these populations belong to the newly reached objects with their features and attributes. The population is called as clusters and the objects are presented by machine in the form of a feature vector. The idea of machine learning is employed for statistical pattern recognition and regulates in the data. The machine learning approach is classified in two approaches: **supervised learning**, which trains a model on identified input and output data so that it can expect future outputs, and **unsupervised learning**, which finds hidden patterns to develop predictive model based on input and output data or intrinsic structures in input data [86], [87], [134], [136].

6.1.1. SUPERVISED LEARNING

In supervised learning, the prior information is available about the class of subset of data. The pattern analysis-based systems are provided with the training from characterized training data. It builds the model to make the predictions based on the evidence available for uncertainty. The supervised learning algorithms are applied for known set of input-output data, which we are trying to predict and get the response of new data values. The supervised learning follows regression and classification techniques to develop analytical and prediction models.

Fig. 6.1 presents the machine learning approach and Classification techniques. The techniques are based on the prediction on distinct responses - for example, to know whether an e-mail is actual or spam, or whether a tumour detection is benign or cancerous. The dataset applied for junk mails filtering would have junk messages

76

and "ham" (= not-junk) messages. In the supervised knowledge problem, it is required to distinguish the message in the trained data set is junk or ham. We should be able to process this data to train our classical system in the way that it can classify new invisible messages. Classification models organize input data into categories. Some of the applications of classification are speech recognition, medical imaging, and credit scoring. The technique is employed, if the data can be categorized into groups, tagged, categorized or distributed in the groups of classes. The general algorithms used for classification are support vector machine (SVM), discriminant analysis, naive Bayes, K nearest neighbour, neural networks, boosted and bagged decision trees and logistic regression. The different learning models are presented with the help of Fig. 6.2.

Regression techniques are used in which the prediction is experienced as continuous responses. The examples of regression are the changes in temperature, pressure, level or fluctuations in electricity demand etc. It is good to apply when the response in real numbers. The regression method models are based on the investigation of associations between variables and leanings to create expectations about constant variables. In case of regression model, the pattern organization is done against discrete class tags to specific comments as the output of the predictions. The temperature regression in weather forecasting can predict that the day is sunny, snowy or rainy. The general algorithms used for regression are linear model, nonlinear model, decision trees, ensemble methods, regularization, stepwise regression, Support vector regression (SVR), Gaussian process regression (GPR), Generalized Linear Model (GLM) and adaptive neuro-fuzzy learning [88].
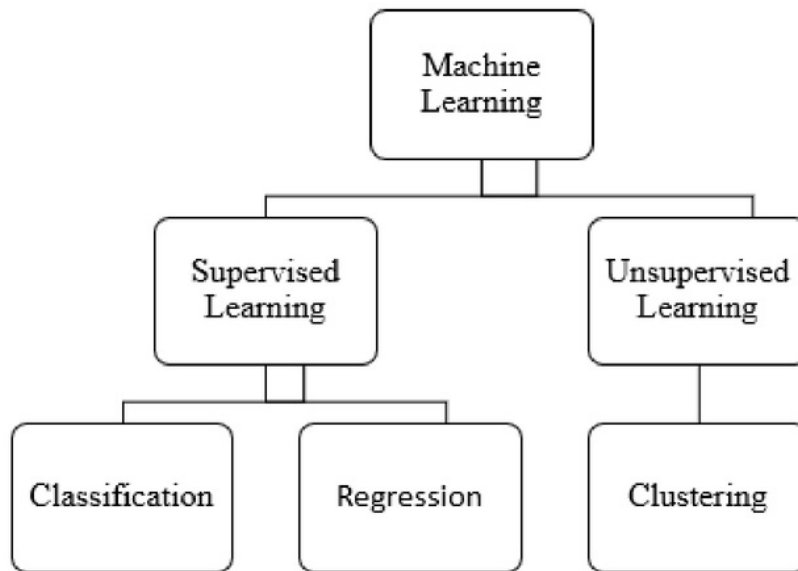
Fig. 6.1 Machine Learning Approach
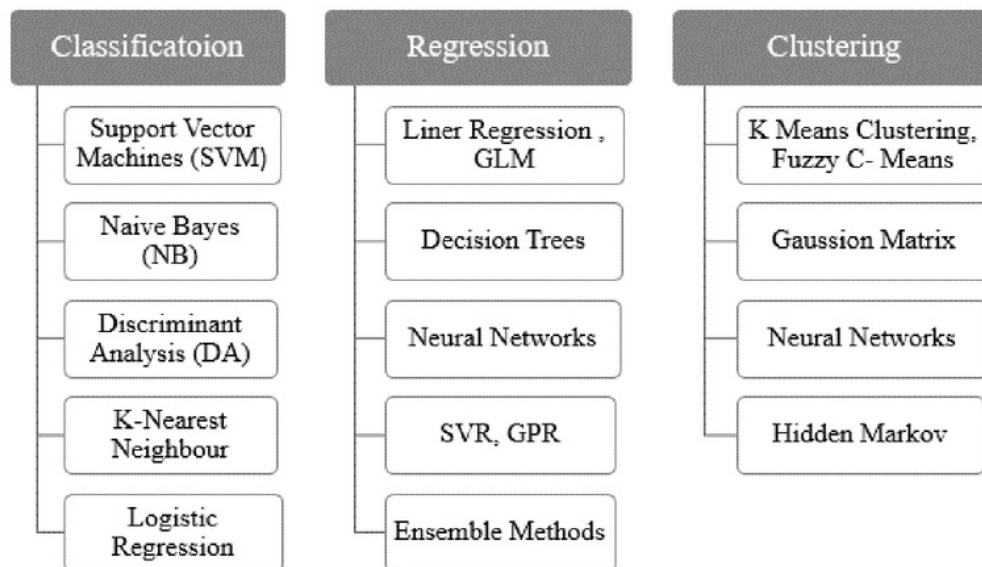
Fig. 6.2 Machine Learning Methods

6.1.2. UNSUPERVISED LEARNING

This learning approach is based on the unlabeled examples, and all the modules are incidental from the unorganized input dataset values. The learning technique is applicable to find out hidden patterns in data of unlabeled input data and draw the inferences from datasets consisting of unknown values. The method follows the clustering technique to set the unlabeled samples constructed on similar distance measurement. This technique is explicitly for data analysis to get groupings or hidden patterns in data. The general techniques for clustering approaches are K-Medoids algorithm or K-means mathematical algorithm, Fuzzy based C-means algorithms, Gaussian matrix model, Neural networks, Hidden Markov models and self-organizing maps etc [88], [89].

6.2. K-MEANS CLUSTERING

The k means clustering technique is a method based on the iterative technique applied for clustering a set of 'N' vector points into 'k' number of groups, refereed as clusters of points. The clustering is the procedure of separating a collection of data set points into insignificant size of groups.

A numerical approach is applied to quantify certain attributes of the goods, such as the percentage of milk products and others, and foods with greater ratio of milk would be composed. Cluster, in a general way, it can be understood for 'n' data points (X_i), where i = 1, 2.......n, that essentially be subdivided in 'k' number of clusters. The objective is to allocate a bunch against individual data point. The K-means algorithm is a clustering technique, used to determine the locations μ_i, where, i = 1, 2,...k of the bunches that diminish the least distance from the data set points to the cluster or bunch. The K-means clustering solves

$$\text{arg.} \min \sum_{i=1}^{k} \sum_{x \in c_i} d(x, \mu_i) = \text{arg.} \min \sum_{i=1}^{k} \sum_{x \in c_i} \|x - \mu_i\|_2^2 \qquad (6.1)$$

Here, c_i = set points that have its place to cluster 'i'. The partitioning in the K-means clustering technique follows the concept of Euclidean distance calculation based on square distance.

$$d(x, \mu_i) = \|x - \mu_i\|_2^2 \tag{6.2}$$

The situation is not trivial as it is N-P, hard in statistics. The K-means process only anticipates determining the universal minimum, probably getting trapped into a different result [134], [137], [139].

6.2.1. K-MEANS ALGORITHM

The K- means the process was suggested by Lloyd's, to obtain the k-means groups and its behaviour is given stepwise. In the beginning, choose the number of clusters 'k' and follow the following steps.

Step-1: Begin the midpoint as the centre of the clusters

$$\mu_i = some\ value, i = 1, 2, \dots, k$$

Step-2: Feature the neighbouring cluster against each data point

$$c_i = \{j: d(x_j, \mu_i) \leq d(x_j, \mu_l), l \neq i, j = 1, 2, \dots, n\} \tag{6.3}$$

Step-3: Fix the location of an individual cluster for the means of all set data-points associated with that group,

$$\mu_i = \frac{1}{c_i} \sum_{j \in c_i} x_j, \forall\ i \tag{6.4}$$

Step-4: Replicate the step-2 and step-3 until convergence is obtained

$|c| = $ Count of present elements in c

The procedure ultimately meets to a point, even though it is not essential to maintain the least distance of the summation of squares. It is for the fact that the algorithm is based on heuristic approach, meeting to a local minimum. The method is also discontinued when the coursework is not transformed from one repetition to the next. This approach is depicted in Fig. 6.3 [134], [137]

80
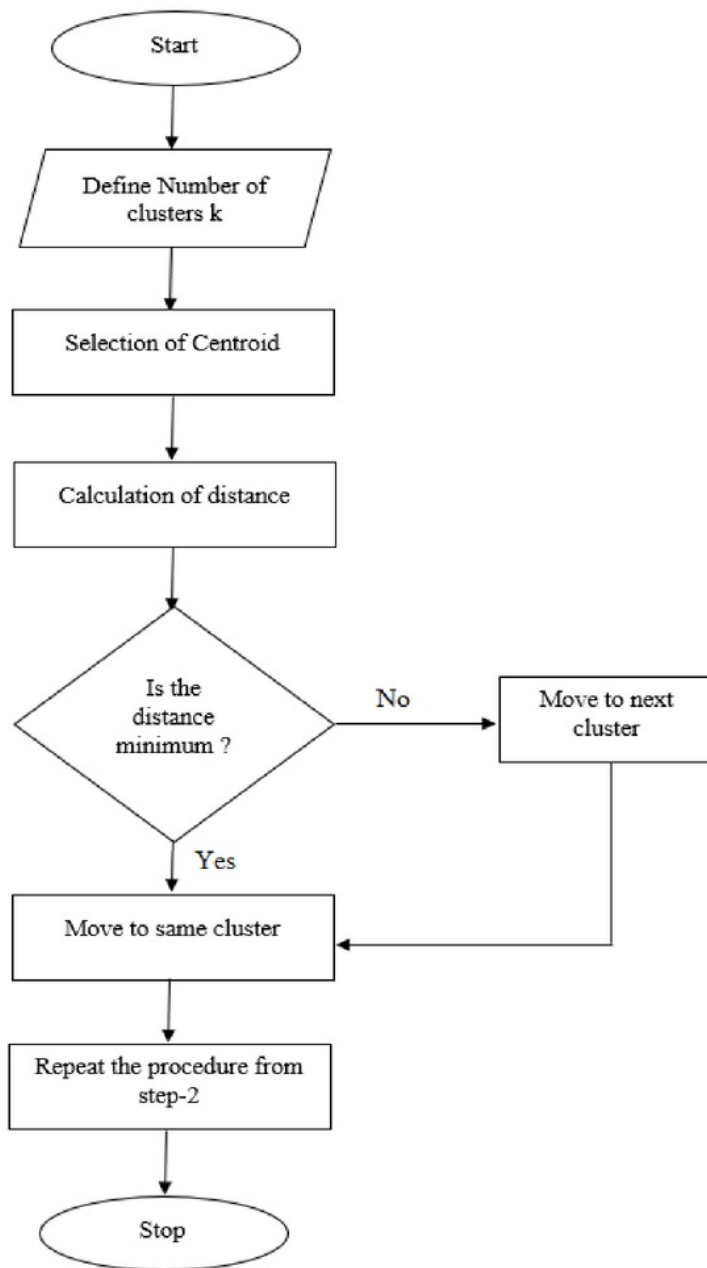
Fig. 6.3 K Means Clustering

6.3. PROCEDURE FOR IMAGE ANALYSIS

The procedure for image processing and analysis is depicted in Fig. 6.4 . The general steps for the processing are input the FESEM image, image preprocessing, image segmentation, image feature extraction, image analysis and score prediction using machine learning approach.

```
┌─────────────────────────────────────┐
│            FESEM Image               │
└─────────────────────────────────────┘
                  ↓
┌─────────────────────────────────────┐
│         Image Preprocessing          │
└─────────────────────────────────────┘
                  ↓
┌─────────────────────────────────────┐
│         Image Segmentation           │
└─────────────────────────────────────┘
                  ↓
┌─────────────────────────────────────┐
│       Image Feature Extraction       │
└─────────────────────────────────────┘
                  ↓
┌─────────────────────────────────────┐
│            Image Analysis            │
└─────────────────────────────────────┘
                  ↓
┌─────────────────────────────────────┐
│           Score Prediction           │
└─────────────────────────────────────┘
```
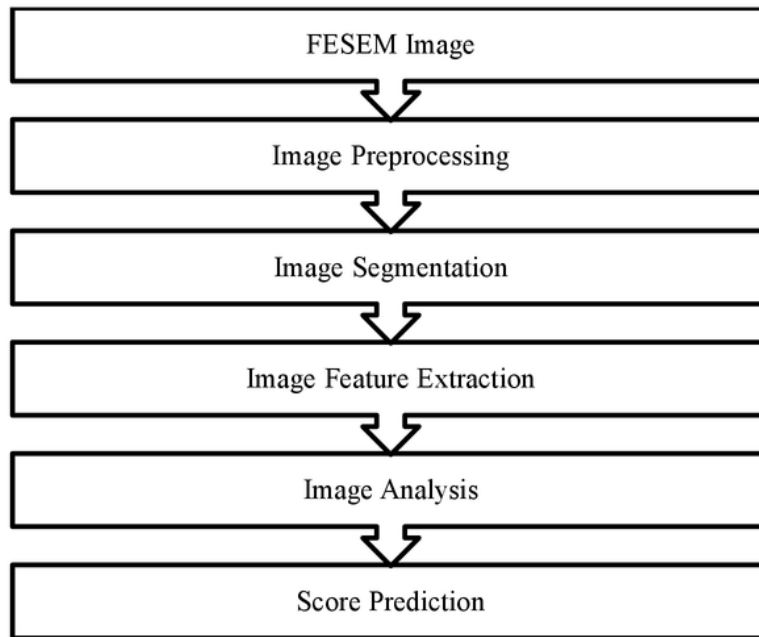
Fig. 6.4 FESEM image processing and analysis.

Step-1 FESEM Images: FESEM images of the SHC material is selected for the estimation of surface roughness. The FESEM images provide exaggeration in three dimensions: x,y and z. The FESEM images always need image processing before optimal inspection of the surface structures.

Step-2 Preprocessing: Preprocessing is the step which is necessary and applied before the image analysis and involves all the processes used for the abstraction of the essential information for the geometric structures and perfection of the original image. The anomalies of the image data are enhanced with the removal of noise, atmospheric noise and unwanted regions. The process highlights the specific

portions, decreases the image noise and shows the significant regions of the digital image.

Step-3 Image Segmentation: Image segmentation is the method in which the digital image is divided into several segments called superpixels. If trails the position of objects such as lines, curves and allocates a label to each pixel for the image that the same label can follow some certain characteristics. There are several different algorithms available that can be used for image segmentation of the images such as 2 D greyscale FESEM images. There is not any predefined algorithm that can generate the best results for all type of FESEM images. The popular segmentation methods are based on Otsu's method, region growing segmentation, thresholding, Sobel operator, support vector machine (SVM), artificial neural network, level set method, wavelet-based processing, watershed algorithms, texture-based segmentation, genetic algorithm and mathematical morphological etc. The image enhancement methods also improve the quality of digital image without the degradation of the data of the source images. The image enhancement methods are referred as direct methods and indirect methods. In the direct segmentation method, the image distinction is improved based on the source of previous information of contrast. In the indirect process, the contrast development is not essential but filtering procedures are used for the image processing.

Step-4 Feature Extraction: The digital image feature extraction is the procedure that starts from a preliminary set of measured statistics and descends the topographies or figure values which are non-redundant and revealing. The extraction is also related to the reduction of image dimensionality instead of completion of full data.

Step-5 Image Analysis: The evocative information of the image is extracted by the image analysis. The progression of image analysis is analogous to bar-coded tags reading and the people reorganization by their face. In the image analysis, the original shape and size of the image are pre-requisites.

Step- 6 Score Prediction: The machine learning-based supervised and unsupervised learning techniques are used for the score prediction of the images. The pattern analysis technique with K-means clustering is used to predict the score based on the test data and training data.

6.4. HAAR DWT WAVELET

Discrete Wavelet transform (DWT) is the wavelet transform in which the wavelets are discretely sampled [140]–[142]. In Fourier Transform of a signal, we simply multiply that signal by an analyzing function, which is a sum of sinusoidal signal. Similarly, in wavelet transform we multiply the signal by a wavelet analyzing function as shown in the mathematical definition of the two transforms. Both transform the given signal, which is a function of time. However, the difference is that the output coefficients of Fourier transform correspond to frequency whereas for wavelet transform the output is a two-dimensional matrix of coefficients which are identified by scale and translation.

Fourier Transform: $X(F) = \int x(t)\, e^{-j2\Pi ft} dt$ from -∞ to +∞   (6.5)

Wavelet Transform: $X(a,b) = \int x(t)\, \phi_{a,b}^*(t) dt$ from -∞ to +∞,   (6.6)

Where 'a' corresponds to scale and 'b' corresponds to translation. The DWT is used in many applications of image processing such as cryptographic security, watermarking, ultra-wideband (UWB) wireless communications, authentication and biomedical signal processing applications such as design of low-power pacemakers and many more. DWT is preferred in many applications of image processing because DWT provides multi-resolution and image compression can be carried out for different stages of resolution as per required and high robustness to signal to process. The Wavelet coefficients distribution remains centred around zero, it means that the major part of the image information is concentrated within a small fraction of coefficients, as a result, it is easy to compress the image efficiently and computations take less time. As far as the application of DWT on images is concerned we apply one-dimensional filters first along the rows of image and the

along the column vice-versa because images are two-dimensional (Fig. 6.5 and Fig. 6.6). In Fig. 6.5, 'j' refers to scale, 'r' refers to row and 'c' refers to column.

It is well-known that a low pass filter does the approximation and a high pass filter extract the features of the original image. So, if we examine the output side, the approximation of the input image is given by the output I_{LL}. The output I_{LH} has passed through a high pass filter which has operated on the rows of the image, so it will give the horizontal properties or features of an input image. Similarly, the vertical features of the input image are given by the output I_{HL} and the output I_{HH} gives the diagonal edges. This was first level decomposition of the input image. If we make the approximation output of the image as input and do the same operation to this input image, then we will get the second level decomposition of the original image.
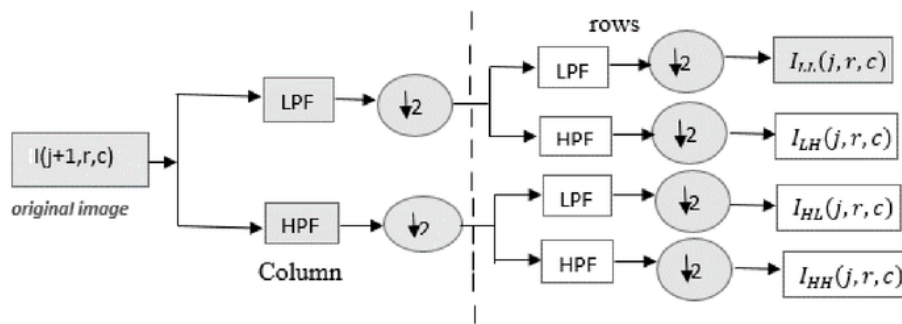
Fig. 6.5 DWT Filtering
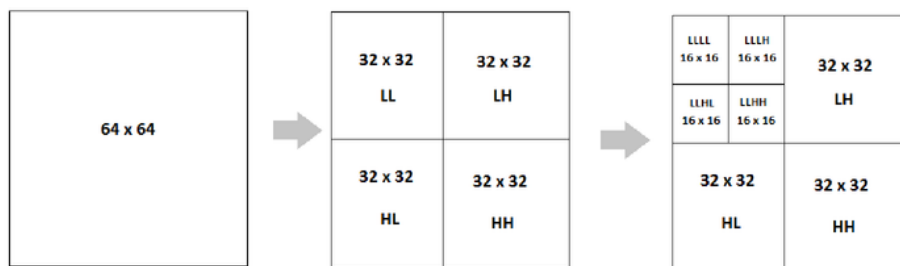
Fig. 6.6 HAAR DWT Processing.

85
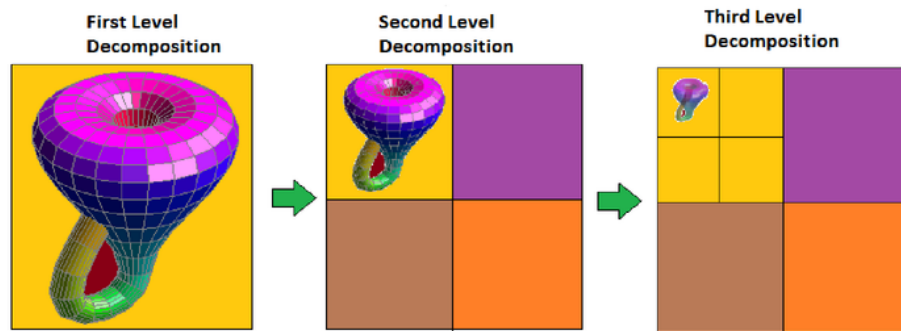
Fig. 6.7 HAAR DWT decomposition of an image.

The wavelet transform decomposes the input image into a set of diverse resolution sub-image, against different frequency regions (Fig. 6.7). The sub-band coding is followed in which the input image is subdivided into different frequency bands. The filter bank is used to perform the sub-band coding. The filter bank is a collection of filters following either a common input or common output. When the filters are having a common input, they form an investigation bank and sharing a common output, to form a fusion bank.

The straightforward use of a filter bank is to divide a signal enthusiastically at the frequency domain. The foremost analysis in the seamless reconstruction measures low filter bank for input signal, and the identical perception is followed for 2D and 3D images. The process of the filter bank operation is given in Figs. 6.8 and 6.9.
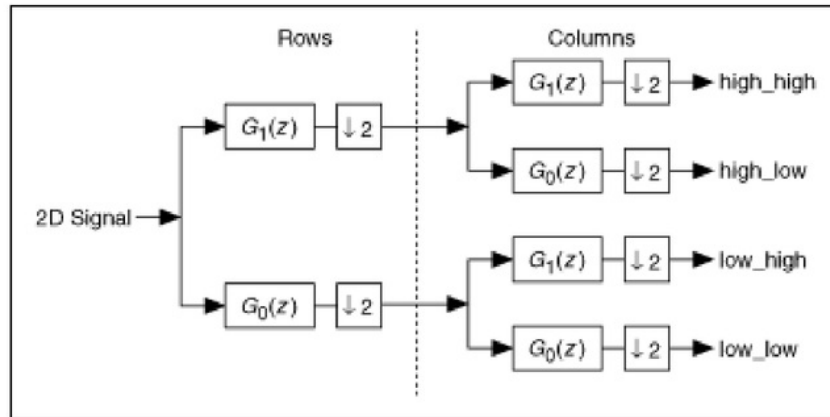
Fig. 6.8 Row and column processing.

(a)

(b)

(c)
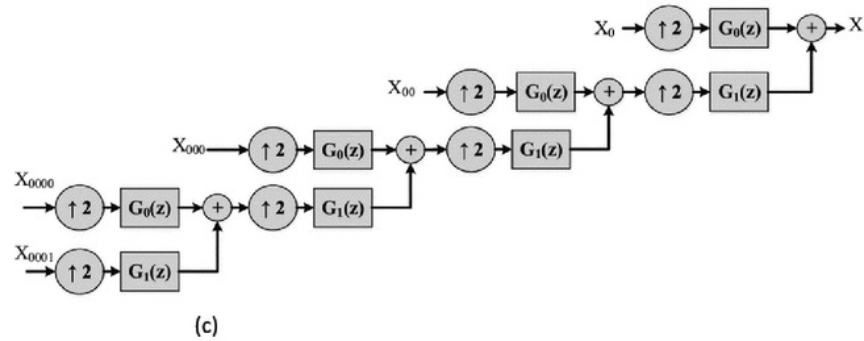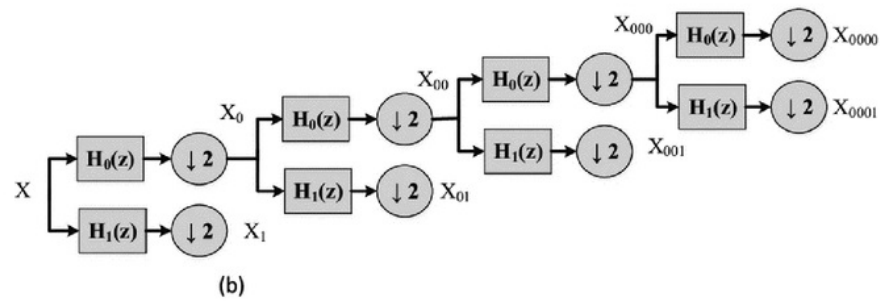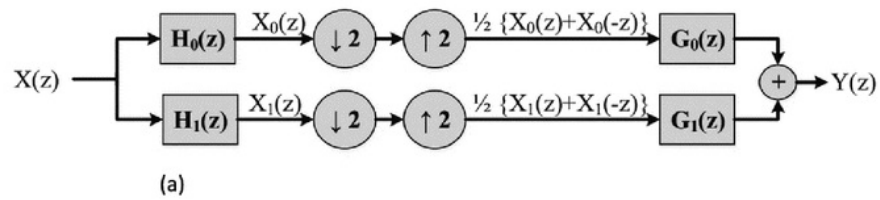
Fig. 6.9 Level processing of DWT.

The filter channel bank is consisting of two sections, first is an analysis section and second is synthesis section. The analysis segment decomposes the input image into a set of sub-band components and the synthesis section is used to reconstruct the original signal from its modules. The sub-band analysis and synthesis filters must design to be free from aliasing and meet to satisfy the perfect signal reconstruction property. The real-time termination of aliasing as well as phase distortion and amplitude should lead to perfect reconstruction of these filter banks which are more appropriate for classification of sub-band coding and decomposition of multi-resolution signal.

The operation of filter bank divides the original image signal into two equal frequency bands. In the DWT these filters banks are low-pass filters $H_0[z]$ and high-pass filters $H_1[z]$. After filtering, these signal outputs at level-1 and level- 2 are given in Eqn. (6.7) and (6.8) respectively.

$$\text{At level (1) :-} X[z]H_0[z] \tag{6.7}$$

$$\text{At level (2) :-} X[z]H_1[z] \tag{6.8}$$

After this filtering operation, the sampling frequency of the signal is too high. Hence, half the samples are rejected by the down-sampling operation. After this, the Z-transform is given in Eqn. (6.8) and (6.9) respectively.

$$\text{At level (3):- } Y[z] = \frac{1}{2}\left\{ X\left[z^{1/2}\right] \cdot H_0\left[z^{1/2}\right] + X\left[-z^{1/2}\right] \cdot H_0\left[-z^{1/2}\right] \right\} \tag{6.8}$$

$$\text{At level (4):-} Y[z] = \frac{1}{2}\left\{ X\left[z^{1/2}\right] \cdot H_1\left[z^{1/2}\right] + X\left[-z^{1/2}\right] \cdot H_1\left[-z^{1/2}\right] \right\} \tag{6.9}$$

The synthesis filter bank restructures the signal based on two filtered and decimated signals. This synthesis technique includes spending the signals in each branch by two which is called expansion or interpolation. This interpolation is attained by introducing zeros between consecutive samples. After the interpolation, the Z-transform of the signal at level- 5 and level-6 are given in Eqn. (6.10) and (6.11) respectively.

At level (5):-$X[z] = \frac{1}{2}\{X[z] \cdot H_0[z] + X[-z] \cdot H_0[-z]\}$ (6.10)

At level (6):-$X[z] = \frac{1}{2}\{X[z] \cdot H_1[z] + X[-z] \cdot H_1[-z]\}$ (6.11)

The above Eqn. (6.10) and (6.11) are written in the form of a matrix and given below as

$$\frac{1}{2} \times \begin{bmatrix} H_0[z] & H_0[-z] \\ H_1[z] & H_1[-z] \end{bmatrix} \begin{bmatrix} X[z] \\ X[-z] \end{bmatrix} \tag{6.12}$$

At level 7 and level-8

$$\frac{1}{2} \times [G_0[z] \quad G_1[z]] \cdot \begin{bmatrix} H_0[z] & H_0[-z] \\ H_1[z] & H_1[-z] \end{bmatrix} \cdot \begin{bmatrix} X[z] \\ X[-z] \end{bmatrix} \tag{6.13}$$

$$\frac{1}{2} \times [G_0[z] \quad G_1[z]]_{1\times2} \cdot \begin{bmatrix} H_0[z] & H_0[-z] \\ H_1[z] & H_1[-z] \end{bmatrix}_{2\times2} \cdot \begin{bmatrix} X[z] \\ X[-z] \end{bmatrix}_{2\times1} \tag{6.14}$$

Combination of both G and H matrices followed by matrix multiplication:

$$\begin{bmatrix} \frac{G_0[z]H_0[z]+G_1[z]H_1[z]}{2} & \frac{G_0[z]H_0[-z]+G_1[z]H_1[-z]}{2} \end{bmatrix}_{1\times2} \cdot \begin{bmatrix} X[z] \\ X[-z] \end{bmatrix}_{2\times1} \tag{6.15}$$

$$F_0[z] = \frac{G_0[z]H_0[z]+G_1[z]H_1[z]}{2} \tag{6.16}$$

$$F_1[z] = \frac{G_0[z]H_0[-z]+G_1[z]H_1[-z]}{2} \tag{6.17}$$

So that

$$[F_0[z]F_1[z]]_{1\times2} \cdot \begin{bmatrix} X[z] \\ X[-z] \end{bmatrix}_{2\times1} \tag{6.18}$$

$$F_0[z]X[z] + F_1[z]X[-z] \tag{6.19}$$

In the above equation, $X[-z]$ denotes to the aliasing constituent. This aliasing will destroy the signal. So, it is required to select the filter coefficients to decrease the aliasing effect of sample, that's will make the $F_1[z]$ as zero to negligence the aliasing effect. Let,

$$H_0[z] = H[z];$$

89

$$H_1[z] = H[-z];$$

$$G_0[z] = 2H[z];$$

$$G_1[z] = 2H[-z];$$

The above equations and discussions provide that the four filters designs based on single filter co-efficient. This is the main feature of sub-band coding. After substituting the above assumptions

$$F_1[z] = \frac{G_0[z]H_0[-z] + G_1[z]H_1[-z]}{2} => 0$$

$$F_0[z] = \frac{G_0[z]H_0[z] + G_1[z]H_1[z]}{2}$$

$$= \frac{2H[z]H[z] + (-2H[-z])H[z]}{2}$$

$$= H^2[z] + H^2[-z]$$

So, in the last level-9

$$(H^2[z] + H^2[-z]) \cdot X[z] \qquad (6.20)$$

When the image or the signal is transmitted from one place to another, the delay con not be neglected through the process it may be in milliseconds. So, the reconstructed signal is having the delay and the delayed signal is given as

$$(H^2[z] + H^2[-z]) \cdot X[z] = z^{-k} \cdot X[z] \qquad (6.21)$$

$$(H^2[z] + H^2[-z]) = z^{-k}$$

That is, $H[z] = A[z] \cdot z^{-\left(\frac{N-1}{2}\right)}$

Then the signal value at level-9 is given by

$$A^2[z] \cdot z^{-(N-1)} - A^2[-z] \cdot (-z)^{-(N-1)} = z^{-k}$$

$$A^2[z] \cdot z^{-(N-1)} - A^2[-z] \cdot (-1)^{-(N-1)} \cdot (z)^{-(N-1)} = z^{-k}$$

$$A^2[z] \cdot z^{-(N-1)} - A^2[-z] \cdot (z)^{-(N-1)} \cdot (-1)^{-(N-1)} = z^{-k}$$

If the value of k = N-1 (as the delay is followed by the filter co-efficient)

$$A^2[z] \cdot z^{-(N-1)} - A^2[-z] \cdot (z)^{-(N-1)} \cdot (-1)^{-(N-1)} = z^{-(N-1)}$$

$$A^2[z] - \left(A^2[-z] \cdot (-1)^{-(N-1)}\right) = 1$$

If N is even in that condition

$$A^2[z] + A^2[-z] = 1$$

$$H^2[z] + H^2[-z] = 1$$

Then the condition for perfect reconstruction is given by

$$H^2[z] + H^2[-z] = 1 \qquad (6.22)$$

6.5. RESULTS AND DISCUSSION

K-Means clustering Algorithm is used on FESEM images. The machine learning approach using K-means clustering is applied on PS/TOS-SiO$_2$ coating-Sample 1, PS/TOS-SiO$_2$ coating-Sample 2, PS/TOS-SiO$_2$ coating-Sample 3, PS/TOS-SiO$_2$ coating-Sample 4, PS/TOS-SiO$_2$ coating-Sample 5, PS/ZnO-1 Coating, PS/ZnO-5 Coating, PS/ZnO-10 Coating, PS/ZnO-15 Coating, PS/ZnO-20 Coating, and PS/ZnO-25 Coating. The learning process is shown in Fig. 6.4 in which are observed over the trained data and test data. The MATLAB tool predicts the score when the cluster size is varying. The predicted score is taken when the error is minimum [137].
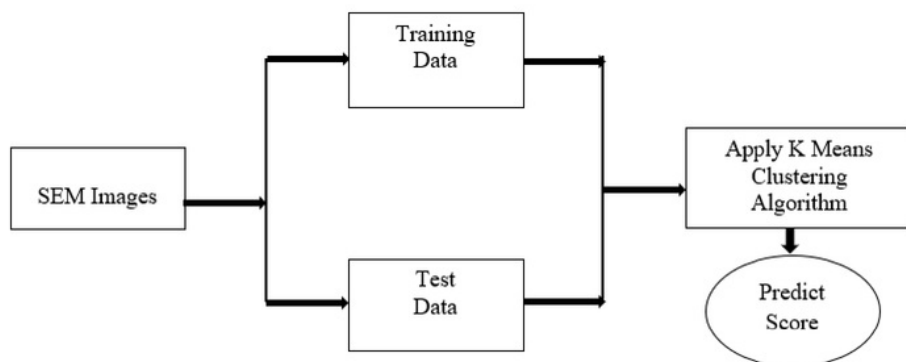
Fig. 6.10 Machine learning approach with FESEM images

The MATLAB simulation of all the images is depicted in Fig. 6.11 to Fig. 6.21 respectively. The MATLAB tool provides the total simulation time and K- means simulation time. Table 6.1 list the simulated results and predicted score against each image.
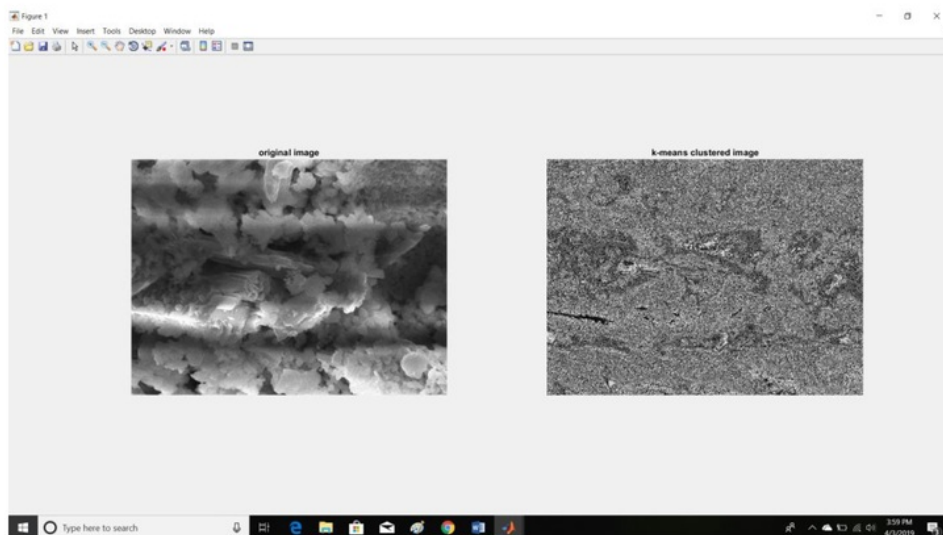
Fig. 6.11 MATLAB simulation of FESEM image of PS/TOS-SiO$_2$ coating-Sample 1.

92
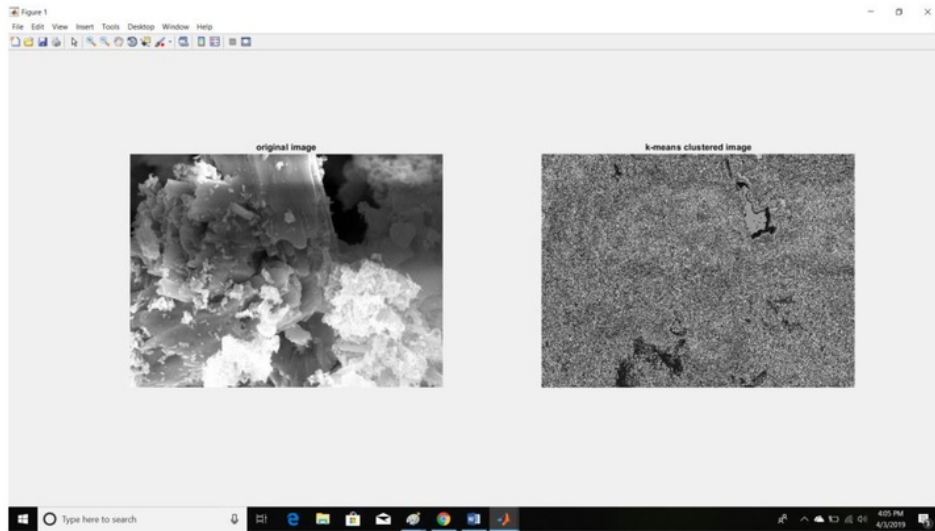
Fig. 6.12 MATLAB simulation of FESEM image of PS/TOS-SiO₂ coating-Sample 2.
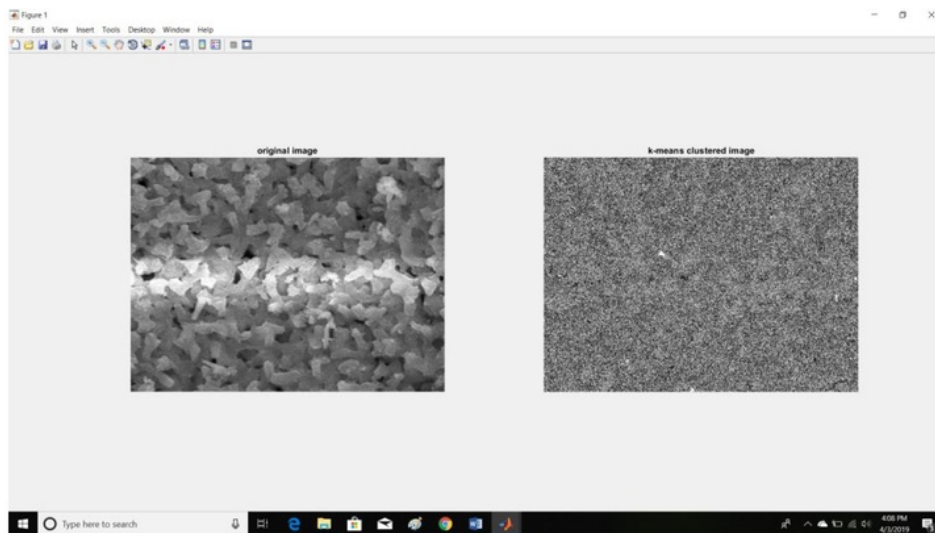
Fig. 6.13 MATLAB simulation of FESEM image of PS/TOS-SiO₂ coating-Sample 3.
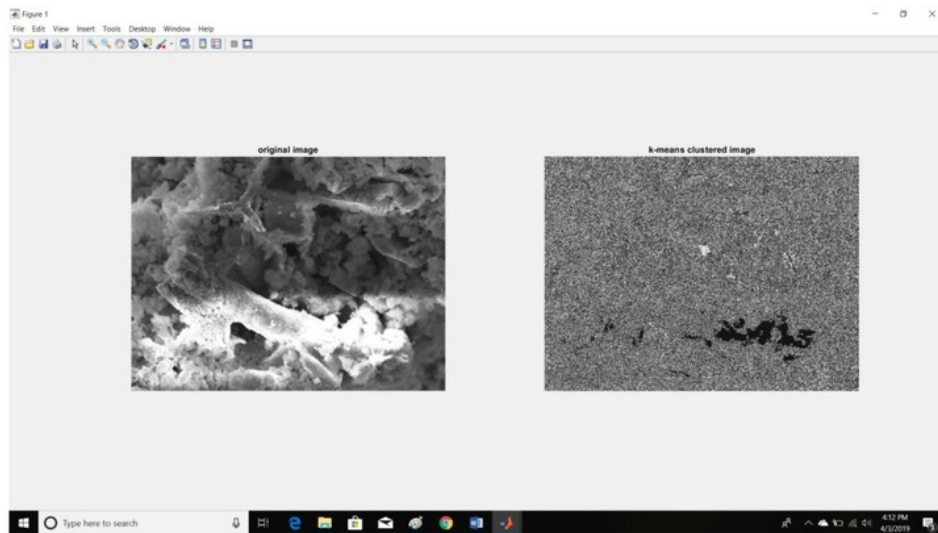
Fig. 6.14 MATLAB simulation of FESEM image of PS/TOS-SiO$_2$ coating-Sample 4.
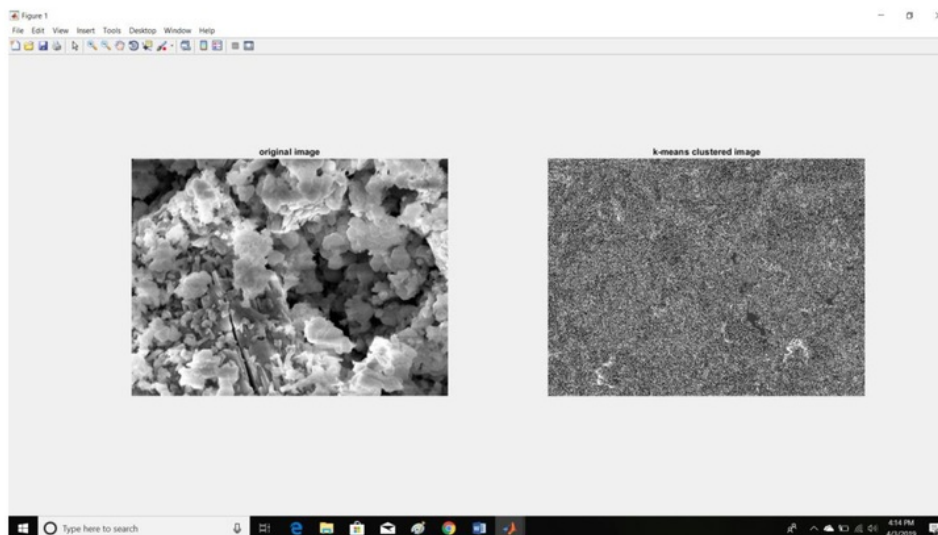
Fig. 6.15 MATLAB simulation of FESEM image of PS/TOS-SiO$_2$ coating-Sample 5.
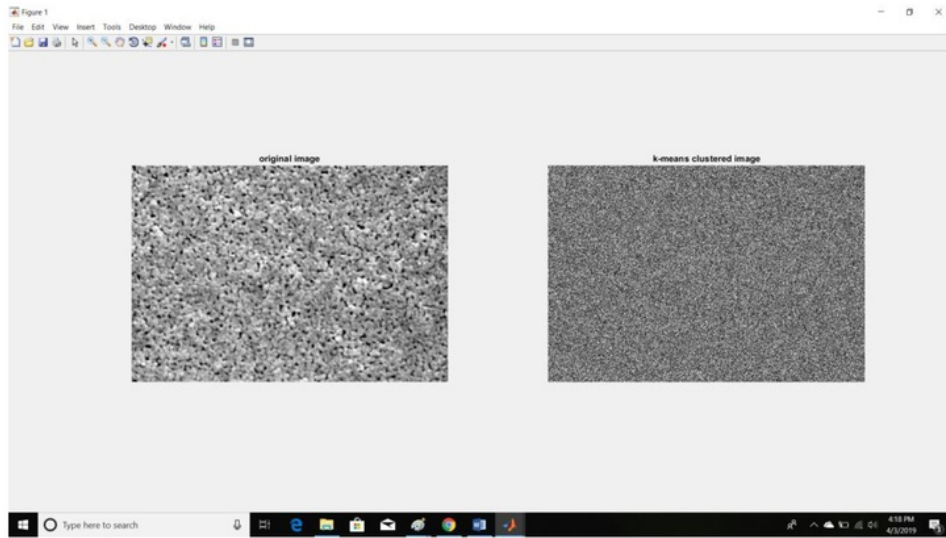
Fig. 6.16 MATLAB simulation of FESEM image of PS/ZnO-1 Coating.
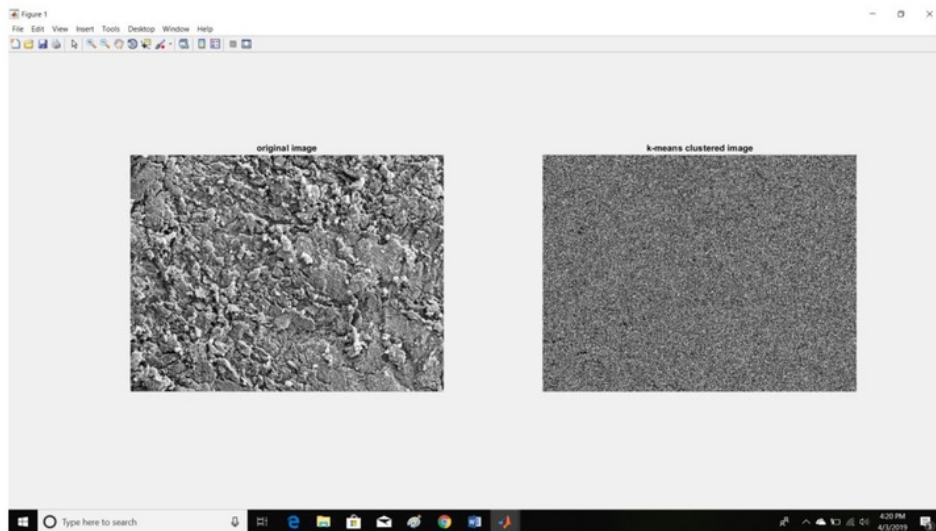
Fig. 6.17 MATLAB simulation of FESEM image of PS/ZnO-5 Coating.
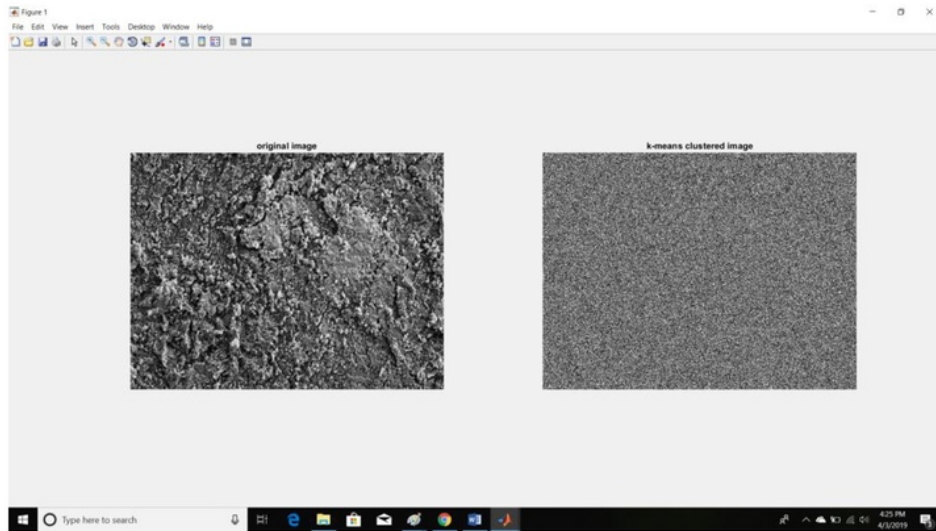
Fig. 6.18 MATLAB simulation of FESEM image of PS/ZnO-10 Coating.
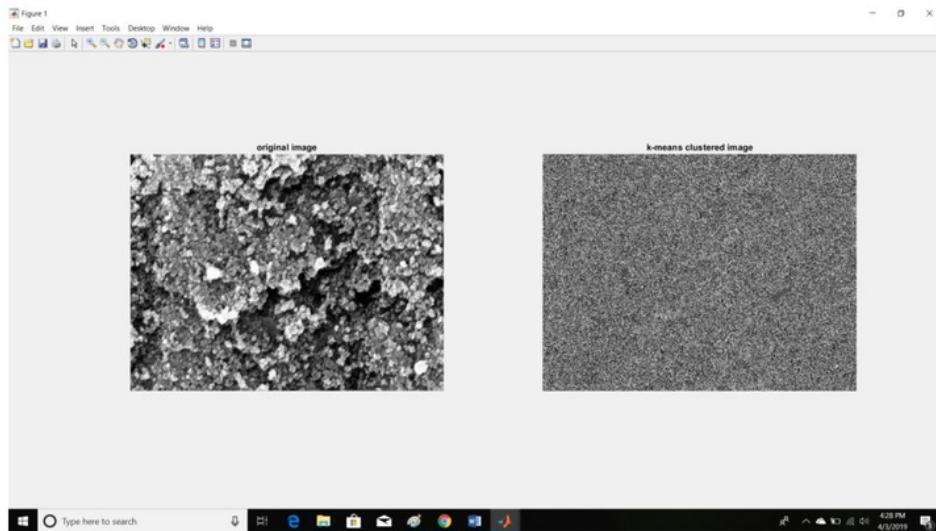
Fig. 6.19 MATLAB simulation of FESEM image of PS/ZnO-15 Coating.
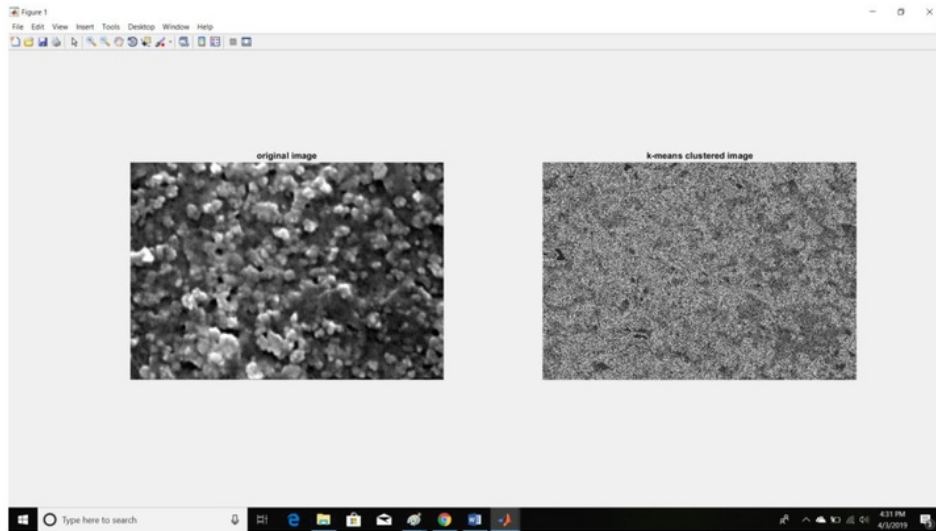
Fig. 6.20 MATLAB simulation of FESEM image of PS/ZnO-20 Coating.
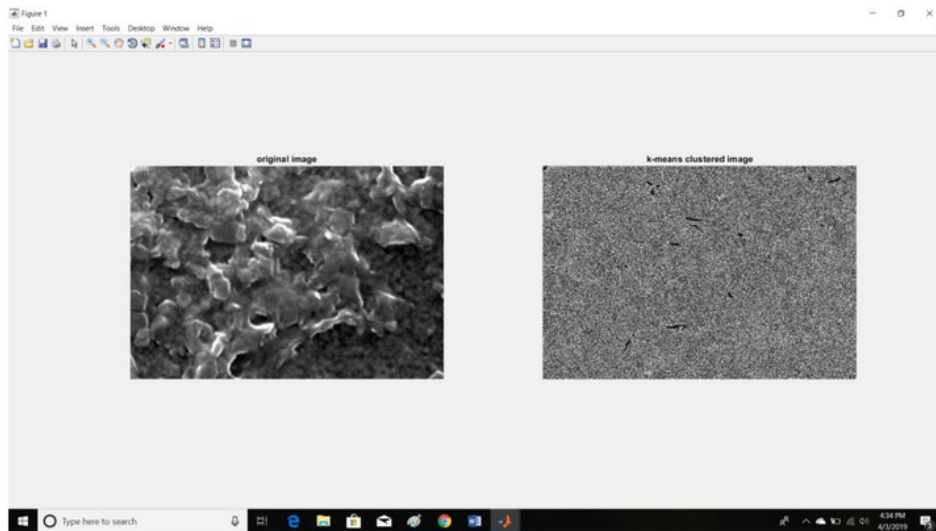
Fig. 6.21 MATLAB simulation of FESEM image of PS/ZnO-25 Coating.

Table 6.1 MATLAB simulation time predicted a score

S. No.	Image	Total Simulation Time (s)	K-Means simulation time (s)	Cluster Size	Error %	Score
1	PS/TOS-SiO$_2$ coating-Sample 1	2.555	2.272	128	7.885	0.921
2	PS/TOS-SiO$_2$ coating-Sample 2	4.240	3.927	128	10.700	0.893
3	PS/TOS-SiO$_2$ coating-Sample 3	2.501	2.205	128	9.292	0.907
4	PS/TOS-SiO$_2$ coating-Sample 4	4.269	3.931	128	8.840	0.911
5	PS/TOS-SiO$_2$ coating-Sample 5	4.358	4.043	128	10.404	0.895
6	PS/ZnO-1 Coating	3.130	2.828	128	10.858	0.891
7	PS/ZnO-5 Coating	4.204	3.883	128	8.922	0.910
8	PS/ZnO-10 Coating	4.291	4.004	128	5.329	0.946
9	PS/ZnO-15 Coating	4.395	4.075	128	7.870	0.921
10	PS/ZnO-20 Coating	1.876	1.605	128	5.773	0.942
11	PS/ZnO-25 Coating	1.933	1.652	128	4.84	0.951

98
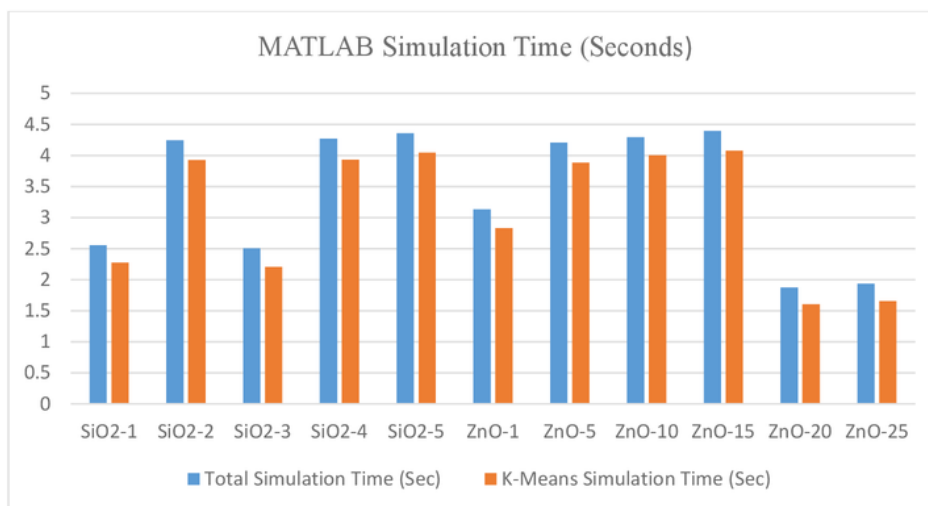
Fig. 6.22 Simulation time graph for FESEM images of SiO_2 and ZnO embedded PS based transparent SHCs.

The Fig. 6.22 Simulation time graph for FESEM images. The machine learning approach for Sample No. 1 to 11 predicts that the score values against samples are 0.921, 0.893, 0.907, 0.911, 0.895, 0.891, 0.910, 0.946, 0.921, 0.942 and 0.951 for PS/TOS-SiO_2 coating-Sample 1, PS/TOS-SiO_2 coating-Sample 2, PS/TOS-SiO_2 coating-Sample 3, PS/TOS-SiO_2 coating-Sample 4, PS/TOS-SiO_2 coating-Sample 5, PS/ZnO-1 Coating, PS/ZnO-5 Coating, PS/ZnO-10 Coating, PS/ZnO-15 Coating, PS/ZnO-20 Coating, and PS/ZnO-25 Coating, respectively. This score estimates the accuracy of the results in terms of roughness. The roughness is also analyzed with MATLAB Image processing tool based Machine learning K means clustering model [86], [89], [134], [143], [144]. The experimental results and machine-learning model based predicated results are closer. The machine learning approach predicates that the achieved results are having 91.70 % accuracy against roughness. The performance of the superhydrophobic coated material is good [89].

6.6. CONCLUSIONS

The pattern recognition and image analysis tools are helpful to handle the large volumes of image data in short time. FESEM images were processed, segmented

and applied under wavelet processing. The machine learning approach based on K-means clustering estimated the roughness of SHCs using FESEM images. The MATLAB tool inbuilt features were used for the FESEM image segmentation, wavelet processing, analysis and score prediction. The computational statistical techniques-based image segmentation follows HAAR DWT sub-band processing in which the images were divided in LL, LH, HL and HH bands with 128 pixels as the common cluster size for all the FESEM images of the SHCs. The performance of the roughness estimation using FESEM images was found good as the tool predicted the score 91.70 % against roughness parameter.

CHAPTER 7. CONCLUSIONS AND FUTURE SCOPE

7.1. CONCLUSIONS

- Surface functionalized nanoparticles filled polymer-based transparent SHCs were successfully prepared using a facile sol-gel route. Polystyrene polymer was used as the host matrix and nano-size ZnO and SiO_2 were used as the fillers to develop the coatings on glass substrates. The roughness of the coatings was optimized with respect to the concentration of the nanoparticles, functionalizing agents and process parameters.

- The ZnO nanoparticles were dual-functionalized using TMCS and MPMS functionalizing agents and uniformly dispersed in PS to achieve the surface roughness of ~ 28 nm with a maximum CA of 152° and SA of 3°. The transparency close to the transmittance of bare glass has been obtained for the PS/ZnO based SHCs.

- TOS-functionalized SiO_2 nanoparticles were embedded in PS to prepare transparent SHC using a simple sol-gel technique. The dip/pull speed and dipping time were optimized to control the superhydrophobicity and the transparency of the developed coating. The maximum roughness of 65.39 ± 6.7 nm with unique morphology was obtained, which was found responsible for the high CA of $162 \pm 2°$ and SA of $3 \pm 1°$. High average transmittance of $91.8 \pm 0.5\%$ which was close to the average transmittance of bare glass ($92.6 \pm 0.2\%$) achieved for the SHC.

- FESEM images were processed, segmented and applied under wavelet processing. The machine learning approach based on K-means clustering

estimated the roughness of SHCs using FESEM images. The MATLAB was used for the FESEM image segmentation, wavelet processing, analysis and score prediction. The performance of the roughness estimation using FESEM images was found good as the tool predicted the score 91.70 % against roughness parameter.

7.2. FUTURE SCOPE

- The sol-gel method assisted with spin coating and dip/pulling route has a great potential to prepare transparent SHCs for many industrial applications.
- The developed transparent SHC can be used for the self-cleaning application of the cover glass of commercial solar panels.
- The efficiency of the uncoated and transparent superhydrophobic film-coated solar panels can be studied and compared to develop a commercial product.
- For the coating of the large area of the cover glass of solar panels, spray-coating can be used.
- The pattern analysis of SHCs using K-Means Clustering can be done for other important parameters such as transparency of the coating, quality of nanoparticle dispersion in a polymer matrix, etc.

CHAPTER 8. REFERENCES

References:

[1]   H. J. Gwon *et al.*, "Superhydrophobic and antireflective nanograss-coated glass for high performance solar cells," *Nano Res.*, vol. 7, no. 5, pp. 670–678, May 2014.

[2]   I. Kartini, S. J. Santosa, E. Febriyanti, O. R. Nugroho, H. Yu, and L. Wang, "Hybrid assembly of nanosol titania and dodecylamine for superhydrophobic self-cleaning glass," *J. Nanoparticle Res.*, vol. 16, no. 7, p. 2514, Jul. 2014.

[3]   M. S. Goyat, S. Ray, and P. K. Ghosh, "Innovative application of ultrasonic mixing to produce homogeneously mixed nanoparticulate-epoxy composite of improved physical properties," *Compos. Part A Appl. Sci. Manuf.*, vol. 42, no. 10, pp. 1421–1431, 2011.

[4]   P. K. Ghosh, A. Pathak, M. S. Goyat, and S. Halder, "Influence of nanoparticle weight fraction on morphology and thermal properties of epoxy/TiO2 nanocomposite," *J. Reinf. Plast. Compos.*, vol. 31, no. 17, pp. 1180–1188, 2012.

[5]   J. Kreuter, "Nanoparticles-a historical perspective," *International Journal of Pharmaceutics*, vol. 331, no. 1. pp. 1–10, 22-Feb-2007.

[6]   S. Chen and D. L. Carroll, "Synthesis and Characterization of Truncated Triangular Silver Nanoplates," *Nano Lett.*, vol. 2, no. 9, pp. 1003–1007, 2002.

[7]   E. Burkarter, C. K. Saul, F. Thomazi, N. C. Cruz, L. S. Roman, and W. H. Schreiner, "Superhydrophobic electrosprayed PTFE," *Surf. Coatings Technol.*, vol. 202, no. 1, pp. 194–198, Nov. 2007.

[8]   R. N. Wenzel, "Resistance of solid surfaces to wetting by water," *Ind. Eng. Chem.*, vol. 28, no. 8, pp. 988–994, Aug. 1936.

[9]   A. B. D. Cassie and S. Baxter, "Wettability of porous surfaces," *Trans. Faraday Soc.*, vol. 40, no. 0, pp. 546–551, Jan. 1944.

[10]   W. Barthlott and C. Neinhuis, "Purity of the sacred lotus, or escape from contamination in biological surfaces," *Planta*, vol. 202, no. 1, pp. 1–8, Apr. 1997.

[11]   C. Neinhuis and W. Barthlott, "Characterization and distribution of water-repellent, self-cleaning plant surfaces," *Ann. Bot.*, vol. 79, no. 6, pp. 667–677, Jun. 1997.

[12]   D. Wang, Z. Zhang, Y. Li, and C. Xu, "Highly transparent and durable superhydrophobic hybrid nanoporous coatings fabricated from polysiloxane," *ACS Appl. Mater. Interfaces*, vol. 6, no. 13, pp. 10014–10021, Jul. 2014.

[13]   T. Zhao, D. Zhang, C. Ding, J. Zhou, J. Zhu, and L. Jiang, "A multi-functional polymer coating that is heat-resistant, hydrophobic and transparent," *Particuology*, vol. 17, pp. 11–14, Dec. 2014.

[14]   L. Cao, A. K. Jones, V. K. Sikka, J. Wu, and D. Gao, "Anti-Icing superhydrophobic coatings," *Langmuir*, vol. 25, no. 21, pp. 12444–12448, Nov. 2009.

[15]   V. Bahadur, L. Mishchenko, B. Hatton, J. A. Taylor, J. Aizenberg, and T. Krupenkin, "Predictive model for ice formation on superhydrophobic surfaces," *Langmuir*, vol. 27, no. 23, pp. 14143–14150, Dec. 2011.

[16]   S. Jung, M. Dorrestijn, D. Raps, A. Das, C. M. Megaridis, and D. Poulikakos, "Are superhydrophobic surfaces best for icephobicity?," *Langmuir*, vol. 27, no. 6, pp. 3059–3066, Mar. 2011.

[17]   S. Jung, M. K. Tiwari, N. V. Doan, and D. Poulikakos, "Mechanism of supercooled droplet freezing on surfaces," *Nat. Commun.*, vol. 3, no. 1, p. 615, Jan. 2012.

[18]   L. Mishchenko, B. Hatton, V. Bahadur, J. A. Taylor, T. Krupenkin, and J. Aizenberg, "Design of ice-free nanostructured surfaces based on repulsion of impacting water droplets," *ACS Nano*, vol. 4, no. 12, pp. 7699–7707, Dec. 2010.

[19]   A. Satyaprasad, V. Jain, and S. K. Nema, "Deposition of superhydrophobic

nanostructured Teflon-like coating using expanding plasma arc," *Appl. Surf. Sci.*, vol. 253, no. 12, pp. 5462–5466, Apr. 2007.

[20] M. S. Kavale *et al.*, "Optically transparent, superhydrophobic methyltrimethoxysilane based silica coatings without silylating reagent," *Appl. Surf. Sci.*, vol. 258, no. 1, pp. 158–162, Oct. 2011.

[21] H. Yu *et al.*, "Bionic micro-nano-bump-structures with a good self-cleaning property: The growth of ZnO nanoarrays modified by polystyrene spheres," *Mater. Chem. Phys.*, vol. 170, pp. 52–61, Feb. 2016.

[22] N. Perkas, G. Amirian, O. Girshevitz, and A. Gedanken, "Hydrophobic coating of GaAs surfaces with nanostructured ZnO," *Mater. Lett.*, vol. 175, pp. 101–105, 2016.

[23] C. Jiang and W. Li, "A facile method for preparations of micro-nanotextured Co3O 4 films with the excellent superhydrophobic and anti-icing behavior," *Mater. Lett.*, vol. 122, pp. 133–138, 2014.

[24] B. Dudem, J. H. Heo, J. W. Leem, J. S. Yu, and S. H. Im, "CH $_3$ NH $_3$ PbI $_3$ planar perovskite solar cells with antireflection and self-cleaning function layers," *J. Mater. Chem. A*, vol. 4, no. 20, pp. 7573–7579, 2016.

[25] N. J. Shirtcliffe, G. McHale, S. Atherton, and M. I. Newton, "An introduction to superhydrophobicity," *Advances in Colloid and Interface Science*, vol. 161, no. 1–2. pp. 124–138, 2010.

[26] J. Kessler, "Air and water: The biology and physics of life's media Mark W. Denny, Princeton University Press, Princeton, 1993. $39.50 (cloth), xvii + 341pp.," *Bull. Math. Biol.*, vol. 58, no. 2, pp. 399–400, Oct. 2003.

[27] A. D. Carlson, "The Extended Organism: The Physiology of Animal-Built Structures . J. Scott Turner," *Q. Rev. Biol.*, vol. 76, no. 2, pp. 270–270, Mar. 2004.

[28] M. Nosonovsky and B. Bhushan, *Multiscale Dissipative Mechanisms and Hierarchical Surfaces*. 2008.

[29] E. Orowan, "Surface Energy and Surface Tension in Solids and Liquids," *Proc. R. Soc. A Math. Phys. Eng. Sci.*, vol. 316, no. 1527, pp. 473–491, 2006.

[30] V. K. Kumikov and K. B. Khokonov, "On the measurement of surface free energy and surface tension of solid metals," *J. Appl. Phys.*, vol. 54, no. 3, pp. 1346–1350, 1983.

[31] S. W. Ip and J. M. Toguri, "The equivalency of surface tension, surface energy and surface free energy," *J. Mater. Sci.*, vol. 29, no. 3, pp. 688–692, 1994.

[32] R. Blossey, "Self-cleaning surfaces - Virtual realities," *Nat. Mater.*, vol. 2, no. 5, pp. 301–306, 2003.

[33] P. G. De Gennes, "Wetting: Statics and dynamics," *Rev. Mod. Phys.*, vol. 57, no. 3, pp. 827–863, 1985.

[34] L. Leger and J. F. Joanny, "Liquid spreading," *Reports Prog. Phys.*, vol. 55, no. 4, pp. 431–486, 1992.

[35] G. McHale, N. A. Käb, M. I. Newton, and S. M. Rowan, "Wetting of a high-energy fiber surface," *J. Colloid Interface Sci.*, 1997.

[36] L. Gao and T. J. McCarthy, "Teflon is hydrophilic. Comments on definitions of hydrophobic, shear versus tensile hydrophobicity, and wettability characterization," *Langmuir*, vol. 24, no. 17, pp. 9183–9188, 2008.

[37] G. McHale, N. J. Shirtcliffe, and M. I. Newton, "Super-hydrophobic and super-wetting surfaces: Analytical potential?," *Analyst*, vol. 129, no. 4. pp. 284–287, 2004.

[38] M. Callies and D. Quéré, "On water repellency," *Soft Matter*, vol. 1, no. 1. pp. 55–61, 2005.

[39] R. N. Wenzel, "Resistance of solid surfaces to wetting by water," *Ind. Eng. Chem.*, vol. 28, no. 8, pp. 988–994, 1936.

[40] R. N. Wenzel, "Surface roughness and contact angle," *J. Phys. Colloid Chem.*, vol. 53, no. 9, pp. 1466–1467, Sep. 1949.

[41] Y. Y. Yan, N. Gao, and W. Barthlott, "Mimicking natural superhydrophobic surfaces and grasping the wetting process: A review on recent progress in preparing superhydrophobic surfaces," *Advances in Colloid and Interface Science*, vol. 169, no. 2. pp. 80–105, 2011.

[42] N. A. Patankar, "Transition between superhydrophobic states on rough surfaces," *Langmuir*, vol. 20, no. 17, pp. 7097–7102, 2004.

[43] K. Koch, B. Bhushan, and W. Barthlott, "Diversity of structure, morphology and wetting of plant surfaces," *Soft Matter*, vol. 4, no. 10, pp. 1943–1963, Sep. 2008.

[44] X. Zhang, F. Shi, J. Niu, Y. Jiang, and Z. Wang, "Superhydrophobic surfaces: From structural control to functional application," *J. Mater. Chem.*, vol. 18, no. 6, pp. 621–633, 2008.

[45] C. J. Long, J. F. Schumacher, and A. B. Brennan, "Potential for tunable static and dynamic contact angle anisotropy on gradient microscale patterned topographies," *Langmuir*, vol. 25, no. 22, pp. 12982–12989, 2009.

[46] C. W. Extrand, "Model for contact angles and hysteresis on rough and ultraphobic surfaces," *Langmuir*, vol. 18, no. 21, pp. 7991–7999, 2002.

[47] H. Kim, M. H. Kim, and J. Kim, "Wettability of dual-scaled surfaces fabricated by the combination of a conventional silicon wet-etching and a ZnO solution method," *J. Micromechanics Microengineering*, vol. 19, no. 9, 2009.

[48] H. E. Jeong, M. K. Kwak, C. I. Park, and K. Y. Suh, "Wettability of nanoengineered dual-roughness surfaces fabricated by UV-assisted capillary force lithography," *J. Colloid Interface Sci.*, vol. 339, no. 1, pp. 202–207, Nov. 2009.

[49] J. T. Simpson, S. R. Hunter, and T. Aytug, "Superhydrophobic materials and coatings: A review," *Reports Prog. Phys.*, vol. 78, no. 8, pp. 21–26, Jul. 2015.

[50] J. Feng, M. T. Tuominen, and J. P. Rothstein, "Hierarchical superhydrophobic surfaces fabricated by dual-scale electron-beam-lithography with well-ordered secondary nanostructures," *Adv. Funct. Mater.*, vol. 21, no. 19, pp. 3715–3722, Aug. 2011.

[51] B. Bhushan and Y. C. Jung, "Natural and biomimetic artificial surfaces for superhydrophobicity, self-cleaning, low adhesion, and drag reduction,"

107

Prog. Mater. Sci., vol. 56, no. 1, pp. 1–108, 2011.

[52] M. A. Aegerter, R. Almeida, A. Soutar, K. Tadanaga, H. Yang, and T. Watanabe, "Coatings made by sol–gel and chemical nanotechnology," *J. Sol-Gel Sci. Technol.*, vol. 47, no. 2, pp. 203–236, Aug. 2008.

[53] N. Miljkovic, R. Enright, and E. N. Wang, "Modeling and optimization of superhydrophobic condensation," *J. Heat Transfer*, vol. 135, no. 11, p. 111004, 2013.

[54] J. Stoddard, J. Crockett, and D. Maynes, "Droplet Train Impingement on Superhydrophobic Surfaces," in *Bulletin of the American Physical Society*, 2014, p. D13.004.

[55] F. M. Chang, Y. J. Sheng, H. Chen, and H. K. Tsao, "From superhydrophobic to superhydrophilic surfaces tuned by surfactant solutions," *Appl. Phys. Lett.*, vol. 91, no. 9, p. 094108, 2007.

[56] G. Barati Darband, M. Aliofkhazraei, S. Khorsand, S. Sokhanvar, and A. Kaboli, "Science and Engineering of Superhydrophobic Surfaces: Review of Corrosion Resistance, Chemical and Mechanical Stability," *Arab. J. Chem.*, 2018.

[57] B. Zhang, X. Zhao, Y. Li, and B. Hou, "Fabrication of durable anticorrosion superhydrophobic surfaces on aluminum substrates via a facile one-step electrodeposition approach," *RSC Adv.*, vol. 6, no. 42, pp. 35455–35465, 2016.

[58] S. He *et al.*, "Preparation and properties of ZnO nanostructures by electrochemical anodization method," *Appl. Surf. Sci.*, vol. 256, no. 8, pp. 2557–2562, Feb. 2010.

[59] H. Meng, S. Wang, J. Xi, Z. Tang, and L. Jiang, "Facile means of preparing superamphiphobic surfaces on common engineering metals," *J. Phys. Chem. C*, vol. 112, no. 30, pp. 11454–11458, Jul. 2008.

[60] M. Zhu, W. Zuo, H. Yu, W. Yang, and Y. Chen, "Superhydrophobic surface directly created by electrospinning based on hydrophilic material," *J. Mater. Sci.*, vol. 41, no. 12, pp. 3793–3797, Jun. 2006.

[61] A. Tuteja *et al.*, "Designing superoleophobic surfaces," *Science (80-.).*, vol. 318, no. 5856, pp. 1618–1622, Dec. 2007.

[62] J. Zheng, A. He, J. Li, J. Xu, and C. C. Han, "Studies on the controlled morphology and wettability of polystyrene surfaces by electrospinning or electrospraying," *Polymer (Guildf).*, vol. 47, no. 20, pp. 7095–7102, Sep. 2006.

[63] J. C. Ge, J. H. Kim, and N. J. Choi, "Electrospun polyurethane/loess powder hybrids and their absorption of volatile organic compounds," *Adv. Mater. Sci. Eng.*, vol. 2016, 2016.

[64] S. Yan, M. Li, L. Sun, Q. Jiao, and R. Huang, "Fabrication of Nano- and Micron- Sized Spheres of CL-20 by Electrospray," *Cent. Eur. J. Energ. Mater.*, vol. 15, no. 4, pp. 572–589, 2018.

[65] B. Ding, T. Ogawa, J. Kim, K. Fujimoto, and S. Shiratori, "Fabrication of a super-hydrophobic nanofibrous zinc oxide film surface by electrospinning," *Thin Solid Films*, vol. 516, no. 9, pp. 2495–2501, 2008.

[66] Z. Cai, J. Lin, and X. Hong, "Transparent superhydrophobic hollow films (TSHFs) with superior thermal stability and moisture resistance," *RSC Adv.*, vol. 8, no. 1, pp. 491–498, 2018.

[67] A. Hozumi, D. F. Cheng, and M. Yagihashi, "Hydrophobic/superhydrophobic oxidized metal surfaces showing negligible contact angle hysteresis," *J. Colloid Interface Sci.*, vol. 353, no. 2, pp. 582–587, Jan. 2011.

[68] C. Te Hsieh, W. Y. Chen, and F. L. Wu, "Fabrication and superhydrophobicity of fluorinated carbon fabrics with micro/nanoscaled two-tier roughness," *Carbon N. Y.*, vol. 46, no. 9, pp. 1218–1224, Aug. 2008.

[69] J. A. Syed, S. Tang, and X. Meng, "Super-hydrophobic multilayer coatings with layer number tuned swapping in surface wettability and redox catalytic anti-corrosion application," *Sci. Rep.*, vol. 7, no. 1, pp. 1–17, 2017.

[70] Y. Zhao, Y. Tang, X. Wang, and T. Lin, "Superhydrophobic cotton fabric fabricated by electrostatic assembly of silica nanoparticles and its

109

remarkable buoyancy," *Appl. Surf. Sci.*, vol. 256, no. 22, pp. 6736–6742, Sep. 2010.

[71] D. Qi *et al.*, "Simple approach to wafer-scale self-cleaning antireflective silicon surfaces," *Langmuir*, vol. 25, no. 14, pp. 7769–7772, Jul. 2009.

[72] M. Li, J. Xu, and Q. Lu, "Creating superhydrophobic surfaces with flowery structures on nickel substrates through a wet-chemical-process," *J. Mater. Chem.*, vol. 17, no. 45, pp. 4772–4776, 2007.

[73] Y. Wang, W. Wang, L. Zhong, J. Wang, Q. Jiang, and X. Guo, "Super-hydrophobic surface on pure magnesium substrate by wet chemical method," *Appl. Surf. Sci.*, vol. 256, no. 12, pp. 3837–3840, Apr. 2010.

[74] L. Pan, H. Dong, and P. Bi, "Facile preparation of superhydrophobic copper surface by HNO 3 etching technique with the assistance of CTAB and ultrasonication," *Appl. Surf. Sci.*, vol. 257, no. 5, pp. 1707–1711, Dec. 2010.

[75] H. S. Khoo and F. G. Tseng, "Engineering the 3D architecture and hydrophobicity of methyltrichlorosilane nanostructures," *Nanotechnology*, vol. 19, no. 34, Aug. 2008.

[76] N. Yang, J. Li, N. Bai, L. Xu, and Q. Li, "One step phase separation process to fabricate superhydrophobic PVC films and its corrosion prevention for AZ91D magnesium alloy," *Mater. Sci. Eng. B Solid-State Mater. Adv. Technol.*, vol. 209, pp. 1–9, Jul. 2016.

[77] W. Song, V. S. Gaware, Ö. V. Rúnarsson, M. Másson, and J. F. Mano, "Functionalized superhydrophobic biomimetic chitosan-based films," *Carbohydr. Polym.*, vol. 81, no. 1, pp. 140–144, May 2010.

[78] A. Pozzato *et al.*, "Superhydrophobic surfaces fabricated by nanoimprint lithography," *Microelectron. Eng.*, vol. 83, no. 4-9 SPEC. ISS., pp. 884–888, Apr. 2006.

[79] Y. Yang, H. He, Y. Li, and J. Qiu, "Using Nanoimprint Lithography to Create Robust, Buoyant, Superhydrophobic PVB/SiO2 Coatings on wood Surfaces Inspired by Red roses petal," *Sci. Rep.*, vol. 9, no. 1, pp. 1–9, 2019.

[80] Y. Chen *et al.*, "Transparent superhydrophobic/superhydrophilic coatings

110

for self-cleaning and anti-fogging," *Appl. Phys. Lett.*, vol. 101, no. 3, 2012.

[81] J. Yuan, J. Wang, K. Zhang, and W. Hu, "Fabrication and properties of a superhydrophobic film on an electroless plated magnesium alloy," *RSC Adv.*, vol. 7, no. 46, pp. 28909–28917, 2017.

[82] A. K. Singh and J. K. Singh, "Fabrication of durable superhydrophobic coatings on cotton fabrics with photocatalytic activity by fluorine-free chemical modification for dual-functional water purification," *New J. Chem.*, vol. 41, no. 11, pp. 4618–4628, 2017.

[83] X. Zhang *et al.*, "A one-pot sol-gel process to prepare a superhydrophobic and environment-resistant thin film from ORMOSIL nanoparticles," *RSC Adv.*, vol. 4, no. 19, pp. 9838–9841, 2014.

[84] P. Zhang and F. Y. Lv, "A review of the recent advances in superhydrophobic surfaces and the emerging energy-related applications," *Energy*, vol. 82, pp. 1068–1087, 2015.

[85] A. Adeem, F. Hammad, and M. Shaban, "Composite Material Surface Analysis based Image Texture Analysis," *Int. J. Comput. Appl.*, vol. 129, no. 1, pp. 22–26, 2015.

[86] Y. Farhang, "Face Extraction from Image based on K-Means Clustering Algorithms," 2017.

[87] S.-J. Byun *et al.*, "An efficient simulation and analysis method of moiré patterns in display systems," *Opt. Express*, vol. 22, no. 3, p. 3128, 2014.

[88] H. Liu, C. Zhang, and D. Huang, "Extreme Learning Machine and Moving Least Square Regression Based Solar Panel Vision Inspection," *J. Electr. Comput. Eng.*, vol. 2017, pp. 1–10, May 2017.

[89] A. Duman, B. Yilbas, H. Pirim, and H. Ali, "Texture Analysis of Hydrophobic Polycarbonate and Polydimethylsiloxane Surfaces via Persistent Homology," *Coatings*, vol. 7, no. 9, p. 139, Sep. 2017.

[90] S. Z. Maw, T. T. Zin, M. Yokota, and E. P. Min, "Classification of shape images using K-means clustering and deep learning," *ICIC Express Lett.*, vol. 12, no. 10, pp. 1017–1023, 2018.

[91] N. A. Hameed, I. M. Ali, and H. K. Hassun, "Calculating surface roughness for a large scale sem images by mean of image processing," *Energy Procedia*, vol. 157, pp. 84–89, 2019.

[92] I. Arzate-Vázquez, J. V. Méndez-Méndez, E. A. Flores-Johnson, J. Nicolás-Bermúdez, J. J. Chanona-Pérez, and E. Santiago-Cortés, "Study of the porosity of calcified chicken eggshell using atomic force microscopy and image processing," *Micron*, vol. 118, no. December 2018, pp. 50–57, 2019.

[93] S. Zhao, Y. Li, Y. Wang, Z. Ma, and X. Huang, "Quantitative study on coal and shale pore structure and surface roughness based on atomic force microscopy and image processing," *Fuel*, vol. 244, no. January, pp. 78–90, 2019.

[94] H. Zhang, C. He, D. Lu, and M. Yu, "SEM image processing of PP/Rice husk composite using MATLAB," *Appl. Mech. Mater.*, vol. 214, pp. 27–30, 2012.

[95] S. Nagappan, J. J. Park, S. S. Park, and C.-S. Ha, "Preparation of superhydrophobic and transparent micro-nano hybrid coatings from polymethylhydroxysiloxane and silica ormosil aerogels," *Nano Converg.*, vol. 1, no. 1, p. 30, Dec. 2014.

[96] J. A. Howarter and J. P. Youngblood, "Self-Cleaning and Anti-Fog Surfaces via Stimuli-Responsive Polymer Brushes," *Adv. Mater.*, vol. 19, no. 22, pp. 3838–3843, Nov. 2007.

[97] S. A. Mahadik *et al.*, "Thermally stable and transparent superhydrophobic sol–gel coatings by spray method," *J. Sol-Gel Sci. Technol.*, vol. 63, no. 3, pp. 580–586, Sep. 2012.

[98] L. Xu, R. G. Karunakaran, J. Guo, and S. Yang, "Transparent, Superhydrophobic Surfaces from One-Step Spin Coating of Hydrophobic Nanoparticles," *ACS Appl. Mater. Interfaces*, vol. 4, no. 2, pp. 1118–1125, Feb. 2012.

[99] Y. Rahmawan, L. Xu, and S. Yang, "Self-assembly of nanostructures towards transparent, superhydrophobic surfaces," *J. Mater. Chem. A*, vol. 1,

112

no. 9, pp. 2955–2969, 2013.

[100] R. G. Karunakaran, C.-H. Lu, Z. Zhang, and S. Yang, "Highly Transparent Superhydrophobic Surfaces from the Coassembly of Nanoparticles (≤100 nm)," *Langmuir*, vol. 27, no. 8, pp. 4594–4602, Apr. 2011.

[101] M. K. Tiwari, I. S. Bayer, G. M. Jursich, T. M. Schutzius, and C. M. Megaridis, "Highly Liquid-Repellent, Large-Area, Nanostructured Poly(vinylidene fluoride)/Poly(ethyl 2-cyanoacrylate) Composite Coatings: Particle Filler Effects," *ACS Appl. Mater. Interfaces*, vol. 2, no. 4, pp. 1114–1119, Apr. 2010.

[102] J. Li *et al.*, "Stable superhydrophobic coatings from thiol-ligand nanocrystals and their application in oil/water separation," *J. Mater. Chem.*, vol. 22, no. 19, pp. 9774–9781, 2012.

[103] H. Budunoglu, A. Yildirim, M. O. Guler, and M. Bayindir, "Highly Transparent, Flexible, and Thermally Stable Superhydrophobic ORMOSIL Aerogel Thin Films," *ACS Appl. Mater. Interfaces*, vol. 3, no. 2, pp. 539–545, Feb. 2011.

[104] A. Nakajima, K. Hashimoto, T. Watanabe, K. Takai, G. Yamauchi, and A. Fujishima, "Transparent superhydrophobic thin films with self-cleaning properties," *Langmuir*, vol. 16, no. 17, pp. 7044–7047, Aug. 2000.

[105] L. Xu and J. He, "Fabrication of Highly Transparent Superhydrophobic Coatings from Hollow Silica Nanoparticles," *Langmuir*, vol. 28, no. 19, pp. 7512–7518, May 2012.

[106] J. Lin, H. Chen, T. Fei, C. Liu, and J. Zhang, "Highly transparent and thermally stable superhydrophobic coatings from the deposition of silica aerogels," *Appl. Surf. Sci.*, vol. 273, pp. 776–786, 2013.

[107] Z. C. Yuekun Lai, Yuxin Tang, Jiaojiao Gong, Dangguo Gong, Lifeng Chi, Changjian Lin, "Transparent superhydrophobic/superhydrophilic TiO2-based coatings for self-cleaning and anti- fogging," *J. Mater. Chem.*, vol. 22, no. 15, pp. 7420–7426, 2012.

[108] S. S. Latthe and A. L. Demirel, "Polystyrene/octadecyltrichlorosilane

superhydrophobic coatings with hierarchical morphology," *Polym. Chem.*, vol. 4, no. 2, pp. 246–249, 2013.

[109] M. Y. Yüce and A. L. Demirel, "The effect of nanoparticles on the surface hydrophobicity of polystyrene," *Eur. Phys. J. B*, vol. 64, no. 3–4, pp. 493–497, Aug. 2008.

[110] A. K. Srivastava, M. Deepa, N. Bahadur, and M. S. Goyat, "Influence of Fe doping on nanostructures and photoluminescence of sol-gel derived ZnO," *Mater. Chem. Phys.*, vol. 114, no. 1, pp. 194–198, Mar. 2009.

[111] N. S. Pesika, Z. Hu, K. J. Stebe, and P. C. Searson, "Quenching of Growth of ZnO Nanoparticles by Adsorption of Octanethiol," *J. Phys. Chem. B*, vol. 106, no. 28, pp. 6985–6990, Jul. 2002.

[112] X. Feng, L. Feng, M. Jin, J. Zhai, L. Jiang, and D. Zhu, "Reversible Super-hydrophobicity to Super-hydrophilicity Transition of Aligned ZnO Nanorod Films," *J. Am. Chem. Soc.*, vol. 126, no. 1, pp. 62–63, Jan. 2004.

[113] G. Li *et al.*, "Tunable wettability in surface-modified ZnO-based hierarchical nanostructures," *Appl. Phys. Lett.*, vol. 92, no. 17, p. 173104, 2008.

[114] R.-D. Sun, A. Nakajima, A. Fujishima, T. Watanabe, and K. Hashimoto, "Photoinduced Surface Wettability Conversion of ZnO and TiO$_2$ Thin Films," *J. Phys. Chem. B*, vol. 105, no. 10, pp. 1984–1990, Mar. 2001.

[115] L. G. Bach *et al.*, "A facile route towards the synthesis of polystyrene/zinc oxide nanocomposites," *J. Nanosci. Nanotechnol.*, vol. 13, no. 1, pp. 694–697, 2013.

[116] R. A. Sperling *et al.*, "Size determination of (bio)conjugated water-soluble colloidal nanoparticles: A comparison of different techniques," *J. Phys. Chem. C*, vol. 111, no. 31, pp. 11552–11559, 2007.

[117] R. A. Sperling and W. J. Parak, "Surface modification, functionalization and bioconjugation of colloidal inorganic nanoparticles," *Phil. Trans. R. Soc. A*, vol. 368, pp. 1333–1383, 2010.

[118] T.-Y. Lo, Y.-C. Huang, Y.-N. Hsiao, C.-G. Chao, and W.-T. Whang, "Preparation of superhydrophobic polyimide films modified with

organosilicasol as effective anticorrosion coatings," *Surf. Coatings Technol.*, vol. 258, pp. 310–319, Nov. 2014.

[119] Y. Zheng, Y. He, Y. Qing, Z. Zhuo, and Q. Mo, "Formation of SiO2/polytetrafluoroethylene hybrid superhydrophobic coating," *Appl. Surf. Sci.*, vol. 258, no. 24, pp. 9859–9863, 2012.

[120] R. Choudhary, S. K. Venkatraman, A. Rana, and S. Swamiappan, "In vitro bioactivity studies of larnite and larnite/chitin composites prepared from biowaste for biomedical applications," *Bull. Mater. Sci.*, vol. 39, no. 5, pp. 1213–1221, 2016.

[121] M. Hu, S. Noda, T. Okubo, Y. Yamaguchi, and H. Komiyama, "Structure and morphology of self-assembled 3-mercaptopropyltrimethoxysilane layers on silicon oxide," *Appl. Surf. Sci.*, vol. 181, no. 3, pp. 307–316, 2001.

[122] K. L. Cho, I. I. Liaw, A. H.-F. Wu, and R. N. Lamb, "Influence of Roughness on a Transparent Superhydrophobic Coating," *J. Phys. Chem. C*, vol. 114, no. 25, pp. 11228–11233, Jul. 2010.

[123] A. Hooda, M. S. Goyat, R. Gupta, M. Prateek, M. Agrawal, and A. Biswas, "Synthesis of nano-textured polystyrene/ZnO coatings with excellent transparency and superhydrophobicity," *Mater. Chem. Phys.*, vol. 193, pp. 447–452, Jun. 2017.

[124] R. G. Karunakaran, C.-H. Lu, Z. Zhang, and S. Yang, "Highly Transparent Superhydrophobic Surfaces from the Coassembly of Nanoparticles (≤100 nm)," *Langmuir*, vol. 27, no. 8, pp. 4594–4602, Apr. 2011.

[125] M. Mani and R. Pillai, "Impact of dust on solar photovoltaic (PV) performance: Research status, challenges and recommendations," *Renew. Sustain. Energy Rev.*, vol. 14, no. 9, pp. 3124–3131, Dec. 2010.

[126] A. Nakajima, K. Hashimoto, T. Watanabe, K. Takai, G. Yamauchi, and A. Fujishima, "Transparent Superhydrophobic Thin Films with Self-Cleaning Properties," *Langmuir*, vol. 16, no. 17, pp. 7044–7047, Aug. 2000.

[127] X. Liu and J. He, "Superhydrophilic and Antireflective Properties of Silica Nanoparticle Coatings Fabricated via Layer-by-Layer Assembly and

Postcalcination," *J. Phys. Chem. C*, vol. 113, no. 1, pp. 148–152, Jan. 2009.

[128] S. Sutha, S. Suresh, B. Raj, and K. R. Ravi, "Transparent alumina based superhydrophobic self–cleaning coatings for solar cell cover glass applications," *Sol. Energy Mater. Sol. Cells*, vol. 165, pp. 128–137, Jun. 2017.

[129] D. M. Giolando, "Transparent self-cleaning coating applicable to solar energy consisting of nano-crystals of titanium dioxide in fluorine doped tin dioxide," *Sol. Energy*, vol. 124, pp. 76–81, 2016.

[130] H. Budunoglu, A. Yildirim, M. O. Guler, and M. Bayindir, "Highly Transparent, Flexible, and Thermally Stable Superhydrophobic ORMOSIL Aerogel Thin Films," *ACS Appl. Mater. Interfaces*, vol. 3, no. 2, pp. 539–545, Feb. 2011.

[131] C. Li, Y. Sun, M. Cheng, S. Sun, and S. Hu, "Fabrication and characterization of a TiO2/polysiloxane resin composite coating with full-thickness super-hydrophobicity," *Chem. Eng. J.*, vol. 333, no. April 2017, pp. 361–369, 2018.

[132] C. Petcu *et al.*, "The Influence of New Hydrophobic Silica Nanoparticles on the Surface Properties of the Films Obtained from Bilayer Hybrids," *Nanomaterials*, vol. 7, no. 2, p. 47, 2017.

[133] N. Venkatathri, "Preparation of silica nanoparticle through coating with octyldecyltrimethoxy silane," *Indian J. Chem. - Sect. A Inorganic, Phys. Theor. Anal. Chem.*, vol. 46, no. 12, pp. 1955–1958, 2007.

[134] J. Pérez Ortega, M. D. R. Boone Rojas, and M. J. Somodevilla García, "Research issues on k-means algorithm: An experimental trial using Matlab," 2009.

[135] A. Likas, N. Vlassis, and J. J. Verbeek, "The global k-means clustering algorithm," *Pattern Recognit.*, vol. 36, no. 2, pp. 451–461, 2003.

[136] Sanyog Dubey and A. Singh, "Research Paper IMPLEMENTATION OF MATLAB-SIMULINK APPROACH IN SHUNT ACTIVE POWER FILTERS TO MINIMIZE THE Address for Correspondence," *Int. J. Adv.*

116

Eng. Res. Stud., no. Jan.-March, pp. 28–35, 2014.

[137] G. Tzortzis and A. Likas, "The MinMax k-Means clustering algorithm," *Pattern Recognit.*, vol. 47, no. 7, pp. 2505–2516, Jul. 2014.

[138] S. F. Hussain and M. Haris, "A k-means based co-clustering (kCC) algorithm for sparse, high dimensional data," *Expert Syst. Appl.*, vol. 118, pp. 20–34, Mar. 2019.

[139] J. M. Peña, J. A. Lozano, and P. Larrañaga, "An empirical comparison of four initialization methods for the K-Means algorithm," *Pattern Recognit. Lett.*, vol. 20, no. 10, pp. 1027–1040, 1999.

[140] M. Agoyi, E. Çelebi, and G. Anbarjafari, "A watermarking algorithm based on chirp z-transform, discrete wavelet transform, and singular value decomposition," *Signal, Image Video Process.*, vol. 9, no. 3, pp. 735–745, 2015.

[141] A. Kumar, P. Rastogi, and P. Srivastava, "Design and FPGA Implementation of DWT, Image Text Extraction Technique," in *Procedia Computer Science*, 2015, vol. 57, pp. 1015–1025.

[142] M. S. Hussain, T. Phuong Loan Hoang, and C. Langen, "A Design for Two-Dimensional Non-Causal Deslauriers-Dubuc Discrete Wavelet Transformation for Real-Time Video Processing on FPGA," in *2018 5th International Conference on Signal Processing and Integrated Networks, SPIN 2018*, 2018, pp. 69–72.

[143] D. O. Wirjadi, "Models and Algorithms for Image-Based Analysis of Microstructures," 2009.

[144] D. S. Bulgarevich, S. Tsukamoto, T. Kasuya, M. Demura, and M. Watanabe, "Pattern recognition with machine learning on optical microscopy images of typical metallurgical microstructures," *Sci. Rep.*, vol. 8, no. 1, p. 2078, Dec. 2018.

PUBLICATIONS

Research Publications in SCI-indexed Journals

1. **Amrita Hooda**, M.S. Goyat, Adesh Kumar, Rajeev Gupta, "A facile approach to develop modified nano-silica embedded polystyrene-based transparent superhydrophobic coating", Materials Letters, 233 (2018) 340–343. (ISSN No.: 0167-577X and **Impact Factor: 3.0**).

2. **Amrita Hooda**, M.S. Goyat, Rajeev Gupta, Manish Prateek, Megha Agrawal, Abhijit Biswas, "Synthesis of nano-textured polystyrene/ZnO coatings with excellent transparency and superhydrophobicity", Materials Chemistry and Physics, 193 (2017) 447-452. (ISSN No.: 0254-0584 and **Impact Factor: 2.78**).

3. **Amrita Hooda**, M.S. Goyat, Jitendra Kumar Pandey, Adesh Kumar, Rajeev Gupta, "A review on fundamentals, constraints, fabrication techniques and potential applications of superhydrophobic coatings, Progress in Organic Coatings, **Under Review**. (**ISSN No.: 0300-9440 and Impact Factor: 3.420).**

4. Adesh Kumar, **Amrita Hooda**, M.S. Goyat, Rajeev Gupta, "Superhydrophobic Coatings Roughness Behavior Study Using Image Processing and Machine Learning Approach" Energy Sources, Part A: Recovery, Utilization, and Environmental Effects, **Under Review**. (**ISSN No.: 1556-7230 and Impact Factor: 0.894).**

Publications in International Conference Proceedings

1. S. Mahato, A. Gupta, J. Justin, A. Tiwari, **A. Hooda**, R.K. Singh, M.S. Goyat, R. Gupta, A. Biswas, M. Agrawal, "Development of environment friendly superhydrophobic polystyrene/SiO_2 coatings via sol-gel route," in

Springer Proceedings in Energy: Nanotechnology for Energy and Water, 2017, pp. 19–24. (ISSN No. : 2352-2534).

2. S. Mahato, A. Gupta, J. Justin, A. Tiwari, **A. Hooda**, R. Gupta, P. Kuchhal, C. Pant, M.S. Goyat, "Development of Polystyrene/SiO$_2$ Superhydrophobic Coating on Metal Substrates for Corrosion Protection," in Springer Proceedings in Energy: Nanotechnology for Energy and Water, 2017, pp. 25–29. (ISSN No. : 2352-2534).

Papers Presented in International/National Conferences

1. **Amrita Hooda**, Rajeev Gupta, Adesh Kumar, "Development of Polymer-based Transparent and Superhydrophobic Coating for Solar Panel", International Conference on "Innovative Research in Engineering, Science and Technology, Akal College of Engineering and Technology, Eternal University, Baru Sahib, Himachal Pradesh, India from 7 – 8th April, 2017.

2. **Amrita Hooda**, Rajeev Gupta, Adesh Kumar, "Synthesis of transparent and superhydrophobic polystyrene-TiO$_2$ based coatings for energy applications", International Conference on " International Conference on Nanomaterials: Synthesis, Characterization and Applications (ICN 2018)", Mahatma Gandhi University, Kottayam, Kerala, India from on 11–13th May 2018.

CURRICULUM VITAE

Ms Amrita Hooda

Department of ECE

University of Petroleum and Energy Studies

Dehradun-248007, Uttarakhand, India

Mobile Nos.: +91-9927339249

E-mail : amu.hooda@gmail.com

ACADEMIC PERFORMANCE

Degree/ Standard	Board/University	Branch/Stream	Year of Passing	Percentage
M. Tech.	Maharshi Dayanand University (MDU), Rohtak	Electronics & Communication	2010	74.87
M.Sc.	Maharshi Dayanand University (MDU), Rohtak	Electronics	2007	69.36
B.Sc.	Maharshi Dayanand University (MDU), Rohtak	Non-medical	2005	60.00

PhD Current Status:- Submitted.

PhD Thesis Title:- Development and pattern analysis of superhydrophobic nanocomposite coating

M.Tech. Thesis Title:- Fabrication and Characterization of Porous Silicon

M.Tech. Project was executed at Kurukshetra University, Kurukshetra (KUK).

RESEARCH EXPERIENCE

Project Title: Development of Superhydrophobic transparent polymeric coating induced by ion beams to increase the efficiency of solar panel by self-cleaning process.

Duration:- 1 year

Funding agency: Inter-university Accelerator Centre (IUAC), New Delhi

Project Handling Institute:- University of Petroleum and Energy Studies (UPES)

TEACHING EXPERIENCE

Organization Name	Position held	Period	
		From	To
Matu Ram Institute of Engineering & Management, Rohtak, Haryana	Assistant Professor	18/08/2010	03/02/2012
Deenbandhu Chhotu Ram University of Science and Technology, Murthal, Sonepat, Haryana	Contractual Faculty	06/08/2012	31/11/2012
Deenbandhu Chhotu Ram University of Science and Technology, Murthal, Sonepat, Haryana	Contractual Faculty	23/01/2013	26/04/2013

COURSES TAUGHT

UG Level

- ➢ Microprocessor and Interfacing
- ➢ MOS IC
- ➢ Microwave and Radar Engineering
- ➢ Digital and Analog Communication

> ➢ Digital Signal Processing

PG Level

> ➢ Advanced Electronic Instrumentation

PUBLICATIONS IN INTERNATIONAL JOURNALS

1) **Amrita Hooda**, M.S. Goyat, Jitendra Kumar Pandey, Adesh Kumar, Rajeev Gupta*, "A review on fundamentals, hurdles, fabrication techniques and potential applications of superhydrophobic coatings, *Progress in Organic Coatings*, **Under Review. (ISSN No.: 0300-9440 and Impact Factor: 3.420).**

2) **Amrita Hooda**, Kamalpreet Kaur, M.S. Goyat, Jitendra Kumar Pandey, Tejendra Kumar Gupta, A.K. Upadhyay, B.S. Tewari, "A review on the toughening mechanisms of oxide nanoparticles reinforced epoxy composites, *Composites Part A: Applied Science and Manufacturing*, **Communicated. (ISSN No.: 1359-835X and Impact Factor: 6.282).**

3) Vipul Sharma, Vipul Sharma, M.S. Goyat*, **Amrita Hooda**, Jitendra Kumar Pandey, Adesh Kumar, Rajeev Gupta, Avani Upadhyay, Rajiv Prakash, John Baptist Kirabira, Prasanta Mandal, Prashant Bhargav, "Recent progress in nano-oxides and CNTs based corrosion resistant superhydrophobic coatings: a critical review", *Progress in Organic Coatings*, **Under Review. (ISSN No.: 0300-9440 and Impact Factor: 3.420).**

4) **Amrita Hooda**, M.S. Goyat, Adesh Kumar, Rajeev Gupta, "A facile approach to develop modified nano-silica embedded polystyrene-based transparent superhydrophobic coating", *Materials Letters,* 233 (2018) 340–343. **(ISSN No.: 0167-577X and Impact Factor: 3.019).**

5) **Amrita Hooda,** M.S. Goyat, Rajeev Gupta, Manish Prateek, Megha Agrawal, Abhijit Biswas, "Synthesis of nano-textured polystyrene/ZnO coatings with excellent transparency and superhydrophobicity", *Materials*

Chemistry and Physics, 193 (2017) 447-452. **(ISSN No.: 0254-0584 and Impact Factor: 2.781).**

6) S. Mahato, A. Gupta, J. Justin, A. Tiwari, **A. Hooda**, R.K. Singh, M.S. Goyat, R. Gupta, A. Biswas, M. Agrawal, "Development of environment friendly superhydrophobic polystyrene/SiO₂ coatings via sol-gel route," in Springer Proceedings in Energy: Nanotechnology for Energy and Water, 2017, pp. 19–24. **(ISSN No. : 2352-2534).**

7) S. Mahato, A. Gupta, J. Justin, A. Tiwari, **A. Hooda**, R. Gupta, P. Kuchhal, C. Pant, M.S. Goyat, "Development of Polystyrene /SiO₂ Superhydrophobic Coating on Metal Substrates for Corrosion Protection," in Springer Proceedings in Energy: Nanotechnology for Energy and Water, 2017, pp. 25–29. **(ISSN No. : 2352-2534).**

8) **Amrita Hooda**, "Performance study of a Multipath Routing in MANETs", *International journal of Electrical, Electronics & Mechanical Fundamentals*, Vol 01, Issue 01, May 2012.

9) **Amrita Hooda**, "New Approach to Avoid Selective Jamming in Wireless Networks", *International journal of Electrical, Electronics & Mechanical Fundamentals*, Vol 02, Issue 01, July 2012.

10) **Amrita Hooda**, "Measuring Efficiency of Random Delays Countermeasures in Embedded Software", *International journal of Electrical, Electronics & Mechanical Fundamentals*, Vol 03, Issue 01, Sept. 2012.

PAPERS PRESENTED IN INTERNATIONAL / NATIONAL CONFERENCES

1) **Amrita Hooda**, "Quantum mechanical effects in MUGFETs" Proceedings of National Conference on Challenges in Emerging Computer Technologies (CECT-2010) on 8th & 9th April, 2010 at Rayat & Bahra Institute of Engg. & Bio-Technology, (Mohali) Punjab.

2) **Amrita Hooda** and Rajiv Sharma, "Fabrication and Characterization of Porous Silicon" Proceedings of National conference on Global Challenges-

Role of Sciences & Technology in Giving Their Solutions, TIT&S" Bhiwani, Haryana, March 3-4, 2012.

3) M.S. Goyat and **Amrita Hooda**, "Synthesis and Characterization of Controlled Porous Silicon", Proceedings of National Conference on Advances in Material Science for Energy Applications (Amsea 2014), University of Petroleum and Energy Studies, Dehradun, Uttarakhand, India, 9-10 January 2014.

4) Manjeet Singh Goyat, **Amrita Hooda**, "Simplistic method for fabrication of superhydrophobic SiO_2/polymer nanocomposite coating" Proceedings of National conference on Biofuels and Bioenergy (NCBB 2015), University of Petroleum and Energy Studies, Dehradun, Uttarakhand, India, 12-13 June 2015.

5) M.S. Goyat, **Amrita Hooda**, "Thermomechanical response and toughening mechanisms of ZrO_2-epoxy nanocomposite", International Conference on Materials Science & Technology 2016 (ICMTech 2016), Conference Centre, Delhi University, New Delhi, India. $1 - 4^{th}$ March 2016.

6) **Amrita Hooda**, Rajeev Gupta, Adesh Kumar, "Development of Polymer-based Transparent and Superhydrophobic Coating for Solar Panel", International Conference on "Innovative Research in Engineering, Science and Technology, Akal College of Engineering and Technology, Eternal University, Baru Sahib, Himachal Pradesh, India from $7 - 8$th April, 2017.

7) **Amrita Hooda**, Rajeev Gupta, Adesh Kumar, "Synthesis of transparent and superhydrophobic polystyrene-TiO_2 based coatings for energy applications", International Conference on " International Conference on Nanomaterials: Synthesis, Characterization and Applications (ICN 2018)", Mahatma Gandhi University, Kottayam, Kerala, India from on $11-13$th May 2018.

COMPUTER SKILLS

➢ Basic knowledge of computer, Windows 2000/XP/98

STRENGTHS

➢ Good Communication Skills & Leadership Qualities.

➢ Interested to work as a Team.

➢ Self-Learning, Highly Motivated, Committed person with Professional attitude.

PERSONAL PROFILE

Date of Birth	: 15-01-1985
Husband's name	: Dr. Manjeet Singh Goyat
Sex	: Female
Marital Status	: Married
Languages Known	: Hindi and English
Hobbies	: Reading, Baseball, Volleyball
Permanent Address	: H.No. 2075, Sector-2(P), Rohtak-124001, Haryana
Contact Nos.	: +91-9927339249

EXTRA-CURRICULAR ACTIVITIES

➢ Participated in National Level Volleyball Tournament at School Level.

➢ Won the Cricket championship in College.

REFERENCES

➢ **Dr. Manish Mathew (Principal Scientist)**

Central Electronics Engineering Research Institute (CEERI)

CSIR, CEERI Pilani,

Rajasthan, India

Email-id: manish@ceeri.res.in

Contact No. : +91-9410542870

➢ **Dr. habil. Yogendra Kumar Mishra (Sr. Research Officer)**

Institute for Materials Science and Technology for Silicon-Based Micro-
and Nanosystems, Institute for Electrical Engineering,
University of Kiel, Kaiserstrasse 2, 24143 Kiel,
Germany
Contact No. : +49-15781879898

➢ **Dr. Rajeev Kumar Gupta (Sr. Associate Prof. & Former Head)**
Department of Physics,
University of Petroleum and Energy Studies,
Dehradun, India.
Email-id: rajeev@ddn.upes.ac.in
Contact No. : +91-9897716629

DECLARATION
➢ I hereby declare that the above-written particulars are true to the best
of my knowledge and belief.

Date: 30/10/2019

Place: Dehradun
(Amrita Hooda)

DEVELOPMENT AND PATTERN ANALYSIS OF SUPERHYDROPHOBIC NANOCOMPOSITE COATING